UNVEILING NOVEL CARDIOPROTECTIVE EFFECTS OF GYY4137, A SLOW-RELEASING HYDROGEN SULFIDE DONOR, AND THEIR RELATIONSHIPS TO NEUROHORMONAL MODULATION AND MICRORNA PROFILES DURING MYOCARDIAL ISCHEMIC INJURY

SHERA LILYANNA

B. Sci (Hons), NUS

A THESIS SUBMITTED

FOR THE DEGREE OF MASTER OF SCIENCE

DEPARTMENT OF MEDICINE

NATIONAL UNIVERSITY OF SINGAPORE

2014

DECLARATION

I hereby declare that this thesis is my original work and it has been written by me in its entirety.

I have duly acknowledged all the sources of information which have been used in the thesis.

This thesis has also not been submitted for any degree in any university previously.

_____

SHERA LILYANNA

AUGUST 2014

ACKNOWLEDGEMENTS

Research is something that cannot be accomplished by one person and this thesis for certain would not have been completed without the support of many, to whom I wish to express my deep gratitude.

First and foremost, I would like to thank Professor Arthur Mark Richards for accepting me in the lab, for giving me the opportunity to undertake this M.Sc. project and for his guidance and advice as my main supervisor to complete this study.

To Dr. Eliana C Martinez, my mentor and co-supervisor, I am deeply and forever grateful for your endless guidance, patience and moral support; for your encouragement during the difficult moments and to finish my study; for understanding my decision. I appreciate our time and friendship for the past 6 years and your concern for my health and my family.

To my past and present colleagues at CVRI. To Dr. Liew Oi Wah, for your guidance and advice on protein studies and moral support when I am down. To Dr. Wong Lee Lee, for your helpful advice in microarray and encouragement for me to finish my study. To Jenny, Yan Xia, Cui Xia, Jia Yuen for the accompaniment and encouragement during my depressed moments.

To my best friends: Felicia, Winny, Karol, Tez and Adel for listening to my complaints, comforting me and accompanying me to de-stress during weekends after stressful weekdays. Thank you for being there and for your listening ears.

Last but not least, to my forever precious family, without whom, I will not be here. Without your physical and moral support and unconditional love, I would not have been able to survive this battle.

TABLE OF CONTENTS

SUMMARY

Myocardial infarction (MI) followed by adverse left ventricular (LV) remodeling is the most frequent proximate cause of heart failure (HF). Following MI, neurohormonal response is activated and in HF, this activation is sustained and has damaging effects on cardiac function. Various microRNAs (miRNAs) have also been identified and linked to the development of typical pathological changes of the myocardium after MI. Hydrogen sulfide (H_2S) is emerging as an important endogenous modulator that exhibits cytoprotective effects in diverse physiological and pathophysiological processes. However, its role in post-ischemic ventricular remodeling and the associated neurohormonal responses, as well as on miRNA profiles has not been well-defined. Sodium hydrosulfide (NaHS) as the prototypical H_2S donor has been extensively studied, however it is highly volatile and might not be physiologically relevant to study the therapeutic potential of H_2S *in vivo*. To this end, we utilized a slow-releasing water-soluble H_2S donor, GYY4137 (GYY) that mimics endogenous physiological release of H_2S. The effect of GYY on LV remodeling and function following myocardial injury has not been previously characterized. Therefore, this study was designed to investigate the cardioprotective effect of GYY following myocardial injury. We postulated that GYY exerts its therapeutic effect by modulating neurohormonal and miRNAs responses to cardiac injury.

The results in this thesis demonstrated that GYY treatment, for 2 and 7 days after acute MI in rats, preserved LV dimensions and function *in vivo* when compared to untreated infarcted (MI), placebo- and DL-propargylglycine- (PAG, an inhibitor of endogenous H_2S synthesis) treated animals. LV dimensions and function in GYY-treated animals were comparable to healthy sham-operated rats at both time-points. GYY-treated hearts

had significantly less LV fibrosis than MI, placebo and PAG hearts. In addition, higher density of blood vessels was observed in the LV scar area of GYY-treated animals in comparison to all other infarcted groups. Despite preserved LV structure and function, GYY treatment increased tissue expression and plasma peptide levels of the natriuretic peptides, atrial natriuretic peptide (ANP) and b-type natriuretic peptide (BNP), in association with enhanced plasma cyclic guanosine 3'5'-cyclic monophosphate (cGMP). These results suggest that GYY may exert its therapeutic effects through modulation of the natriuretic peptides (NPs)-cGMP pathway.

Furthermore, miR-31 was found to be significantly suppressed upon treatment with GYY when compared to MI- and placebo-treated rats at day 7 post-MI. miR-31 has been reported to be higher in serum from patients with coronary artery disease (CAD) with restenosis when compared to CAD patients without restenosis and to healthy controls. In a parallel study, we have found that miR-31 is deleterious to cardiac function and its inhibition *in vivo* prevents the development of HF. Therefore, GYY-mediated modulation of miRNAs may contribute to the cardioprotective effect of GYY.

In conclusion, this study has demonstrated that GYY exerted post-ischemic cardioprotective effects, which are pro-angiogenic and anti-fibrotic. GYY-mediated attenuation of adverse remodeling may be, in part, due to enhanced early post-ischemic endogenous natriuretic peptide activation and miRNAs modulation.

LIST OF TABLES

LIST OF FIGURES

LIST OF ABBREVIATIONS

3'UTR	3' untranslated region
Ang 2	Angiotensin 2
ARBs	Ang 2 type 1 receptor antagonists
ACE	Angiotensin-converting enzyme
ADT-OH	5-(4-hydroxyphenyl)-*3H*-1,2-dithiole-3-thione
ANP	Atrial natriuretic peptide
APJ	Angiotensin II receptor-like 1
B2M	Beta 2 microglobulin
BCL2	B-cell CLL/lymphoma 2
BNP	B-type natriuretic peptide
cAMP	Adenosine 3'-5'-cyclic monophosphate
cGKIα	Guanosine 3'5'-cyclic monophosphate -dependent kinase I alpha
cGMP	Guanosine 3'5'-cyclic monophosphate
CNG	Cyclic nucleotide-gated ion channels
CO	Cardiac output
CSE	Cystathionine γ-lyase
DADs	Diallyl disulfide
DATS	Diallyl trisulfide
EF	Ejection fraction
FC	Fold change
FS	Fractional shortening
GSH	Glutathione
GYY	4-Methoxyphenyl (morpholino) phosphinodithioate morpholinium salt/ GYY4137
H_2S	Hydrogen sulfide

HF	Heart failure
IP	Intra peritoneal
LAD	Left anterior descending coronary artery
LPS	Lipopolysaccharide
LV	Left ventricular
LVAWd	Left ventricular anterior wall in diastole
LVAWs	Left ventricular anterior wall in systole
LVEDD	Left ventricular end-diastolic diameter
LVESD	Left ventricular end-systolic diameter
LVEDP	Left ventricular end-diastolic pressure
LVEDV	Left ventricular end-diastolic volume
LVESV	Left ventricular end-systolic volume
LVIDd	Left ventricular internal dimension in diastole
LVIDs	Left ventricular internal dimension in systole
MI	Myocardial infarction
miRNAs	microRNAs
mRNAs	messenger RNAs
mTOR	mammalian target of rapamycin
NaHS	Sodium hydrosulfide
NF-κB	Nuclear factor kappa-light-chain-enhancer of activated B cells
PAG	D-propargylglycine
PCI	Percutaneous coronary intervention
PDE	Phosphodiesterase enzyme
PKC	Protein kinase C
PRA	Plasma renin activity
NO	Nitric oxide

NPs	Natriuretic peptides
NPR1	Natriuretic peptide receptor 1
NPR3	Natriuretic peptide receptor 3
QPCR	Quantitative real-time polymerase chain reaction
RAAS	Renin-angiotensin-aldosterone system
ROS	Reactive oxygen species
SC	Subcutaneous
SNS	Sympathetic nervous system
STEMI	Reperfused-ST-segment elevation myocardial infarction
TGF-β	Transforming growth factor-β
VEGF-A	Vascular endothelial growth factor-A
VSMC	Vascular smooth muscle cell

1. INTRODUCTION

1.1 Myocardial infarction

Myocardial infarction (MI) occurs when a coronary artery supplying nutrients and oxygen to the left ventricle is abruptly obstructed leading to an inequality between the supply and demand of the heart for oxygenated blood[1]. MI, complicated by adverse left ventricular (LV) remodeling, is the most common proximate cause of heart failure (HF), a principal cause of death world-wide[2]. In Singapore, MI accounted for 16.4% of deaths in 2011[3]. The ischemic event leads to the loss of functional cardiomyocytes and impaired cardiac contractility, resulting in a sudden increase in loading conditions which in turn may trigger a cascade of biochemical intracellular signaling processes leading to LV remodeling[4]. LV remodeling refers to the modifications in shape, size, structure and physiology of the cardiac ventricle and is closely connected to the activation of circulating neurohormones[5]. Initially, neurohormonal activation plays an important role as part of the compensatory mechanisms following MI[6, 7] and the degree of activation is associated to the magnitude of the myocardial injury[8]. This activation comprises increased expression of endothelin and cardiac natriuretic peptides (NPs), activation of the renin-angiotensin-aldosterone system (RAAS), as well as activation of sympathetic nervous system (SNS)[9, 10]. However, long term neurohormonal activation has potentially deleterious consequences on the peripheral circulation and heart leading to further LV adverse remodeling (**Figure 1.1**)[8, 10].

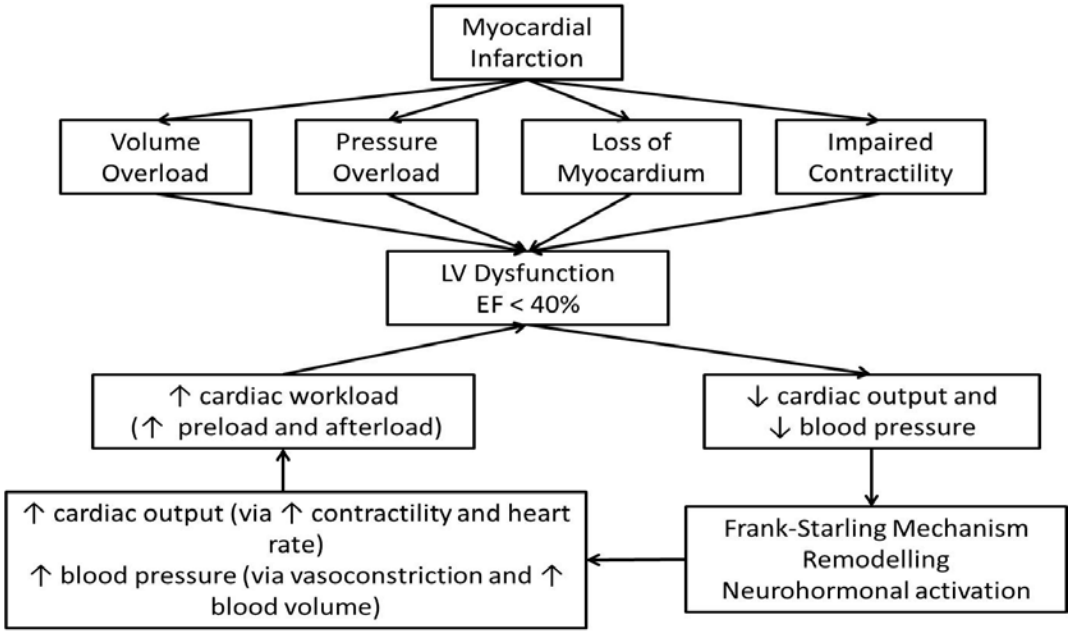

Figure 1.1 The vicious cycle after MI. Adapted with permission from Elsevier Inc: Cardiovascular Pathology 21 (5):365-71, copyright © 2012[10].

The RAAS is vital in the maintenance of water and electrolyte balance and volume of blood. It is stimulated by various stimuli including sympathetic traffic and changes in renal perfusion[11]. Angiotensin 2 (Ang 2), a potent vasoconstrictor, is a product of renin-angiotensin activation and chronic elevation of Ang 2 has potentially harmful cardiovascular effects[12]. Ang 2 has been implicated in interstitial cardiac fibrosis by promoting fibroblast proliferation and adhesion in addition to extracellular matrix proteins synthesis through activation of Ang 2 type I receptor[13]. It has also been shown that Ang 2 receptors expression is up-regulated in hypertrophic cardiomyocytes after MI, and stretching of these cells increased Ang 2 production[14]. Ang 2 also directly triggers aldosterone release from the adrenal zona glomerulosa. Aldosterone is the primary mineralocorticoid hormone regulating systemic salt and water homeostasis[15]. Aldosterone is also involved in the development of myocardial fibrosis and induces vascular inflammatory responses[16].

The NPs, atrial natriuretic peptide (ANP) and B-type natriuretic peptide (BNP) are released by the heart normally in response to myocardial stretch but also in response to ischemia[17]. They are involved in regulating natriuresis and vasodilation, inhibiting RAAS activation and also exerting anti-mitogenic effects on smooth muscle, endothelial, and myocardial cells[18]. Circulating levels of the ANP and BNP are used as predictors in the assessment of cardiac dysfunction and failure, and are currently used as diagnostic and prognostic tools in the management of patients with cardiac injury including MI[18, 19]. On the other hand, increased levels of the vasoactive peptide endothelin-1 (ET-1) has been associated with infarct extension and reduction of coronary blood flow[20, 21]. Furthermore, ET-1 promotes myocardial hypertrophy[22]. The C-terminal portion of pro-ET-1, which is more stable in circulation than ET-1, can also potentially be used as a prognostic marker after MI[23]. In addition, the increase in adrenergic nervous activity has been associated to arrhythmias and LV remodeling[11]. Circulating norepinephrine, the product of adrenergic activation, is toxic to cardiomyocytes[24]. Antagonism of neurohormonal pathways constitutes the mainstay of current pharmacotherapy for cardiac ischemic injury through the use of angiotensin converting enzyme (ACE) inhibitors, Ang 2 type 1 receptor antagonists (ARBs), blockers of β-adrenoceptors and mineralocorticoid receptor antagonists.

1.2 Treatment options after MI

One of the most effective treatments during MI is reperfusion of the infarcted myocardium. Fibrinolytic therapy and primary percutaneous coronary intervention (PCI) have been demonstrated to effectively reduce the infarct size, improve LV function and decrease mortality of MI patients[25, 26]. In addition, current pharmacological therapies

ameliorate post-MI adverse LV remodeling and suppress the detrimental effects of neurohormonal activation (ARBs, β-adrenoceptors blocker therapy, ACE inhibitors, and mineralocorticoid receptor antagonist therapy).

Captopril and enalapril, ACE inhibitors, impair conversion of angiotensin 1 to Ang 2, whereas ARBs, such as valsartan and losartan, directly occupy and block Ang 2 type 1 receptors preventing their activation by Ang 2[27]. Both ACE inhibitors and ARBs decrease fibrosis formation in the non-infarcted myocardium and proliferation of fibroblasts following MI, which is associated with improved cardiac function and survival[28-30]. β-adrenoceptors blocking agents, such as carvedilol and metoprolol, neutralize the harmful effects of SNS activation and have been proven clinically to improve LV function after MI[10, 31]. Intravenous treatment of metoprolol in reperfused-ST-segment elevation myocardial infarction (STEMI) patients has recently been demonstrated to reduce infarct size[32]. Mineralocorticoid receptor antagonists have also been demonstrated to reduce post-MI mortality[27, 31].

Despite the clear benefits of these agents in reducing mortality from 20-30% to 5-10% over the last 30 years[33, 34], post-MI adverse remodeling remains a common event and carries high risk of subsequent HF and mortality[35]. With the increased immediate survival following MI because of percutaneous reperfusion and adjunctive pharmacotherapies together with an aging population, we have a growing population having survived acute cardiac injury which contributes to the increasing prevalence of HF[36, 37]. Currently, available treatments are insufficient for full prevention of post MI adverse ventricular remodeling and the search for new treatment strategies that are more effective in protecting the heart against MI, preventing LV remodeling and its subsequent cardiovascular events are urgently needed.

1.3 Hydrogen sulfide (H_2S) as cardioprotectant

1.3.1 H_2S in cardiovascular system

Hydrogen sulfide (H_2S), traditionally recognized as a noxious gas in external environmental settings, has now been acknowledged as the third gasotransmitter after carbon monoxide and nitric oxide (NO)[38, 39]. It is highly lipophilic, easily permeable and diffusive in the plasma membranes[40]. Because of its nature, it is difficult to accurately measure H_2S concentration in blood and tissue. Depending on the method being used, H_2S in blood and tissue has been reported at concentrations varying between 15nM and 301μM[40]. H_2S is endogenously generated through enzymatic pathways (i.e. cystathionine γ-lyase (CSE), cystathionine β-synthase (CBS), and cysteine aminotransferase (CAT) together with mercaptopyruvate sulfurtransferase (3-MST)), non-enzymatic pathways (reduction of thiol-containing molecules) and from intracellular sulfane sulfur[41-43]. The key H_2S-synthesizing enzyme in the cardiovascular system is CSE[44]. In recent years, various studies have established the involvement of H_2S in cell signaling processes[43]. Noteworthy effects of H_2S on cell signaling processes, relevant to the cardiovascular system, can be divided into four: protein modifications, transcription factors and intracellular signaling proteins, ion channels, and metabolism (**Figure 1.2**)[43].

H_2S s-sulfhydrates cellular proteins by adding sulfide to the thiol groups of cysteine residues to generate –SSH moiety that may be similar to the s-nitrosylation by NO[45]. This process enhances the biological activity of the s-sulfhydrated GAPDH[45]. Although the effect on other cellular proteins is yet to be investigated, s-sulfhydration could be one of the key mechanisms underlying the various effects of H_2S on the cardiovascular system. H_2S also targets various transcription factors, including signal transducer and activator of transcription 3 (STAT3) and nuclear factor-E2-related factor 2 (Nrf-2). STAT3 was

activated after H_2S administration to lipopolysaccharide (LPS)-injected rats[46]. STAT3 has been reported to promote cell survival (through increased survivin), angiogenesis (up-regulation of vascular endothelial growth factor; VEGF) and proliferation (activation of c-fos)[47]. H_2S was found to cause Nrf-2 to localize to the nucleus in ischemic rat hearts[48]. Nuclear Nrf-2 subsequently regulates the expression of heme oxygenase-1 gene and thioredoxin-1 gene to limit cardiac injury[48]. In addition, cardiac Akt and protein kinase C (PKC) have been demonstrated to be activated after sodium hydrosulfide (NaHS), a fast-releasing H_2S donor, was briefly infused into isolated hearts of ischemia model. This activation resulted in the reduction of myocardial injury and improved cardiac mechanical performance[49]. Other targets of H_2S include the ion channels. H_2S causes vasodilatation via the opening of vascular smooth muscle K_{ATP} channels[50-53]. H_2S effects on K_{ATP} channels also aid in protecting hearts in the ischemia/reperfusion injury model[54-56]. Lastly, H_2S was also found to suppress oxidative stress in mitochondria by increasing intracellular reduced glutathione (GSH) levels[57]. The antioxidant activity of H_2S was demonstrated to protect the isolated heart against ischemia/reperfusion injury[58].

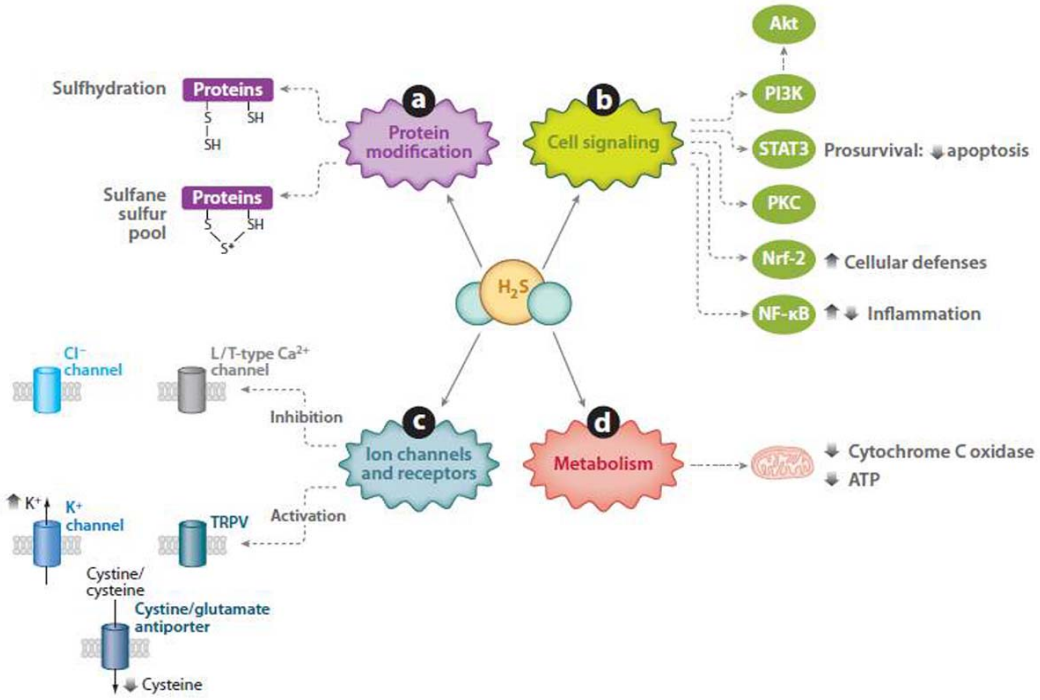

Figure 1.2 Molecular targets of H_2S in cardiovascular system. H_2S is known to affect (**a**) protein (cysteine thiol) modifications, (**b**) intracellular signaling proteins and transcription factors, (**c**) ion channels, and (**d**) metabolism. Reprinted with permission from Li L, *et al.* Annu Rev Pharmacol Toxicol. 2011; 51:169-87. Copyright © 2011 Annual Reviews[43].

1.3.2 H_2S and MI

Recent studies have demonstrated that under ischemic conditions, activity of CSE in the isolated heart[49] and endogenous H_2S level in ventricular myocytes[44] were reduced. Moreover, plasma H_2S was decreased in infarcted rats[59] and in patients with coronary disease[60]. These observations suggest that impaired endogenous H_2S production might possibly be involved in the development of MI. In view of this, various groups have investigated and demonstrated H_2S-mediated cardioprotective effects in MI model *in vivo*. A study done by Zhu and colleagues demonstrated that NaHS, administrated from 7 days prior to left anterior descending coronary artery (LAD) ligation to 2 days after ligation, significantly reduced mortality (~20%) and infarct size (~18%) compared to

placebo group[61]. Similarly, another group reported that treatment with NaHS for 3 days after LAD ligation significantly reduced infarct size, prevented LV dilatation and preserved the anterior wall thickness compared to placebo group[62]. The cardioprotective effect of H_2S treatment post-MI could be explained by several possible mechanisms. One study reported that exogenous H_2S treatment, after LAD ligation, reduced the infarct size and preserved LV function by promoting angiogenesis. Expression of VEGF, a key growth factor for angiogenesis, and its receptor (tyrosine kinase receptor and fms-like tyrosine kinase) were elevated whereas anti-angiogenic factors such as endostatin, angiostatin and parstatin were decreased upon H_2S treatment[63]. Another study implicated the involvement of NADPH oxidase 4 (Nox4). Nox4 is one of the important sources of reactive oxygen species (ROS) in activated cardiac fibroblast and regulates the transcription of pro-fibrotic genes and the redox-dependent pathway[64]. Administration of NaHS decreased activation of Nox4 expression after MI. Reduction of Nox4 was complemented with decreased fibrotic response as shown by the reduction of matrix metalloproteinase-2 and -9 (MMP-2 and MMP-9) expression level and the activity of MMP-2, suggesting that H_2S could attenuate LV remodeling after MI through the suppression of myocardial fibrosis[65]. NaHS treatment also exerted its effect via the regulation of bcl-2-associated X (BAX)/ B-cell CLL/lymphoma 2 (BCL-2) apoptotic signaling pathway. The expression level of BAX, a pro-apoptotic protein, was down-regulated while BCL-2, an anti-apoptotic protein, was up-regulated upon H_2S treatment, thus resulting in reduction of caspase-3 activity[66]. All of these studies demonstrated that H_2S therapeutic treatment is beneficial to the heart post-MI through the regulation of multiple signaling pathways.

1.3.3 Various H_2S donors

In the initial years, the majority of studies investigating the therapeutic potential of H_2S utilized commercially available sulfide salts such as NaHS. However, NaHS is highly volatile and short-lived. It releases H_2S rapidly in aqueous solution and does not reflect the slow and constant H_2S synthesis *in vivo*[67]. Thus, NaHS might not be a physiologically relevant compound to use to study the therapeutic potential of H_2S. Because of the limitations related to NaHS, researchers have developed novel H_2S donors that mimic the sustained physiological release of endogenous H_2S *in vivo*. H_2S donors that are available currently can be grouped as follows.

1) Naturally occurring H_2S donors

Garlic is a natural organic sulfur-containing plant, derivatives of which have been demonstrated to induce H_2S release by red blood cells, in the presence of GSH[68]. Allicin (diallyl thiosulfinate) found in garlic is very unstable and decays in water to a number of lipid-soluble sulfur-containing molecules such as diallyl sulfide, diallyl disulfide (DADS) and diallyl trisulfide (DATS)[69]. DADS and DATS have been reported to vasodilate rat aortae by releasing H_2S, suggesting that these compounds could be useful as H_2S donors[68]. S-allyl-cysteine (SAC) is a water–soluble component formed in the preparation of aged garlic extract[70]. It can also be generated synthetically from allyl bromide and cysteine hydrogen chloride salt[70]. SAC is the only cysteine analogue that has been reported to possibly function as a substrate for H_2S production by CSE[71]. SAC significantly increased plasma H_2S concentration and could up-regulate expression and activity of CSE in the infarcted heart[72]. These findings suggested that SAC potentially acts as an H_2S donor. However, there is still no direct evidence on how these natural organic sulfur containing compounds may be a source of H_2S.

2) Synthetic H_2S –releasing drugs

Synthetic H_2S-releasing drugs are predominant among H_2S donors. Most studies used modified existing pharmacological compounds such as NSAIDs (non-steroidal anti-inflammatory drugs) that contain releasing moiety of H_2S, ADT-OH [5-(4-hydroxyphenyl)-*3H*-1,2-dithiole-3-thione]). These S-NSAIDs drugs comprise of *S*-aspirin, *S*-diclofenac, *S*-naproxen, and *S*-sulindac. *S*-diclofenac has been demonstrated to have better anti-inflammatory effects compared to diclofenac[73, 74]. It also has the ability to inhibit smooth muscle cell proliferation[75], and exhibits anti-ischemic[58] and anticancer properties[76]. Anti-cancer properties of *S*-diclofenac and *S*-sulindac seem to be mediated through the inhibition of carcinogen-activating enzymes[77]. *S*-NSAIDs have shown promising therapeutic potential in cardiovascular diseases and cancers. The reported biological effects of these *S*-NSAIDs, however, could result from ADT-OH moiety itself rather than the release of H_2S. This is because ADT-OH is biologically active and the exact mechanism on how ADT-OH releases H_2S has not been fully investigated[78, 79]. Recently, another synthetic H_2S-releasing drug, which is not based on structural modification of existing drug molecules, has been synthesized and characterized. This compound is covered in the next section.

1.3.4 GYY4137

GYY4137 (morpholin-4-ium-4-methoxyphenyl (morpholino) phosphinodithioate; **Figure 1.3A**), a derivative of Lawesson's reagent, is a slow-releasing H_2S donor that has been shown to decompose gradually to generate small quantities of H_2S *in vitro* (**Figure 1.3B and C**) and *in vivo* (**Figure 1.3D and E**)[53]. In their study, Li *et al* demonstrated that NaHS released H_2S *in vitro* rapidly within 5 to 8 seconds (**Figure 1.3B**) as measured by

amperometry, whereas GYY4137 (GYY) released H_2S slowly, peaking at around 6-10 minutes (**Figure 1.3C**). *In vivo*, intravenous and intraperitoneal administration of GYY to anesthetized rats increased plasma H_2S concentration at 30 minutes and it remained elevated over the 180-minute time course of the experiment (**Figure 1.3D**). In contrast, administration of NaHS did not increase plasma H_2S level at the same time points of evaluation (**Figure 1.3E**). GYY mimics endogenous physiological release and was shown to be more effective in relaxing rat aortae compared to NaHS with no toxicity *in vitro*[53]. In recent years, the beneficial effects of GYY have been reported in several systems. GYY has been reported to be protective against endotoxic shock in rat by decreasing LPS-induced inflammatory markers in plasma such as tumor necrosis factor alpha (TNF-α), creatinine, nitrite/nitrate level, and c-reactive protein, as well as inhibiting activation of nuclear factor kappa-light-chain-enhancer of activated B cells (NF-κB) in liver[46]. It also decreased the production of pro-inflammatory mediators from human joint cells *in vitro*[80], supporting a possible role of GYY as an anti-inflammatory agent. In addition, anti-cancer effects of GYY have been demonstrated *in vitro* and *in vivo*[81]. GYY treatment significantly reduced *in vitro* proliferation of various cancer cell lines. In a mouse xenograft model, GYY reduced tumor growth of myelomonocytic leukemia and acute promyelocytic leukemia by 52.5% and 55.3% respectively after 14 days, thus confirming the anti-cancer effect of this H_2S donor. Moreover, GYY relaxed oxytocin-stimulated and spontaneous contractions of human myometrial biopsies and pregnant myometrium in rat[82]. In the lung disease model of bronchopulmonary dysplasia, GYY has been reported to decrease ROS in hyperoxia-exposed human pulmonary artery endothelial cells, enhance capillary-like network formation and also protect mitochondrial function in alveolar epithelial cells[83]. *In vivo*, GYY treatment attenuated pulmonary artery remodeling and right ventricular hypertrophy in the rat pups pulmonary hypertension model[83].

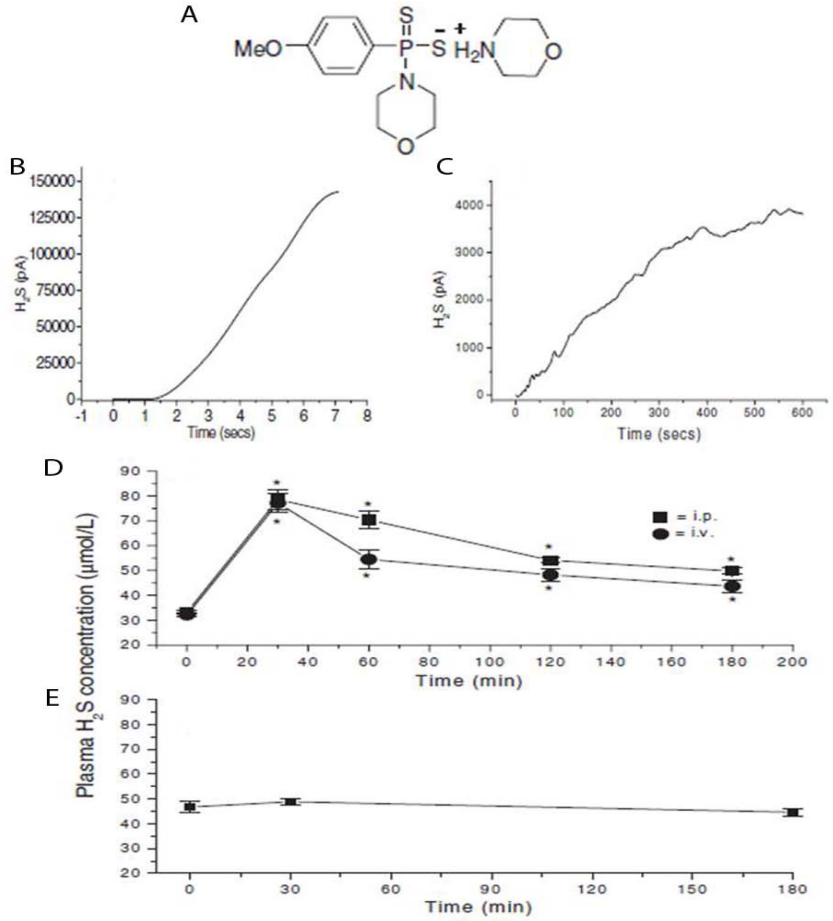

Figure 1.3 GYY4137. (**A**) Chemical structure of GYY4137. *In vitro* release rate of H_2S from (**B**) NaHS (100 μmol/L) and (**C**) GYY4137 (1 mmol/L) in phosphate buffer pH 7.4 as determined by amperometry or spectrophotometrically. Plasma concentration of H_2S in animals administered with (**D**) GYY4137 (133 μmol/kg intravenously (i.v) or intraperitoneally (i.p) or (**E**) NaHS (20 μmol/kg i.v). Reprinted with permission from Li L, *et al.* Circulation. 2008; 117:2351-2360. Copyright © 2008[53].

GYY has significant therapeutic effects in models of cardiovascular disease. Grambow *et al.* demonstrated that GYY prolonged the venular thrombus formation in mice by interfering with platelet activation and adhesion molecule-mediated aggregation through reduction of circulating soluble P-selectin concentration, suggesting that GYY can function as an anti-thrombotic agent[84]. In addition to its involvement in thrombogenesis, GYY also exhibits anti-atherosclerotic activity. GYY treatment in apoE−/− mice fed with high-fat diet prevented further aortic atherosclerotic plaque formation and moderately

recovered aortic endothelium-dependent vasodilation, most likely through the induction of endothelial nitric-oxide synthase (eNOS) phosphorylation[85]. In a diabetic myocardial injury model, GYY was able to reduce the harmful effects of high glucose treatment in rat cardiomyoblast cells as seen from preservation of cell viability and reduction of lactate dehydrogenase enzyme activity. This GYY-mediated cytoprotection was demonstrated to be the result of AMP-activated protein kinase/mammalian target of rapamycin (AMPK/mTOR) signaling pathway activation[86]. Based on the various beneficial effects of GYY, this slow-releasing H_2S donor is involved in multiple pathways and could be a potential therapeutic agent against adverse post-MI cell loss and adverse ventricular remodeling.

1.4 Natriuretic peptides (ANP and BNP) pathway

ANP and BNP, members of the natriuretic peptide family, are expressed mainly in the heart[87]. Gene expression of ANP is highest in the atria whereas BNP is expressed predominantly in the cardiac ventricles[88]. proANP is stored in the atrial granules and is cleaved into the mature peptide upon release from the atrial granules[89]. The main stimulus for proANP release is atrial stretch caused by increased intravascular volume[88]. Though BNP is also deposited in atrial granules along with ANP[90], in the ventricle, BNP is not deposited in granules and is constitutively transcribed as required, proportional to ventricular myocyte mechanical stretch[91]. Degradation of ANP and BNP occur through the actions of neutral endopeptidase (NEP)[92, 93] and by binding to the natriuretic peptide clearance receptor (NPR3) [88]. Both ANP and BNP bind and activate the transmembrane guanylyl cyclase, natriuretic peptide receptor-1 (NPR1) to catalyze the synthesis of the intracellular second messenger, cyclic guanosine 3',5'-monophosphate (cGMP)[94]. In the

cardiovascular system, cGMP exerts its biological action through cGMP-dependent protein kinase 1 (cGKI), cGMP-regulated phophodiesterases (PDE2 and PDE3) and cGMP-gated cation channels (CNGs)[94]. The ANP/BNP-cGMP pathway regulates various physiological processes in the cardiovascular system such as fibrosis, angiogenesis and cardiac hypertrophy and remodeling[95].

1.4.1 ANP/BNP in cardiac hypertrophy and remodeling

Horio *et al.* demonstrated that endogenous ANP inhibited cardiomyocyte hypertrophy possibly via a cGMP-dependent pathway[96]. The authors treated cultured cardiomyocytes with HS-142-1, a specific antagonist of NPR1, and showed that this antagonist increased basal and phenylephrine (PE)-stimulated protein synthesis and enhanced the size of myocytes. Treatment with zaprinast, an inhibitor for a cGMP-specific PDE as well as a cGMP analogue, attenuated the basal and PE-stimulated protein synthesis. In accordance to this observation, animal studies with a modified ANP/BNP-cGMP pathway have shown similar results. Mice with cardiac-restricted NPR1 deletion displayed minor cardiac hypertrophy, accompanied by an increase in circulating ANP level and gene expression of cardiac hypertrophy markers including skeletal-actin, ANP, and alpha-myosin heavy chain[97]. Furthermore, these transgenic mice developed enhanced cardiac hypertrophy and marked deterioration of cardiac function in response to aortic constriction. In contrast, mice with cardiac overexpression of NPR1 displayed reduction in cardiomyocyte size and ANP mRNA expression[98]. Moreover, cardiac overexpression of constitutive active guanylyl cylase (GC) prevented pressure-overload-derived hypertrophy in a mouse model[99]. Taken together, these observations suggest the ANP and BNP/NPR1/cGMP system is anti-hypertrophic.

1.4.2 ANP/BNP modulation of fibroblasts

Natriuretic peptide receptors are expressed in cardiac fibroblasts, as well as cardiomyocytes[100]. However, in contrast to cardiomyocytes that express predominantly NPR1, cardiac fibroblasts express both NPR1 and natriuretic peptide receptor-2 (NPR2). ANP and BNP treatment of cultured cardiac fibroblasts increased cGMP and inhibited Ang 2-induced DNA synthesis[101]. Furthermore, myocyte-conditioned medium and exogenous application of ANP inhibit collagen synthesis in cardiac fibroblasts, while treatment with HS-142-1, a specific antagonist of NPR1, reverses this effect[102]. These observations suggest that ANP and BNP generated by myocytes could suppress cardiac fibroblast proliferation through paracrine effects; this concept is further reinforced by a recent animal study. In response to aortic constriction, ANP knock-out mice developed robust cardiac interstitial and perivascular fibrosis with collagen deposition[103]. Mice lacking BNP exhibited multifocal ventricular fibrotic lesions in response to abdominal aortic constriction[104]. These findings demonstrated the anti-fibrotic effects of ANP and BNP.

1.4.3 ANP/BNP modulation of angiogenesis

Evidences suggest that the ANP/BNP-cGMP pathway is involved in promoting angiogenesis in ischemic tissues. Exogenous application of ANP increased cGMP level in human umbilical vein endothelial cells and promoted endothelial tube formation[105]. Likewise, BNP stimulated migration and proliferation of cultured microvascular endothelial cells[106]. *In vivo* study of the hind-limb ischemia mice model demonstrated that systemic BNP injection significantly improved blood flow and capillary density[107]. Yamahara *et al.* also reported that transgenic mice, overexpressing BNP had enhanced

neovascularization in the hind-limb ischemia model[108]. Vascular remodeling was significantly impaired in NPR1 knock-out mice in response to limb ischemia[106, 109]. Furthermore, a significant association between circulating N-terminal proBNP level and endothelial progenitor cells (EPCs) colony forming unit in HF patients has been reported[107], supporting the involvement of ANP/BNP in angiogenesis.

1.4.4 Clinical application of ANP/BNP

Preclinical studies in patients with congestive HF have reported that infusion of ANP improved cardiac function by regulating loading conditions for LV[110-112]. Since then, the use of recombinant ANP (carperitide) to treat acute MI has been approved in Japan whereas recombinant BNP (nesiritide) is approved by the Food and Drug Administration (FDA), USA for treatment of acute decompensated heart failure (ADHF)[113]. Hayashi *et al*. demonstrated that infusion of carperitide to 30 patients with acute myocardial infarction (AMI) after coronary intervention improved LV remodeling as indicated by significantly higher ejection fraction (EF) when compared to control group[114]. In a bigger study, Kitakaze *et al*. reported that infarct size was significantly reduced by 15% and EF was markedly higher in the carperitide group relative to placebo group[115]. Both studies demonstrated that treatment with ANP is beneficial as an adjunct therapy in patients with AMI. However, further studies are needed to address the controversy surrounding the safety side of these drugs pertaining to adverse renal effects[87, 113].

1.5 microRNAs (miRNAs)

MicroRNAs (miRNAs), short non-coding RNA molecules of 20-22 nucleotides length, have been recognized as physiological regulators of gene expression through translational repression or degradation of messenger RNAs (mRNAs) by binding to the target sequences in the 3' untranslated region (3'UTR) of mRNAs[116, 117]. The expression of miRNAs has been shown to be closely regulated and is specific to different organs and cell types[118]. In recent years, various miRNAs have been identified and recognized as playing a role in the pathophysiology of many diseases including cancers and cardiovascular diseases[119, 120]. The emerging interest in miRNAs stems from their two potential clinical applications. Firstly, it is known that many diseases are characterized by abnormal miRNAs expression. As such, comparison of miRNA profiles between normal and diseased samples allows for the identification of crucial miRNAs that are changed during the development of pathological conditions. Identification of these dysregulated miRNAs in the circulation might potentially render miRNAs useful as early disease biomarkers. The second application is the therapeutic targeting of miRNAs that are linked to pathways related to the disease pathophysiology. In the cardiovascular field, specific miRNAs have been found to be related to the progression of typical pathological changes of the heart after MI which include induction of apoptosis (miR-1 and miR-206)[121], arrhythmia (miR-1)[122], neo-angiogenesis (miR-92a and miR-210)[123, 124], cardiac fibrosis (miR-21 and miR-101)[125, 126] and inflammatory response (miR-223 and miR-29)[127, 128]. These associations suggest that miRNAs could be useful as new diagnostic and prognostic markers of MI and therapeutic targets in treatment or prevention of post-MI remodeling. Moreover, plasma levels of specific miRNAs (miR-1, miR-208a, miR-133, and miR-499) are altered after MI, thus demonstrating the potential use of miRNAs as biomarkers[129-131].

1.6 Hypotheses and study aims

The effect of the slow releasing-H_2S donor, GYY, has never been evaluated in the myocardial infarction model and the relationship of GYY with neurohormonal modulation and miRNA profiles have not been well-defined. Hence, we hypothesized that GYY is cardioprotective against myocardial infarction and exerts its effect, in part, through modulation of the neurohormonal response and miRNAs.

The specific aims of this study are:

1. To assess the effects of GYY with respect to cardiac function and structure, as well as its therapeutic effects in the early and late post-MI period in a rat model of myocardial infarction.
2. To investigate the relationship of observed potential therapeutic effects of GYY with neurohormonal response upon ischemic cardiac injury.
3. To explore the effect of post ischemic GYY treatment on miRNAs profiles in the early and late post-MI phases.

2. MATERIALS AND METHODS

2.1 Experimental design

Overview of the experimental design could be seen in **Figure 2.1**. Male wistar rats underwent baseline echocardiography were distributed randomly to sham/healthy control group or disease groups. Rats in disease groups underwent LAD coronary artery ligation and were assigned randomly to untreated (MI) group and treated groups: including placebo (injected with 0.9% saline solution), GYY (treated with GYY4137) and PAG (treated with DL-propargylglycine (PAG)) 30 minutes (min) after LAD ligation. At each of two time-points (2 days and 7 days), final echocardiography and hemodynamic measurement were performed. Tissues and blood were collected for further analyses.

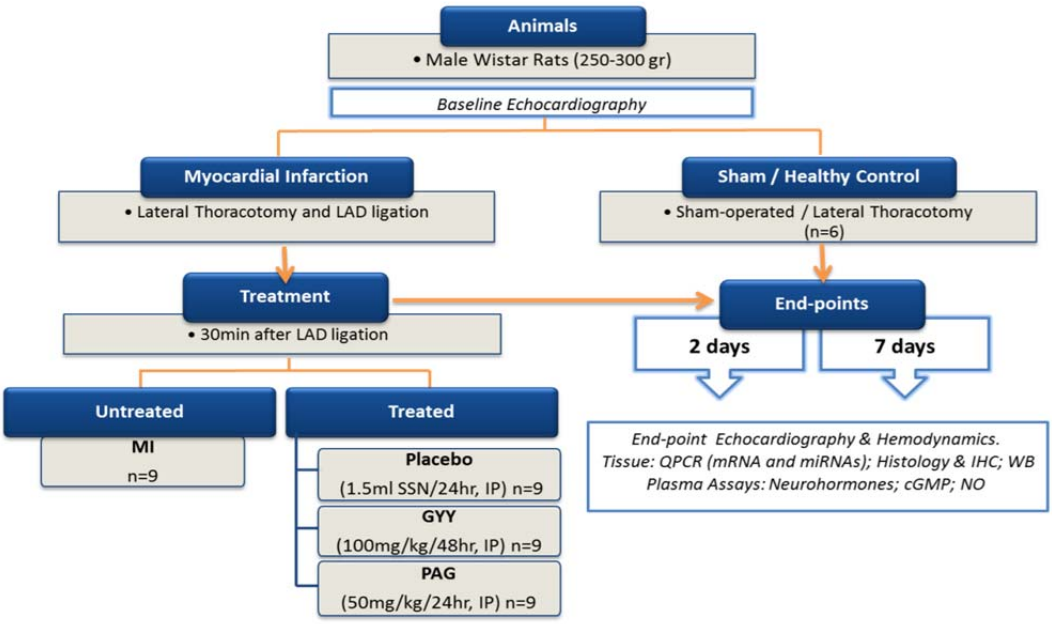

Figure 2.1 Schematic of the experimental design of the study.

LAD, left anterior descending coronary artery; MI, infarcted untreated; Placebo, infarcted placebo-treated group; GYY, infarcted GYY-treated group; PAG, infarcted PAG-treated group; SSN, saline; IP, intra peritoneal; QPCR, quantitative real-time polymerase chain reaction; mRNA, messenger RNA; miRNAs, microRNAs; IHC, immunohistochemistry; WB, western blot; cGMP, Guanosine 3'5'-cyclic monophosphate; NO, nitric oxide.

2.2 Treatment drugs

2.2.1 H_2S donor

The slow releasing-H_2S donor, GYY, used in this project was synthesized in-house by the Department of Pharmacology and Department of Chemistry, National University of Singapore. For intra peritoneal (IP) injection, appropriate dosage (100mg/kg) was aliquoted and diluted in 1.5ml of 0.9% saline. In order to completely dissolve GYY, solution was then sonicated for 10 seconds (sec) and repeated for three times with 5sec interval on ice (sonicator XL-2000 series; QSonica LLC, CT, USA). Next, solution was passed through 0.2µm syringe filter (Sartorius AG, Goettingen, Germany) inside the biological safety cabinet and loaded into sterile 3ml syringe for IP injection.

2.2.2 Cystathionine γ-lyase (CSE) antagonist

PAG, a CSE antagonist (Sigma Aldrich, St. Louis, MO, USA) was used at a dosage of 50mg/kg. It was diluted in 1.5ml of 0.9% saline for IP injection. Solution was passed through 0.2µm-syringe filter (Sartorius AG, Goettingen, Germany) inside the biological safety cabinet and loaded into sterile 3ml syringe for IP injection.

2.3 Rat model of myocardial infarction

All animal experiments were consented by the Institutional Animal Care and Use Committee (IACUC) of the National University of Singapore and performed in accordance to the established guiding principles for animal research. Eighty-four male Wistar Rats ((250-300g); NUS Care) were used in this study. Anesthesia was induced and maintained with inhalational isoflurane (2%; Baxter, Deerfield, IL, USA). Rats were

intubated with 16G catheter (Terumo Corporation, Tokyo, Japan) attached to the ventilator (Harvard Apparatus, MA, USA) throughout the procedure. The heart was exposed by fourth intercostal space incision (left-thoracotomy) and pericardium incision (pericardectomy). A myocardial infarction was created with an LAD ligation, which was performed by inserting a 7-0 polypropylene suture stitch (B.Braun, Germany) from the left border of the pulmonary conus to the right border of the left atrial appendage. An acute myocardial infarction was evaluated by immediate observation of myocardial blanching and ST segment changes in electrocardiogram. After the procedure, the chest was closed in three layers as follows: ribs and muscle were closed with 5-0 absorbable glyconate suture and skin was closed with 5-0 polypropylene suture (B.Braun, Germany).

Animals that only underwent lateral thoracotomy and pericardectomy were used as sham healthy controls. Animals were randomly assigned to receive therapeutic treatment 30min after ligation and were allowed to recover in a small-animal intensive care unit. Treatments were followed for 2 days and 7 days in rats that survived the first 24 hours (hr) after LAD ligation as follows for each time point (**Figure 2.1**): healthy sham-operated (n=6), untreated myocardial infarction (MI; n=9), placebo (infarcted injected with 0.9% saline solution, 1.5ml/24hr IP; n=9), GYY (infarcted treated with GYY4137, 100mg/kg/48hr IP; n=9) and PAG (infarcted treated with PAG, 50mg/kg/24hr IP; n=9). The dose of GYY used in this study was based upon prior studies of effective doses of this compound in other animal models[46, 85]. Animals received Carprofen (5mg/kg, once daily, subcutaneous (SC)) and Enrofloxacin (25mg/kg, twice daily, SC) postoperatively for the next 5 days after thoracotomy.

2.4 Echocardiography

Transthoracic echocardiography was carried out in all animals at baseline (before surgery) and on the same day of euthanasia at day 2 and day 7 post-MI using Vivid 7 Dimension ultrasound system equipped with a broadband 10S transducer (GE VingMed, Horten, Norway). Rats were induced and maintained with inhalational isoflurane (2%; Baxter) during the procedure. LV wall thickness and internal diameter during diastole and systole were obtained from M-mode recordings of the LV in the para-stemal short-axis view. LV end diastolic diameter (LVEDD) and LV end systolic diameter (LVESD) were obtained from M-mode recordings. LV volumes were calculated using a modified Teichholz formula where LV end diastolic volume was calculated as LVEDV= [(π x (LV diastolic internal diameter)^3)/(6 x (ellipticity factor of ⅓)] and LV end systolic volume was calculated as LVESV=[(π x (LV systolic internal diameter)^3)/(6 x (ellipticity factor of ⅓)]. LV fractional shortening (%FS) was calculated as [(LVEDD- LVESD)/LVEDD] x 100. LV ejection fraction (%EF) was calculated as [(LVESV - LVEDV)/LVEDV] x 100. Offline measurements of LV dimensions and areas were made from three consecutive cardiac cycles using EchoPac software (version 6; GE VingMed, Horten, Norway).

2.5 Hemodynamic measurements

Assessment of LV pressure and volume were carried out 2 days and 7 days post-treatment. Animals were induced and maintained with inhalational isoflurane (3%; Baxter) during the procedure. Similar to the myocardial injury procedure, animals were intubated with 16G catheter attached to ventilator (Harvard Apparatus). Mid-thoracotomy was done to expose the heart and the ascending aorta. A 2-mm transient-time flow probe

was positioned around of the ascending aorta for cardiac output (CO) measurement (Transonic Systems, Inc, Ithaca, NY, USA). Subsequently, a pressure transducer catheter (Millar Micro-Tip® model SPR-838; Millar, Inc, TX, USA) was inserted to the apex of LV. Aortic flow and pressure waves were recorded with the Powerlab 8/30 data acquisition system (ADInstruments Pte Ltd, Castle Hill, NSW, Australia). Data were analyzed with Lab Chart Pro software (version 7.0; ADInstruments).

2.6 Tissues and blood collection

Following hemodynamic measurements, terminal injection of pentobarbitone (150mg/kg, IP) was injected. Five ml of blood was collected in 7.2mg EDTA tube through cardiac puncture. Plasma was obtained by blood centrifugation (3,000g for 5 min, at 4°C) and stored at -80°C until processing for biochemical assays. The heart was excised and perfused with ice cold 1 x Phosphate Buffered Saline (1st Base, Singapore) to remove excess blood. Perfused heart was then cut into 2 cross sections. The upper slice was further halved and fixed in 10% formalin (Sigma Aldrich, St. Louis, MO, USA) for histology. Tissue from the lower portion encompassing infarct and peri-infarct areas (or the corresponding antero-inferior left ventricular region in sham animals) was divided equally for RNA and protein extraction, and immediately flash-frozen in liquid nitrogen. The liver was excised and immediately flash-frozen in liquid nitrogen. Tissues were stored at -80°C until further processing.

2.7 Histology for LV infarct size

One of the upper-halved formalin-fixed heart slices was embedded in paraffin. Paraffin-embedded heart tissue was then cut into 5μm sections, and then stained for Masson's

trichrome as follows. Paraffin-embedded heart tissue was de-paraffinized and rehydrated by washing the tissue section twice with xylene at 5min each, followed by twice 100% ethanol rinses (5min each), followed by 95% ethanol (5min), 70% ethanol (5min), 50% ethanol (5min), 30% ethanol (5min) and finally washed with water. Tissue section was then stained with weigert's iron hematoxylin working solution for 10min (Sigma Aldrich, St. Louis, MO, USA) followed by rinsing in running warm tap water for 10min and washing with water. Next, tissue section was stained with biebrich scarlet-acid fuchsin solutions (Sigma Aldrich, St. Louis, MO, USA) for 15min and washed with water followed by incubation in phosphomolybdic-phophotungstic acid solution (Sigma Aldrich, St. Louis, MO, USA) for 10min. Without rinsing, tissue section was then stained with aniline blue solution (Sigma Aldrich, St. Louis, MO, USA) for 5min, rinsed with water and incubated in 1% acetic acid solution (Sigma Aldrich, St. Louis, MO, USA) for 2 min. Following washing in water, tissue section was dehydrated through 95% ethanol (2min), 100% ethanol (2min) and xylene (2min). Then, tissue sections were mounted with resin mounting medium (Sigma Aldrich, St. Louis, MO, USA). Collagen fibers were stained green and represented the infarcted area whereas viable muscle cells were stained red. For infarct size determination, Masson's trichrome-stained heart cross sections were imaged using a Nikon Eclipse Ti microscope (4x objective; Nikon, Tokyo, Japan) and the whole heart cross sections' image was obtained using NIS-Elements AR 3.2 software (Nikon, Tokyo, Japan). Subsequently, the percentage of the scarred LV wall was determined using the area measurement (calculated by dividing the infarcted area by the total LV area) using a semi-automated software (MIQuant).

2.8 Immunohistochemistry

The second upper-halved formalin-fixed heart slices were then cryoprotected in 20% sucrose at 4°C overnight. The cryoprotected heart was then embedded in OCT (optimal cutting temperature; Sakura Finetek, CA, USA) and stored at -80°C overnight prior to cryosection. OCT-embedded heart tissue was then cut into 10μm sections and subjected to immunohistochemistry with procedures as follows. Tissue sections on the slides were allowed to air-dry inside the fume hood for 15min. PAP pen (LifeTechnologies, Carlsbad, CA, USA) was used to demarcate the area surrounding the tissue sections. Tissue sections were then re-fixed in cold 10% formalin for 15min and then air-dried for another 15min. Subsequently, tissue sections were re-hydrated in 1x Tris Buffered Saline (TBS; 1st Base) for 5min followed by incubation in blocking solution (5% goat serum, 0.5% triton-X 100, 5% bovine serum albumin (BSA) in 1x TBS) for 30min. Following blocking, tissue sections were incubated with antibody against rat endothelial cells (1:50 mouse monoclonal anti-RECA-1; Hycult biotechnology, Uden, The Netherlands) for 2hr at room temperature (r.t). Tissue sections were then washed three times with 1x TBS at 5min each followed by secondary antibody incubation (goat anti mouse Alexa Fluor-594; LifeTechnologies, Carlsbad, CA, USA) for 1hr at r.t. Next, after repeated washing, sections were incubated with anti-actin-α-smooth muscle (SMA) (FITC conjugated, 1:500, mouse monoclonal clone 1A4, Sigma Aldrich, MO, USA) for 1.5hr at r.t. Following three times wash, tissue sections were mounted with prolong gold with DAPI (LifeTechnologies, Carlsbad, CA, USA) to stain the nuclei and kept at 4°C until imaging. Tissue sections were imaged using Nikon Eclipse Ti microscope (Nikon Instruments Inc, Melville, NY, USA) and captured using NIS-Elements AR 3.2 software. Images from 10 random high power fields per LV infarct zone (200x) were taken from four animals per infarcted group per time point. Quantifications of RECA-1 positive and SMA positive

blood vessels were done using ImageJ software (1.42q, National Institutes of Health, Bethesda, MD, USA).

2.9 Plasma H_2S measurement

Plasma H_2S was measured by a high-performance liquid chromatography (HPLC) method using monobromobimane (MBB). Rat plasma samples (15µl) and NaHS standards were derivatized with fluorescent probe MBB (2mM) for 30min at r.t in hypoxic chamber (1% O_2) in the dark to form sulfide-dibimane. Excess MBB was quenched by addition of 2-mercaptoethanol. Mixture was extracted with ethyl acetate. Organic layer was transferred into a fresh 50ml tube, evaporated under nitrogen steam and dissolved in water and methanol mixture (10:90). Derivatized NaHS stock solution was used to prepare a standard curve of NaHS (0.018–1.5µM). HPLC analysis of derivatized rat plasma and NaHS solution was performed on a C18 column using an Agilent 1100 Series HPLC System (Santa Clara, California, USA) with mobile phases comprising of 10% v/v methanol and 0.25% v/v acetic acid and 90% v/v methanol and 0.25% v/v acetic acid. Excitation and emission wavelengths were 385 nm and 475 nm respectively. Retention time of the derivatized H_2S in this system was 24.4 ± 0.01min. Concentration of the H_2S in the rat plasma was measured from linear plots of the HPLC peak areas of sulfide-dibimane versus known concentration of NaHS solution.

2.10 Measurement of tissue H_2S synthesizing enzyme activity

Tissue H_2S synthesizing enzyme activity was determined as follows. Liver tissue from placebo-treated and PAG-treated rats obtained 2 and 7 days after myocardial infarction

(n=6/group/time-point) was homogenized (1:30 v/v) in ice-cold potassium phosphate buffer (100mM, pH 7.4). The assay mixture (500µl) containing tissue homogenate (430µl), L-cysteine (10mM; 20µl), pyridoxal 5'-phosphate (2mM; 20µl) (Sigma Aldrich, MO, USA), and saline solution (30µl) was incubated at 37°C for 30 min in parafilm-sealed microcentrifuge tubes. Next, zinc acetate (1% w/v, 250µl) was added to trap H_2S followed by addition of trichloroacetic acid (10% w/v, 250µl) to halt the reaction. Subsequently, N,N-dimethyl-p-phenylenediamine sulfate (20mM; 133µl) in 7.2M HCl was added followed immediately by $FeCl_3$ (30µM; 133µl) in 1.2M HCl. All standards and samples were assayed in duplicate and absorbance (670 nm) was read using a 96-well microplate reader (Tecan Systems Inc., USA). The concentration of H_2S in each sample was calculated from the standard curve of sodium hydrosulfide (NaHS, 3.125−250µmol/L). Results are presented as nanomoles of H_2S generated per milligram soluble protein. Soluble protein concentration was determined using Bradford assay (BioRad Laboratories, Herculer, CA, USA).

2.11 Plasma neurohormones assays

2.11.1 Plasma renin activity assays

Plasma renin activity assay was done according to an established method. The angiotensinase inhibitors- dimercaprol and 8-hydroxyquinoline and incubation buffer (pH 7.4) were added to the plasma samples and incubated at 37°C for 3hr. Identical control incubation at 4°C was also carried out on each plasma sample. Reaction of renin on its endogenous substrate angiotensinogen produced angiotensin 1 in these samples and the level of angiotensin 1 was measured by radioimmunoassay as follows. Incubated plasma (25µl) or Angiotensin 1 standard, [^{125}I] Angiotensin 1 (50µL) and Angiotensin 1 specific

antiserum (50µl) were incubated for 24hr at 4°C. Bound and free radio labelled Angiotensin 1 was separated by addition of solid phase second antibody method in which 0.5ml of 5% Sac-Cel (Immunodiagnostic Systems, Boldon, UK) plus 5% Dextran (Sigma Aldrich, St. Louis, MO, USA) in assay buffer was added, vortexed, stood at r.t. for 30 min and then centrifuged at 2,000g for 15min at 20°C. Bound labelled Angiotensin 1 was pelleted and counted in a Gammamaster gammacounter (LKB, Uppsala, Sweden). Using the standard curve, the amount of Angiotensin 1 in each sample was calculated and the net amount generated over the 3hr incubation was obtained by subtraction of the endogenous Angiotensin 1 that was measured in the identical control incubations. Plasma renin activity referred to nanomol Angiotensin 1 produced/liter of plasma/hour).

2.11.2 Endothelin assay

Endothelin was firstly iodinated by a Lactoperoxidase method as follows. 7.5µg Endothelin-1 and 25µl 0.4M Sodium Acetate buffer were reacted with 18MBq of $Na^{125}I$ (Amersham – UK), 20µg Lactoperoxidase and 100ng H_2O_2 for 10min followed by addition of another 100 ng H_2O_2 for an additional 10 min incubation. Next, the solution was separated using a gradient of 20-100% acetonitrile in 49mM phosphate buffer pH 2.9 for 40min on a 10cm Brownlee Aquapore RP300 7micron HPLC column. Monoiodinated endothelin was eluted, purified and used as a tracer. For radioimmunoassay, endothelin was extracted from plasma by C18 SepPak cartridges (Waters Associates, Millford, MA, USA), washed with 5mL methanol followed by 5mL of 0.1% trifluroacetic acid (TFA). Endothelin was then eluted from plasma with 2ml of 80% isopropanol in 0.1% TFA, dried at 37°C, and dissolved in assay buffer (0.5ml of 0.1M phosphate buffer (pH 7.4), 0.05M NaCl, 0.1% BSA, 0.1% Triton x-100 and 0.01% NaN_3). Endothelin was assessed

by adding 50µl of standard or plasma samples with 50µl of endothelin antiserum (cat. number RAS6901, Bachem, Torrance, CA, USA). The assay was incubated at 4°C for 22-24hr, followed by addition of 50µl of tracer ^{125}I labelled endothelin (2,000-2,500 cpm) and then incubated at 4°C for another 22-24hr. Bound and free endothelin were separated using a solid phase second antibody method (refer to section 2.11.1). After removal of supernatant, the pellet was then counted in a Gammamaster gammacounter (LKB, Uppsala, Sweden). Using the standard curve, the amount of endothelin in each sample was calculated.

2.11.3 ANP assay

ANP was extracted from plasma by C18 SepPak cartridges (Waters Associates, Millford, MA, USA) similar to endothelin assay, and then subjected to radioimmunoassay as follows. 100µl of radioactively labelled human ANP was allowed to react with 100µl of ANP antibody in the presence of varying amounts of rat ANP-28, standard or plasma extracts. The assay was incubated for 22-24hr at 4ºC. The amount of ANP in the plasma extract was estimated by evaluating the extent of binding of the labelled ANP to the antibody. After incubation, bound and free radiolabelled ANP was separated using a solid phase second antibody method (refer to section 2.11.1) and centrifuged to precipitate the bound radiolabelled ANP. The bound ANP was counted using a Gammamaster gammacounter (LKB, Uppsala, Sweden) to generate dose response curve of radioactivity versus peptide concentration from which the ANP concentration in plasma extracts and controls was determined.

2.11.4 BNP assay

BNP assay was determined with competitive binding assay ratBNP enzyme immunoassay kit (Phoenix Pharmaceuticals, Inc, Burlingame, CA, USA) in accordance to the manufacturer's protocol as follows. Firstly, peptide was extracted from plasma samples using C18 Sep-column and the extracted peptide was dried and reconstituted in 1x assay buffer. The plate used in this kit was pre-coated with secondary antibody and the nonspecific binding sites were blocked. 50µl of extracted peptide from plasma samples, 50µl of standard (0.01ng/ml-100ng/ml), 50µl of positive controls was added to the respective well. Then, 25µl of anti-BNP antibody and 25µl of biotinylated BNP was added to each well and incubated for 2hr at r.t with orbital shaking at 300-400rpm. . At the end of incubation, solution was decanted and plate was washed for 4 times with 1x assay buffer. Subsequently, 100µl of streptavidin-horseradish peroxidase (SA-HRP) was added and incubated for 1hr at r.t with orbital shaking at 300-400rpm. Plate was then washed again for 4 times with 1x assay buffer. 100µl of 3.3'5,5'-tetramethylbenzidinee (TMB) substrate solution was then added and incubated for 1 hour at r.t with orbital shaking 300-400rpm protected from light. Finally, 100µl of 2N HCl was added to the well to halt the reaction. The colour of the solution would change from blue to yellow and the absorbance was read at 450nm. The intensity of the change in color (yellow) generated was directly proportional to the total of biotinylated peptide-SA-HRP complex but inversely proportional to the amount of the peptide in standard solutions or plasma samples. This was due to the competitive binding of the biotinylated peptide with the standard peptide or samples to the BNP antibody. A standard curve of known concentration of standard peptide was established and the unknown concentration in plasma samples was determined by extrapolation to the standard curve.

2.11.5 Aldosterone assay

Aldosterone was measured by direct radioimmunoassay. Aldosterone standard in 100µl of charcoal stripped plasma, or 100µl of plasma sample were mixed with aldosterone antiserum and [^{125}1] aldosterone-3-carboxymethyl oxime in 400µl of assay buffer (citrate 68 mmol/L and phosphate 64 mmol/L, containing 2 g of BSA/L; pH 3.6) and incubated for 24hr at 4°C. The assay was separated by addition of dextran coated charcoal solution followed by centrifugation. Supernatant was then decanted and the charcoal pellet was counted using a Gammamaster gammacounter (LKB, Uppsala, Sweden). Standard curve was generated from the aldosterone standard and the amount of aldosterone in plasma was then calculated from the curve.

2.12 Plasma cGMP measurement

Guanosine 3'5'-cyclic monophosphate (cyclic GMP; cGMP) was measured using the cyclic GMP complete Enzyme-Linked Immunosorbent Assay (ELISA) kit (Enzo Life Sciences Inc., NY, USA) with the acetylated format to increase the sensitivity according to the manufacturer's protocol as described below.

2.12.1 Sample preparation

Plasma samples were directly used for the assay. Standards for plasma samples were diluted in assay buffer 2 to concentrations of 50, 10, 2, 0.4 and 0.08 pmol/ml. All standards and samples were acetylated by adding 10µl of the acetylating reagent for each 200µl of the standard or sample.

2.12.2 Assay Procedure

Neutralizing reagent was added first to each well of goat anti-rabbit antibody-coated plate when measuring cGMP from tissue samples but not for plasma samples. Next, 100µl of standards and samples were added to the appropriate wells followed by 50µl of cGMP conjugate and 50µl of cGMP antibody. Plate was sealed and incubated for 2hr on a plate shaker (500rpm) at r.t. After that, contents of the wells were removed and wells were washed with 400µl of wash buffer repeated for a total of 3 washes. Wash buffer was completely aspirated and 200µl of substrate solution was added to each well. Plate was incubated for 1hr at r.t without shaking. Finally, reaction was stopped by adding 50µl of stop solution and the absorbance readout at 405nm was obtained using Enspire 2300 multilable reader (Perkin Elmer, MA, USA). A standard curve was generated using non-linear logistic regression analysis with 4 parameters (4-PL). The cGMP level was calculated using the cGMP standard curve after subtraction of the background reading (substrate blank). Level of cGMP was expressed as picomole per ml (pmol/ml).

2.13 Plasma nitric oxide measurement

Plasma samples were purified by passing them through a 10kDa molecular weight cut-off centrifugal filter (Merck Millipore, Danstadt, Germany) to remove high molecular weight proteins that may confound the result. Nitric Oxide metabolites were measured using nitric oxide fluorometric assay kit (BioVision Inc., Milpitas, CA, USA) according to the manufacturer's protocol as follows. After filtration, 75µl of sample was combined with 5µl of 1mM enzyme cofactor and 5µl of nitrate reductase. Sample was incubated at r.t. for 4hr to allow 99% conversion of nitrate into nitrite. Then, 5µl of enhancer was added and incubated for 30min at r.t. to quench interfering compounds. 5µl of DAN reagent (2,

3-diaminonaphthalene) was added and incubated for 10min at r.t. to allow reaction with nitrite. Finally, 5µl of NaOH was added and incubated for 10min at r.t to enhance the fluorescent yield. Fluorescent intensity reading at excitation wavelength of 360nm and emission wavelength at 450nm was obtained by Enspire 2300 multilable reader (Perkin Elmer, MA, USA). Standard curve was obtained using nitrate/nitrite standards. Total nitrate/nitrite concentration (µM) was calculated as C = [nitrate+nitrite] (µM) = [(fluorescence – y intercept/slope)/sample volume (µl)] x dilution factor.

2.14 RNA extraction and quality control

2.14.1 Total RNA isolation

Total RNA was isolated using TRIzol (Life Technologies, Carlsbad, CA, USA) method according to the manufacturer's protocol as follows. Firstly, heart tissue from the infarct and peri-infarct area was ground into a fine powder using pestle and mortar under liquid nitrogen to prevent degradation. 1ml of TRIzol (per heart tissue sample) was added and transferred to microcentrifuge tube, resuspended and incubated for 10min at r.t. Resuspended sample was then subjected to phase separation by adding 200µl of chloroform and shaken vigorously for 30sec, followed by 3min incubation at r.t. After incubation, mixed suspension was then subjected to 13,000rpm centrifugation for 15min at 4°C. Three separate layers can be observed after centrifugation. The uppermost aqueous transparent phase was then carefully transferred into new pre-chilled tube. 600µl mixture of phenol acid and chloroform in the 2:1 ratio was then added into the transferred supernatant, vortexed briefly and subjected to centrifugation at 13,000rpm for 5min at 4°C. The resulting uppermost layer was then transferred again to a new tube and 600µl of chloroform was added. Mixture was vortexed briefly twice and centrifuged at 13,000rpm

for 5min at 4°C. The uppermost supernatant was then transferred into a new tube, added with 3U/ µl of DNase I (Life Technologies, Carlsbad, CA, USA) and incubated at 37°C for 20min. Sample was then added with 500µl isopropanol, mixed thoroughly and incubated at -80°C overnight. The next day, mixture was then subjected to centrifugation at 13,000rpm for 10min at 4°C. The resulting white pellet should be visible after centrifugation and supernatant was carefully discarded. RNA pellet was then washed three times with 1ml 75% ethanol and subjected to centrifugation at 13,000rpm for 5min at 4°C. Supernatant was then discarded and pellet was air-dried for 5-10min and resuspended in 30-50µl of RNase free water gently. RNA suspension was then incubated in heatblock for 10min at 55°C. RNA concentration was determined with NanoDrop ND-2000C (Thermo Scientific, Rockford, IL, USA) and the remaining of RNA was stored at -80°C.

2.14.2 Quality control for total RNA

The overall quality of the total RNA preparation was assessed by electrophoresis on denaturing agarose gel and polyacrylamide–urea (PAGE) gel.

2.14.2.1 Agarose gel

Denaturing agarose gel (1%) was prepared by dissolving 0.5g of agarose Life Technologies, Carslbad, CA, USA) in 43.5ml of H_2O in microwave and cooled down to 60°C in water bath. After the flask has cooled down to 60°C, 5ml of 10x MOPS running buffer, 1.5ml 12.3M (37%) formaldehyde and 1µl gel red (Biotium, Inc., CA, USA) were added to the agarose solution inside the fume hood. Mixture was then poured to the gel

cassette and was allowed to set. Sample was prepared by mixing 300ng of total RNA with 2µl of 10x MOPS running buffer, 3.5µl of 12.3M (37%) formaldehyde, 10µl of deionized formamide and 2µl of RNA loading buffer. Sample mixture was incubated at 65°C for 10min and put on ice immediately. Sample was run with constant voltage of 80V for 40min and gel was visualized using GelDoc (BioRad Laboratories, Herculer, CA, USA).

2.14.2.2 PAGE gel

Urea (3.6g) was dissolved with 2.8ml of 40% acrylamide/bis-acrylamide (29:1) solution and 0.75ml of 10x TBE buffer in 60°C water bath. Then 0.95ml H_2O, 37µl of 10% ammonium persulfate (APS) and 7.5µl TEMED was added to the mixture. Solution mixture was poured to the gel cassette and allowed to set for 15min. Casted gel was pre-run at 120V for 15min. Meanwhile, sample was prepared by combining 500ng of total RNA with 10µl deionized formamide, 3µl RNA loading buffer and 2µl 10x TBE buffer. Sample was incubated at 95°C for 5min and kept in ice immediately after heated. Sample was run at 120V for 2 hr. After running, gel was stained for 30min with staining buffer containing 1M NaCL and 15µl gel red for a total volume of 50ml. Gel was visualized using GelDoc (BioRad Laboratories, Hercules, CA, USA).

2.15 mRNA quantitative real-time PCR

A total of 500ng of RNA was used for first strand cDNA synthesis. cDNA was synthesized using the MultiScribe-based high-capacity cDNA archive kit (Applied Biosystems®, LifeTechnologies, Carlsbad, CA, USA). Quantitative real-time polymerase

chain reaction (QPCR) was performed to quantify genes encoding ANP, BNP, APLN, APJ, NPR1, NPR3, VEGF-A, BCL-2, B2M, and Actin according to manufacturer's protocols using TaqMan gene specific primers and TaqMan universal master mix from Applied Biosystems® (LifeTechnologies, Carlsbad, CA, USA). Assay Id for all mRNAs validated were listed in Table 2.1. All QPCR reactions were conducted in triplicates on CFX96 Real Time System (BioRad Laboratories, Hercules, CA, USA). Beta-2 microglobulin (B2M) was used as a normalizer to get the normalized expression for all genes and Actin was used as an inter-plate calibrator.

Table 2.1 Assay Id of TaqMan gene specific primers used for quantitative real-time PCR

Gene	Assay Id
ANP (NPPA)	Rn00561661_m1
BNP (NPPB)	Rn00676450_g1
NPR1	Rn00561678_m1
NPR3	Rn00563495_m1
BCL-2	Rn99999125_m1
VEGF-A	Rn00582935_m1
APLN	Rn00581093_m1
APJ	Rn00580252_s1
B2M	Rn00560865_m1
Actin	Rn00667869_m1

2.16 Protein study

2.16.1 Expression and purification of recombinant rat CSE

The synthetic DNA sequence specifying rat CSE (*Rattus norvegicus*; GenBank Accession No. NP_058770) cloned into the vector, pJexpress404, were obtained from DNA2.0

(Menlo Park, CA, USA). The coding sequence was designed with an N-terminal His_6-tag to facilitate protein purification by immobilized metal affinity chromatography (IMAC) and custom optimized to *E. coli* preferred codons. Authenticity of the synthetic coding fragment was verified by DNA sequencing.

E. coli host strain BL21 (DE3) *trxB* (Novagen, Merck Millipore, Darmstadt, Germany) was used for the expression of recombinant rat CSE. Mini-scale expression studies to determine the solubility of the rat protein were performed by growing the bacterial host containing the recombinant expression vector at 37ºC under ampicillin selection (100µg/ml) in 50ml of LB broth in a shaking flask. Isopropyl-β-D-thiogalactopyranoside (IPTG) was added when the culture reached an OD_{690} of 0.8 to a final concentration of 0.5nM to induce the expression of the recombinant protein. 1ml culture samples were collected just prior to induction, at 2, and at 4hr post-induction for further analysis. The pattern of the recombinant protein accumulation was analyzed by sodium dodecyl sulfate polyacrylamide gel electrophoresis (SDS-PAGE) analysis. Solubility of the fusion proteins was assessed by separating the total proteins into soluble and insoluble fractions as follows. 1ml of culture were pelleted by centrifugation, reconstituted in 300µl BugBuster protein extraction reagent (Novagen) and lysed at r.t by vortexing for 5min. Next, addition of 60µl of 6x SDS dissociation buffer (10.28% w/v SDS, 0.35 mM Tris–HCl pH 6.8, 5% mercaptoethanol, 30% v/v glycerol, and 0.012% bromophenol blue) was carried out and then heated at 95ºC for 10min to solubilize the proteins. Centrifugation was performed to pellet the insoluble protein fraction at 12,000 g for 10min and the supernatant containing the soluble protein fraction was transferred to another tube. The insoluble fraction was washed with buffer (0.1% Na_2HPO_4, 0.8% NaCl, 0.02% KCl, and 0.02% KH_2PO_4 adjusted to a final pH 7.3), collected with centrifugation and reconstituted in 300µl BugBuster (Novagen). Following that, 60µl of 6x SDS dissociation buffer was

added to both fractions, boiled for 10min, separated on a 12% SDS-PAGE gel and stained with coomassie blue. The expression profile was imaged by G:Box (Syngene, Synoptics Ltd, Cambridge, UK) and densitometry analysis of the relative band intensities was analyzed using the Quantity One quantitation software (Bio-Rad).

For large scale purification, the bacterial host harboring the recombinant expression vector was grown at 37ºC under ampicillin selection (100µg/ml) in a shake flask containing 200ml of Terrific Broth (Conda Pronadisa,Spain). When the culture reached an OD_{690} of 0.8, IPTG was added to a final concentration of 0.5 mM to induce the expression of the recombinant protein. The culture was harvested at 4hr post-induction. Cells were pelleted at 5,000g for 10min at 4ºC and lysed in 40ml of BugBuster® (Novagen) at room temperature by vortexing for 5min. The lysate was subjected to centrifugation at 8000g for 20min at 4ºC and supernatant was decanted off. The inclusion body pellet containing rat cystathionine-gamma lyase was washed with phosphate buffer and solubilized overnight at 4ºC in Wash buffer (5mM imidazole, 500mM NaCl, 100mM sodium phosphate, pH 8.0) containing 6M guanidium hydrochloride. Unsolubilized material was removed by centrifugation at 8500 rpm for 20min at 4ºC. The supernatant was clarified through a 0.45µm syringe filter and loaded onto the IMAC cartridge for purification under default program settings of the Denaturing IMAC method on the Profinia Purification System. The protein of interest was eluted with 4ml Elution buffer (250mM imidazole, 500mM NaCl, 100mM sodium phosphate, pH 8.0) containing 6M guanidium hydrochloride. The eluant was placed in a dialysis tubing (MWCO 10kDa) and dialysed overnight at 4ºC against 2L of 100mM sodium phosphate (pH 7.2) and a final dialysis against a further 2L of fresh phosphate buffer for 2hr. The aggregated rat CSE was recovered from the dialysis tubing as a white precipitate and solubilized in 1%SDS. Protein quantitation was performed using the BCA assay as described below

(section 2.16.2) (Pierce, Rockford, IL, USA) and purity was analyzed by SDS-PAGE (16% gel) analysis followed by coomasie blue staining.

2.16.2 Protein isolation and quantitation

Heart tissue from the infarct and per-infarct area obtained from 4-5 rats per group and liver tissue obtained from 3 rats per group were ground into a fine powder using pestle and mortar under liquid nitrogen to prevent degradation. Total protein was extracted by adding 200-300µl lysis buffer (50mM Tris-HCL at pH 7.4, 150mM NaCl, 5mM EDTA, 2% SDS, and 10% glycerol) containing a protease inhibitor and phosphatase inhibitor (Thermo Scientific, Waltham, MA, USA) for 1hr at 4ºC. Samples were then boiled at 100ºC for 10min. The insoluble materials were pelletted at 14,000 rpm for 30 min at 4ºC. Total protein concentration was measured by the bicinchoninic acid (BCA) method (Thermo Scientific, Waltham, MA, USA) according to the manufacturer's protocol. Sample was diluted 20x with the lysis buffer for concentration measurement. Standard curve was generated with BSA as standard. After adding samples and standards to the BCA reagents, reaction was incubated at 37ºC for 30min. Absorbance reading at 562nm was obtained using Enspire 2300 multi-label reader (Perkin Elmer, MA, USA). Concentration of the total protein was measured from linear plots of the samples absorbance reading versus known concentration of BSA solution.

2.16.3 Western blot analysis

Bis-Tris SDS-PAGE was carried out according to the manufacturer's instruction (Life Technologies, Carlsbad, CA, USA). NuPage 10% Bis-Tris pre-casted gels (Life

Technologies, Carlsbad, CA, USA) were used for the experiment. Protein samples (30μg) or 50ng of CSE recombinant protein (used as positive control for CSE analysis) were mixed with an equal volume of SDS-PAGE loading buffer (Life Technologies, Carlsbad, CA, USA) and heated at 70ºC for 10min. Electrophoresis was carried out at 150V for 50min in 1X NuPage MES SDS running buffer (Life Technologies, Carlsbad, CA, USA). polyvinylidene difluoride (PVDF) membrane (BioRad Laboratories, Hercules, CA, USA) was activated in 100% methanol for 2-3min. The SDS-PAGE gel, PVDF membrane, scotchbrite and filter paper were soaked in pre-cooled (4°C) 1X NuPage Transfer buffer (Life Technologies, Carlsbad, CA, USA) for 10 min. They were assembled according to manufacturer's instruction (BioRad Laboratories, Hercules, CA, USA) for electro-transfer at 110V for 2hr in cold room (4°C). At the end of blotting, the PVDF membrane was stained with Ponceau S solution (Sigma Aldrich, St. Louis, MO, USA) to verify the efficiency of protein transfer. The membrane was then blocked with 5% non-fat milk in tris-buffered saline (1st Base) with 0.1% Tween 20 (TBS-T; Biorad) for 1hr at r.t. Subsequently, membrane was probed with the following primary antibodies: CSE, VEGF-A, BCL-2, cGKIα, α-tubulin and β-actin (SantaCruz, Biotechnology, Inc, Dallas, Tx USA) diluted in 5% skim milk in TBS-T and applied overnight at 4ºC. The membrane was subsequently washed 3 times in TBS-T, for 5min each time.

For blot detection, goat anti-rabbit IgG HRP-conjugated or goat anti-mouse IgG HRP-conjugated (Rockland Immunochemicals, PA, USA) at a dilution of 1:1000 in 5% skim milk in TBS-T, was added to the membrane. After 1 hr of incubation at r.t, the membrane was thoroughly washed as described above. Protein bands were visualized using chemiluminesence by adding ECL substrate solution containing luminol in peroxide buffer (Thermo Scientific, Waltham, MA, USA) to the membrane for 5min and then exposed using G:Box (Syngene, Synoptics Ltd, Cambridge, UK). Expression level of

protein of interest was measured by densitometry analysis using ImageJ software (1.42q, National Institutes of Health, Bethesda, MD, USA). Protein expression was quantified by normalizing it against β-actin or α-tubulin levels.

2.17 miRNAs microarray

miRNA profiling was performed on pooled samples of 3 animals per group per time point using LNA™-modified oligonucleotide (Exiqon, Vedbaek, Denmark) probes (Sanger miRBase release v11.0). Total RNA of the pooled samples (1μg) was first 3′-end-labeled with Hy3 dye using the miRCURY LNA™ Power Labeling Kit and hybridized on miRCURY LNA™ Arrays according to the manufacturer's protocol (Exiqon, Vedbaek, Denmark) as follows. Samples were firstly incubated with calf intestinal alkaline phosphatase enzyme (CIP) for 30min at 37° C to remove the 5' phosphates from the microRNA terminals. Reaction was stopped and RNA was denatured by incubation at 95°C followed by snap cooling on ice. Next, a fluorescent label (Hy3™) was attached enzymatically to the 3' end of the microRNAs in the total RNA samples by incubating samples with a fluorescent label for 2hr at 16°C protected from light. The labeling procedure was stopped by incubating reaction for 15min at 65°C and kept at 4°C until hybridization on the array. Hybridization of samples on the array chip was done using MAUI® hybridization system (BioMcro® Systems Inc, Salt Lake City, UT, USA). Labeled samples were denatured for 2min at 95°C after addition of hybridization buffer. The array chip was first pre-washed with wash buffer and primed with hybridization buffer. 50μl of labeled samples were injected to the chip and hybridized for 16hr at 56°C. At the end of the hybridization, chip was washed and scanned using InnoScan700, microarray scanner (Innopsys, Carbonne, France). Microarray data was analyzed using

GeneSpring GX v11 (Agilent Technologies Inc, Santa Clara, CA, USA). Background-subtracted median signal intensity with conditions of at least four groups out of five groups expressing raw value of 300 was selected as a threshold value for inclusion of significantly detected miRNAs followed by normalization using global quantile normalization. Differentially regulated miRNAs (all infarcted groups versus healthy control) with fold change (FC) ≥ 1.1 and ≤ -1.1, at least in one group or more, were considered and subjected to unsupervised hierarchical clustering analysis. Hierarchical clustering plot (heatmap) of miRNAs was generated using Multiple Experiment Viewer v4.9 software with average linkage and Euclidean distance metric as clustering criteria (Dana-Farber Cancer Institute, Boston, MA, USA). Top 13 miRNAs from this list were selected for further validation with miRNAs QPCR.

2.18 miRNAs QPCR

Stem-loop real-time RT-PCR quantification of miRNA expression was performed using TaqMan microRNA assays (Applied Biosystems®, LifeTechnologies, Carlsbad, CA, USA) with specific miRNA primers according to the manufacturer's protocol. A total of 10ng of total RNA was used for reverse transcription reaction and followed by QPCR using TaqMan universal master mix from Applied Biosystems® (LifeTechnologies, Carlsbad, CA, USA). Assay Id for all miRNAs validated were listed in Table 2.2. All QPCR reactions were conducted in triplicates on CFX96 Real Time System (BioRad Laboratories, Hercules, CA, USA). 4.5sRNA was used as a normalizer to get the normalized expression for all genes and miR-16 was used as an inter-plate calibrator.

Table 2.2 Assay Id of TaqMan miRNAs specific primers used for quantitative real-time PCR

Gene	Assay Id
Rno-miR-31	000185
Rno-miR-214	000517
Rno-miR-221	000524
Rno-miR-21	000397
Rno-miR-34a	000426
Rno-miR-30d	000420
Rno-miR-29b	000413
Rno-miR-222	002276
Rno-miR-223	000526
Rno-miR-206	000510
Rno-miR-199a-3p	002304
Rno-miR-193	002250
Rno-miR-195	000494
4.5sRNA(H)	001716
Rno-miR-16	000391

2.19 Statistical analysis

Data are presented as mean ± standard error of mean (SEM). To test for statistical significance between-group comparisons of echocardiographic indexes, hemodynamic parameters and miRNAs expression were performed using a 2-way ANOVA with repeated measures followed by pair-wise comparisons using Bonferroni's post-test. The ANOVA model for echocardiographic indexes included healthy control versus treatment and baseline versus 2 or 7 days after MI as factors, as well as the interaction between the two factors. The ANOVA model for hemodynamic parameters and miRNAs expression included healthy control versus treatment and day 2 versus day 7 as factors, as well as the

interaction between the two factors. For other comparisons, one-way ANOVA followed by the Bonferroni's post hoc test and the unpaired Student's t-test were used when appropriate. Differences were considered significant when $P<0.05$. All statistical analyses were performed using GraphPad Prism® software version 5.04 for Windows (GraphPad Software Inc., San Diego, CA).

3. RESULTS

3.1 Animal survival

To evaluate the effect of GYY on the response to cardiac injury, all rats except the sham group underwent LAD ligation. All the rats from the sham-operated group survived the surgical procedure (n=6/time-point). In total, 12 out of 84 rats that underwent LAD ligation died within 24hr after surgery (treatment group as indicated in **Figure 2.1**): 3 out of 21 MI (14.3%), 3 out of 21 placebo (14.3%), 2 out of 20 GYY (10%) and 4 out of 22 PAG (18.2%). Thus, 9 infarcted rats /group/time-point were subsequently included in this study.

3.2 Effect of GYY on the H_2S system during ischemic injury

To assess the effect of GYY on plasma H_2S level, plasma were collected from rats from each group and assessed through HPLC. Evaluation on plasma H_2S level showed that exogenous application of GYY induced a 2.8 fold increase in plasma H_2S relative to sham rats ($P<0.0001$) at both time points (**Figure 3.1**). Similarly, plasma H_2S level in GYY-treated animals (2265.4 ± 231.5 and 3078.5 ± 417.1nmol/L) were significantly enhanced at both time-points of evaluation compared to untreated MI animals (1234.7 ±86.8 and 1452.0 ± 134.7nmol/L; $P<0.01$ and $P<0.001$), placebo- (1055.9 ± 80.5 and 1704.7 ± 244.8nmol/L; $P<0.001$ and $P<0.01$) and PAG-treated rats (1352.7 ± 144.0 and 1588.8 ± 193.4nmol/L; $P<0.01$ and $P<0.01$) (**Figure 3.1**).

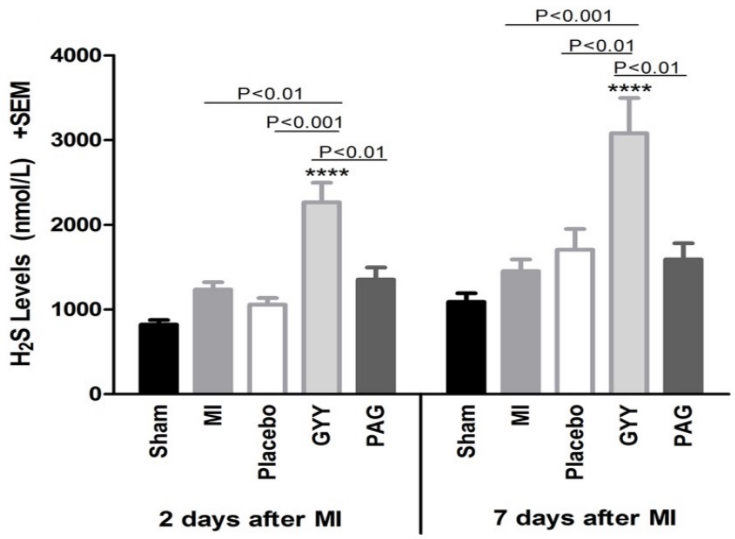

Figure 3.1 Plasma H_2S levels at day 2 and day 7 post-MI. Assessment of plasma H_2S levels by HPLC of healthy sham-operated rats, infarcted untreated rats (MI), placebo-, GYY-, and PAG-treated rats (n=5-6/group; P<0.0001 vs. Sham). Data were presented as mean ± SEM.

We then examined if GYY treatment increased the expression of CSE. Authenticity of the synthetic coding fragment of rat CSE was firstly verified by DNA sequencing (**Figure 3.2A**). A polyhistidine tag to facilitate protein purification by IMAC was incorporated at the N-terminus. Gene expression under the T5 promoter resulted in the production of an expected 44.5 kDa protein of amino acid sequence as shown in **Figure 3.2B**. Rat CSE was highly expressed in bacteria and accumulated rapidly to 34.6% of total bacterial proteins at 2hr post induction as determined by densitometric band quantitation with rolling disk baseline correction set at a rolling disk radius of 50 pixels. No further increase in band intensity was observed at 4hr post-induction (**Figure 3.2B**). Partitioning of total proteins into soluble and insoluble protein fractions showed that rat CSE was produced primarily in the aggregate form. As CSE is abundantly expressed in liver[78, 132], we evaluated CSE protein expression level in liver tissue. We found that CSE

protein expression level was not significantly altered in all groups at both time-points as shown by densitometry analysis and quantification (**Figure 3.2C and D**). While the effect of daily treatment with PAG did not alter plasma H_2S level and CSE protein expression level, its enzyme activity in liver tissue of PAG-treated rats was significantly reduced (**Figure 3.2E**). Homogenates of livers from PAG-treated animals produced 31-fold less H_2S (nmol/mg of soluble protein) at day 2 (0.20 ±0.01) and day 7 post-MI (0.14 ±0.01) compared to placebo-treated animals (5.97±0.37, and 4.38 ±0.31; $P<0.0001$ for both) suggesting that dose of PAG used was efficient to inhibit CSE activity (**Figure 3.2E**). These results demonstrated that GYY treatment increased plasma H_2S level but did not alter CSE expression at protein level.

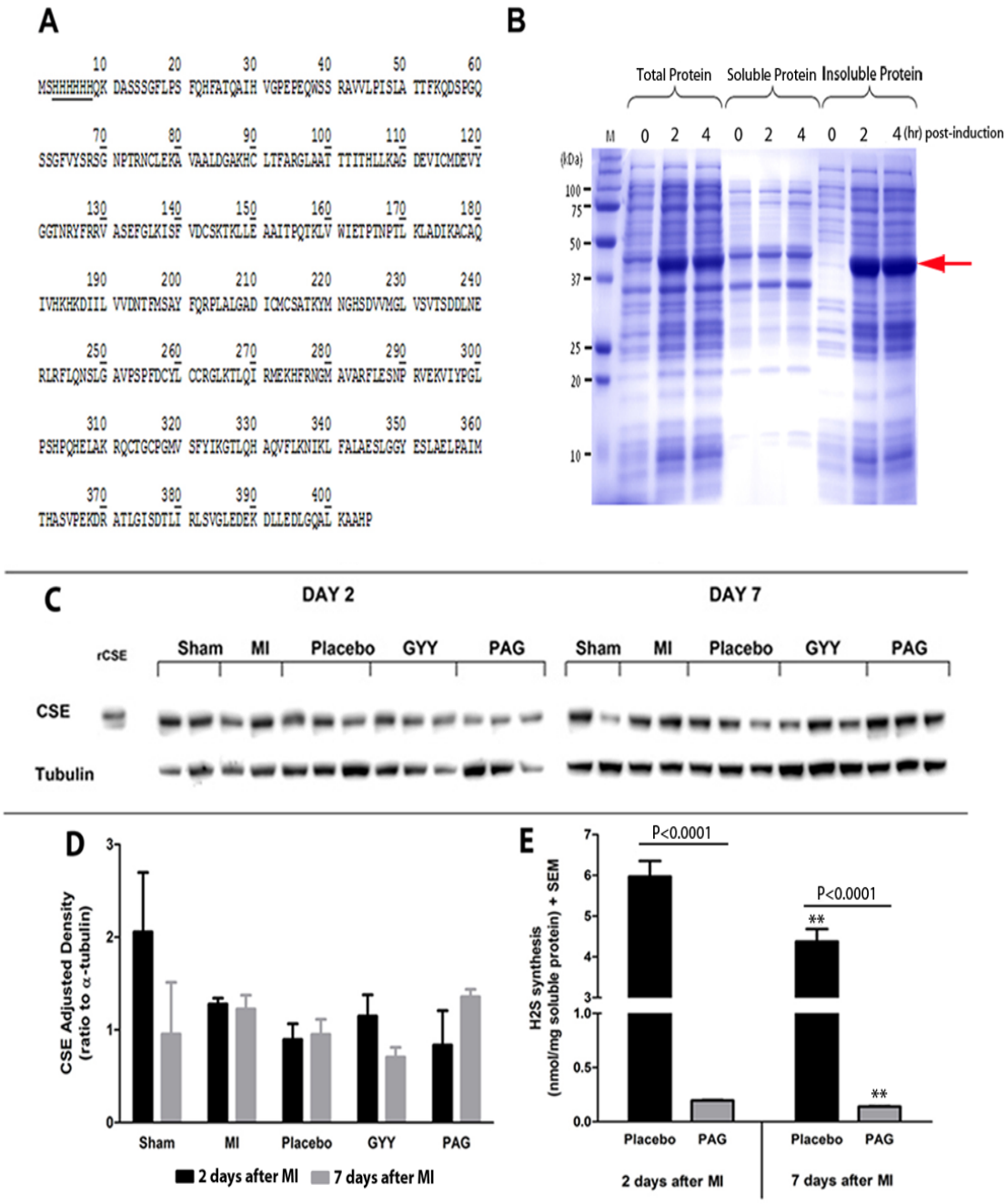

Figure 3.2 Evaluation of GYY treatment on CSE during ischemic injury. (**A**) Amino acid sequence of expressed recombinant rat CSE. Underlined sequence represents position of the polyhistidine tag. (**B**) Expression pattern of rat CSE in *E. coli* strain BL21 (DE3) trxB. Red arrow indicates the expressed CSE at the expected 44.5 kDa position. (M = Precision Plus Protein™ All Blue Standards) (**C**) Representative blot showing the expression of CSE protein in liver tissue (**D**) Densitometry analysis of CSE expression level in liver tissue normalized to α-tubulin (n=2-3) (**E**) Measurement of tissue H_2S-synthesizing enzyme activity in liver tissue at 2 days and 7 days post-MI in placebo- and PAG-treated rats. (n=6/group/time-point; **P<0.01 vs. day 2). Data were presented as mean ± SEM.

3.3 Therapeutic effects of post-ischemic treatment with GYY in the acute and late phases following MI

3.3.1 Post-ischemic treatment of GYY preserved LV function and structure

We evaluated the effect of post-ischemic treatment of GYY with transthoracic echocardiography. We found that, at both time points, GYY treatment led to attenuation of LV remodeling and preservation of cardiac function. At 2 days post-MI, treatment with GYY preserved the cardiac structure as seen from the wall thickness measurement during diastole (**Figure 3.3A**) and systole (**Figure 3.3B**). LV wall thickness in diastole and systole were comparable to baseline and healthy control (sham) whereas during systole, MI-, placebo- and PAG-treated rats displayed significant thinner wall compared to GYY-treated rats ($P<0.0001$, $P<0.001$ and $P<0.01$). Treatment with GYY also prevented early adverse cardiac remodeling as LV internal dimension in diastole (LVIDd) and systole (LVIDs) was comparable to baseline and sham animals, and LVIDs was significantly preserved compared to MI ($P<0.001$), placebo ($P<0.01$) and PAG ($P<0.0001$) group (**Figure 3.3C and D**).

Similar results were observed at 7 days post-MI. LV wall thickness during diastole in GYY-treated rats was still comparable to baseline and sham group (**Figure 3.3E**). Although LV wall thickness in systole (**Figure 3.3F**), LVIDd (**Figure 3.3G**) and LVIDs (**Figure 3.3H**) of GYY-treated rats were statistically significantly different compared to baseline ($P<0.05$, $P<0.01$ and $P<0.001$ respectively), these values were close to those of the sham animals. Moreover, LV wall thickness during systole in GYY-treated rats was still significantly thicker compared to MI ($P<0.01$) and PAG ($P<0.05$) group (**Figure 3.3F**). Similarly, LVIDs was significantly smaller compared to MI- ($P<0.0001$), placebo- ($P<0.0001$) and PAG- ($P<0.0001$) treated rats (**Figure3.3H**). In contrast, the other

infarcted groups exhibited a marked decrease in wall thickness during systole (**Figure 3.3B**) and marked increase in LVIDs (**Figure 3.3D**) when compared to sham group and baseline.

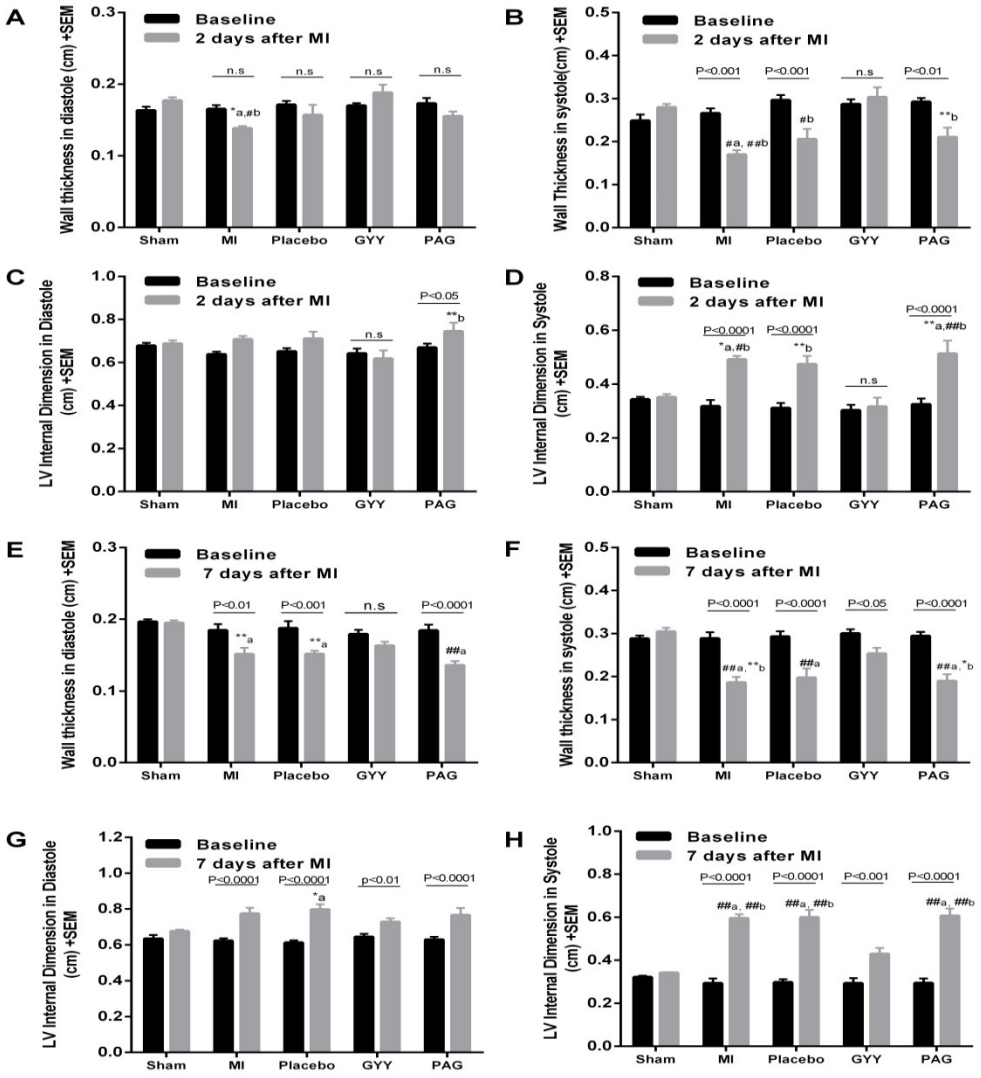

Figure 3.3 Echocardiographic evaluation of LV remodeling. LV wall thickness of healthy sham-operated rats, infarcted untreated rats (MI), placebo-, GYY-, and PAG-treated rats were measured in (**A**) diastole and (**B**) systole 2 days post-MI and (**E-F**) 7 days post-MI. LV internal dimension of the animals were also measured in (**C**) diastole and (**D**) systole 2 days post-MI and (**G-H**) 7 days post-MI. Group-time interaction: n.s, not significant; *a P<0.05 vs. Sham; **a P<0.01 vs. Sham; #a P<0.001 vs. Sham; ##a P<0.0001 vs. Sham; *b P<0.05 vs. GYY; **b P<0.01 vs. GYY; #b P<0.001 vs. GYY; ##b P<0.0001 vs. GYY (n=6 for sham/time point, n=9 for other groups/time point). Data were presented as mean ± SEM.

Cardiac dysfunction was also evaluated based on 4 parameters: (1) left ventricular end-diastolic volume (LVEDV), (2) left ventricular end-systolic volume (LVESV), (3) left ventricular fractional shortening (FS), and (4) left ventricular ejection fraction (EF). Attenuation of cardiac dysfunction in GYY-treated group can be observed at both time-point post-MI. At day 2 post-MI, measurement readouts for LVEDV (**Figure 3.4A**), LVESV (**Figure 3.4B**), FS (**Figure 3.4C**) and EF (**Figure 3.4D**) in GYY-treated rats were comparable to sham group and to the baseline reading. In addition, LVESV, a cardinal post-MI predictor of adverse remodeling and increased risk of adverse clinical outcomes[133], was significantly preserved in GYY-treated group (0.079±0.016ml) when compared to MI ($P<0.01$), placebo ($P<0.001$) and PAG ($P<0.0001$) group (**Figure 3.4B**). Moreover, FS (48.82±4.19%; **Figure 3.4C**) and EF (83.54±2.40%; **Figure 3.4D**) at day 2 post-MI were significantly preserved compared to MI ($P<0.001$ and $P<0.0001$ respectively), placebo ($P<0.01$ and $P<0.001$) and PAG ($P<0.001$ and $P<0.0001$) group.

At day 7 post-MI, measurement of LVEDV in GYY-treated rats was not statistically significant compared to baseline and sham rats while other infarcted groups had significantly elevated LVEDV relative to baseline (**Figure 3.4E**). Importantly, LVESV was significantly preserved in GYY-treated group (0.136±0.022ml) when compared to MI ($P<0.001$), placebo ($P<0.0001$) and PAG ($P<0.0001$) group (**Figure 3.F**). Furthermore, the decrease in FS (41.13±3.08%; **Figure 3.4G**) and EF (75.70±2.22%; **Figure 3.4H**) in GYY-treated rats, when compared to its baseline readings (54.94±2.97%; $P<0.001$ and 88.50±1.11%; $P<0.05$), were markedly ameliorated, contrasting the severe decrease observed in FS and EF ($P<0.0001$, respectively) in the other infarcted groups.

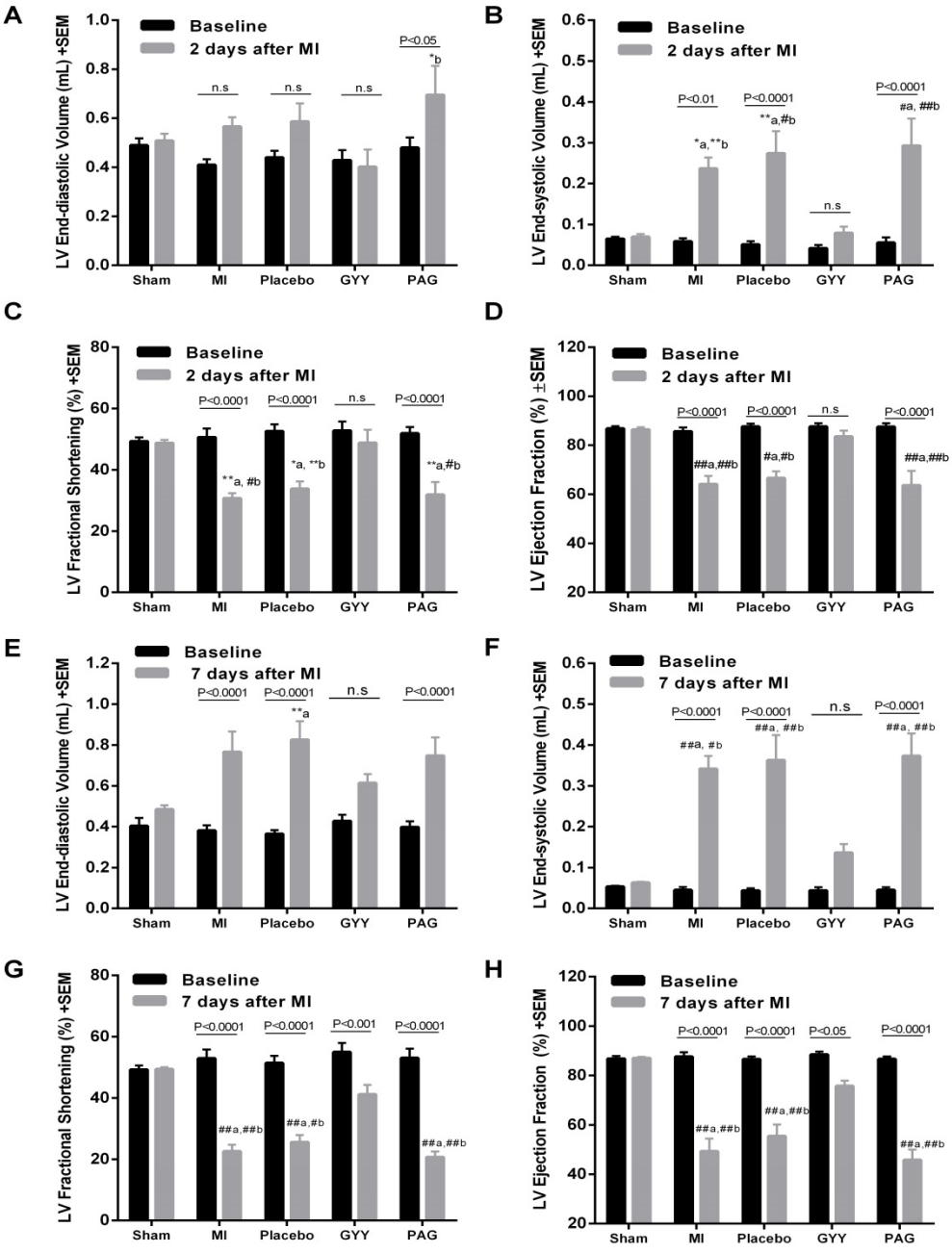

Figure 3.4 Echocardiographic evaluation of LV function. (**A**) LV end-diastolic volume and (**B**) LV end-systolic volume of healthy sham-operated rats, infarcted untreated rats (MI), placebo-treated, GYY-treated and PAG-treated rats were evaluated 2 days post-MI and (**E-F**) 7 days post-MI. (**C**) LV fractional shortening and (**D**) ejection fraction were also evaluated 2 days post-MI and (**G-H**) 7 days post-MI. Group-time interaction: n.s, not significant; *a P<0.05 vs. Sham; **a P<0.01 vs. Sham; #a P<0.001 vs. Sham; ##a P<0.0001 vs. Sham; *b P<0.05 vs. GYY; **b P<0.01 vs. GYY; #b P<0.001 vs. GYY; ##b P<0.0001 vs. GYY (n=6 for sham/time point, n=9 for other groups/time point**).** Data were presented as mean ± SEM.

Additionally, we also performed hemodynamic analyses to further confirm the effect of GYY treatment. As seen in **Table 3.1**, hemodynamic analyses revealed that preservation of cardiac function in GYY-treated rats was paralleled by conservation of LV end-diastolic pressure (LVEDP) at both-time points (3.38 ± 0.37 mmHg and 3.58 ± 0.39mmHg) and that these values were comparable to that of sham group (2.06 ±0.34 mmHg and 2.82 ± 0.15 mmHg). In contrast, all other infarcted groups had significantly higher LVEDP than sham group (in mmHg): MI rats (4.62 ± 0.65 and 4.86 ± 0.27, $P<0.05$, for days 2 and 7 respectively), placebo- (4.46 ± 0.32; $P<0.05$, and 5.26 ± 0.61; $P<0.01$), and PAG-treated (4.94 ± 0.63; $P<0.001$, and 4.92 ± 0.37; $P<0.05$) (**Table 3.1**). GYY also preserved cardiac output as demonstrated with readout values that were comparable to sham animals at both time-points. Notably, cardiac output in GYY group at 2 days post-MI were also significantly higher compared to all infarcted groups ($P<0.05$ respectively) (**Table 3.1**). There was no significant difference in the stroke volume of GYY-treated rats compared to that of sham animals at both time-points, but the stroke volume of other infarcted groups was significantly lower when compared to sham animals ($P<0.05$) at day 7 post-MI. There was no significant change in other hemodynamic parameters across all groups at both time-points (**Table 3.1**). Collectively, these results demonstrated that GYY attenuated LV remodeling and preserved cardiac function 2 days and 7 days post-MI.

Table 3.1 Hemodynamic parameters in healthy sham-operated rats, infarcted untreated rats (MI), infarcted placebo-, GYY-, and PAG- treated rats, 2 and 7 days after myocardial injury.*

Groups	Sham n= 6	MI n=8-9	Placebo n= 8-9	GYY n= 8-9	PAG n= 9
LVEDP (mmHg)					
2 days post-MI	2.06±0.34	4.62±0.65 *[a]	4.46±0.32 *[a]	3.38±0.37	4.94±0.63 **[a]
7 days post-MI	2.82±0.15	4.86±0.27 *[a]	5.26±0.61 **[a]	3.58±0.39	4.92±0.37 *[a]
Mean Pressure (mmHg)					
2 days post-MI	27.10±2.19	23.76±0.96	26.16±1.27	25.32±1.67	29.18±1.65
7 days post-MI	26.27±3.40	29.21±1.43	29.42±1.33	25.29±1.35	29.52±1.66
Systolic Duration (s)					
2 days post-MI	0.10±0.003	0.10±0.003	0.10±0.003	0.10±0.004	0.09±0.002
7 days post-MI	0.09±0.004	0.10±0.003	0.10±0.003	0.09±0.002	0.10±0.003
Diastolic Duration (s)					
2 days post-MI	0.09±0.01	0.11±0.005	0.10±0.01	0.10±0.004	0.10±0.004
7 days post-MI	0.11±0.005	0.11±0.01	0.11±0.005	0.10±0.005	0.10±0.01
Cycle Duration (s)					
2 days post-MI	0.19±0.01	0.21±0.01	0.20±0.01	0.20±0.01	0.20±0.01
7 days post-MI	0.20±0.01	0.21±0.01	0.20±0.01	0.19±0.01	0.20±0.01
Heart Rate (BPM)					
2 days post-MI	323.52±19.57	292.04±9.03	303.80±10.56	305.37±9.86	308.18±8.23
7 days post-MI	303.93±8.30	300.23±12.21	296.49±10.21	319.44±9.00	303.84±12.66
Max dP/dt (mmHg/s)					
2 days post-MI	3025.69±426.61	2669.92±246.37	2937.20±226.25	2789.54±220.28	3642.22±260.62
7 days post-MI	3777.48±539.87	3434.60±348.65	3590.00±264.07	3077.21±215.94	3535.51±284.44
Contractility Index (1/s)					
2 days post-MI	100.68±4.31	93.28±3.80	98.75±2.15	95.10±2.34	102.59±2.50
7 days post-MI	108.25±3.97	97.96±3.33	99.92±3.36	101.33±3.01	103.81±2.97
Min dP/dt (mmHg/s)					
2 days post-MI	-2226.92±347.74	-1854.88±171.62	-2159.77±175.48	-1999.00±208.22	-2437.31±204.06
7 days post-MI	-2818.28±474.04	-2489.29±296.19	-2549.04±229.01	-2174.41±138.82	-2539.06±244.10
Tau (ms)					
2 days post-MI	15.43±1.31	20.46±1.19	18.14±1.07	19.44±1.35	17.73±1.00
7 days post-MI	15.66±1.93	18.04±1.59	19.01±2.76	17.03±1.05	14.36±2.19
Cardiac Output (mL/min)					
2 days post-MI	51.38±2.20	44.37±3.18 *[b]	44.37±2.67 *[b]	57.19±3.35	44.38±4.70 *[b]
7 days post-MI	66.08±4.73	48.43±3.14 *[a]	48.25±4.03 *[a]	60.29±3.27	46.75±4.21 **[a]
Stroke volume (mL/beat)					
2 days post-MI	0.16±0.01	0.15±0.01	0.15±0.01	0.19±0.01	0.15±0.02
7 days post-MI	0.22±0.02	0.16±0.01 *[a]	0.16±0.01 *[a]	0.19±0.01	0.16±0.01 *[a]

**LVEDP, left ventricular end-diastolic pressure; BPM, beats per minute; s, seconds; ms, milliseconds.* Data were presented as mean ± SEM. Group-time interaction statistical significance indicated as follows: *a P<0.05 vs. Sham; **a P<0.01 vs. Sham; *b P<0.05 vs. GYY.

3.3.2 Post-ischemic treatment of GYY reduced LV fibrosis

Fibrosis has been shown to play a critical role in LV remodeling and LV dysfunction post-MI[134]. In order to investigate the effect of post-ischemic treatment of GYY on LV fibrosis, morphometric studies on heart tissue were performed. As seen in **Figure 3.5A and B**, GYY treatment preserved LV dimensions comparable to sham at day 2 and day 7 post-MI. In addition, GYY-treated rats displayed significantly smaller LV cross-sectional area containing fibrosis (as indicated by area stained green) at day 2 (**Figure 3.5A**) and day 7 (**Figure 3.5B**) post-MI. Quantification of the fibrotic area confirmed that GYY treatment resulted in significantly lower percentage of fibrosis (8.0 ±1.4% and 15.3 ± 3.4%) compared to MI (38.1 ±5.4%; $P<0.01$ and 36.9 ±4.6%; $P<0.05$), placebo (39.4 ± 6.5%; $P<0.01$ and 36.7 ± 8.0%; $P<0.05$) and PAG (39.6 ±5.4%; $P<0.01$ and 39.3 ±2.4%; $P<0.01$) group (**Figure 3.5C**). Therefore, in agreement with the results of the echocardiographic data, treatment with GYY attenuated adverse LV remodeling and preserved LV dimensions 2 and 7 days after MI.

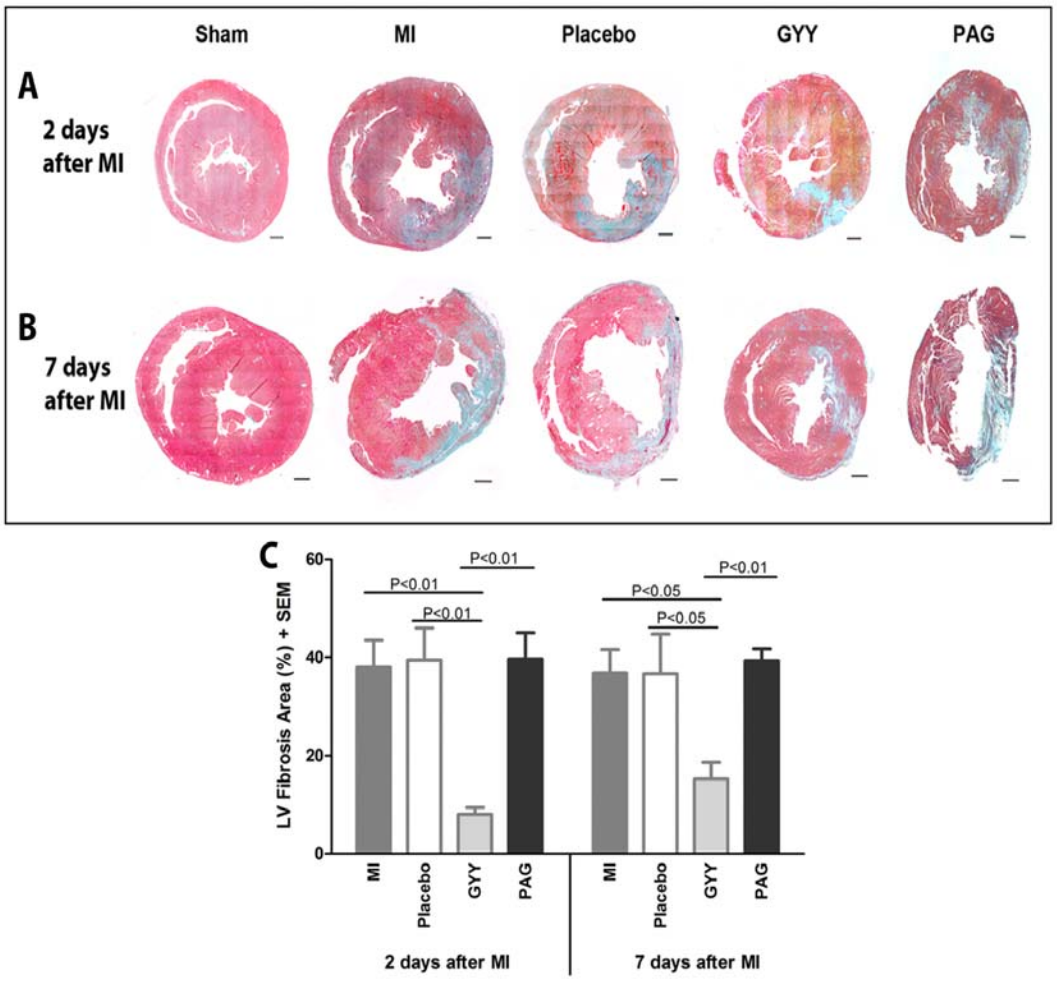

Figure 3.5 Morphometric evaluations of explanted hearts after treatment. Representative mid-ventricular cross-section of Masson's trichrome-stained sections (40x) of infarcted untreated rats (MI), infarcted placebo-, GYY-, and PAG- treated rats, (**A**) 2 days and (**B**) 7 days after MI showing more conserved LV dimensions and less collagen deposition in GYY-treated rats. Scale bars, 1,000μm. (**C**) Measurement of the percentage of LV area containing fibrosis at both time-points (n=7-8/group). Data were presented as mean ± SEM.

3.3.3 Post-ischemic treatment of GYY enhanced vascularization in the infarct area

Angiogenesis is necessary for cardiac repair following cardiac injury[27]. Thus, the effect of GYY on vascular density was assessed by performing immunofluorescence staining against rat endothelial cell antigen-1 (RECA-1) and α-smooth muscle actin (SMA) on LV scar region of infarcted hearts in all treatment groups (**Figure 3.6**). RECA-1-positive ($RECA\text{-}1^+$) vessels were stained in red and SMA-positive (SMA^+) vessels were stained in green, whereas nuclei were stained in blue. Disruption of blood vessels or reduction in $RECA\text{-}1^+$ and SMA^+ vessels, at both evaluation time-point, could be observed in infarcted MI group (**Figure 3.6A** and **B**), placebo-treated group (**Figure 3.6C and D**) and PAG-treated group (**Figure 3.6G** and **H**). In contrast, GYY treatment seemed to promote angiogenesis as indicated by a marked increase in the number of $RECA\text{-}1^+$ vessels at day 2 (**Figure 3.6E**) and day 7 (**Figure 3.6F**) post-MI. The number of blood vessels was then quantified by counting $RECA\text{-}1^+$ and SMA^+ vessels in the LV scar area per 200x field. Based on the quantification presented in **Figure 3.6I,** more of $RECA\text{-}1^+$ blood vessels were seen in GYY-treated hearts at day 2 (118.06 ±11.98) and 7 post-MI (110.42 ±14.81) compared to MI-treated (45.72 ±3.21 and 37.51 ±11.58; $P<0.01$ respectively), placebo-treated (41.08 ± 11.69; $P<0.001$ and 36.74 ± 6.73; $P<0.01$) and PAG-treated groups (42.07 ±10.03 $P<0.001$ and 37.77 ±6.57; $P<0.01$). Likewise, SMA^+ blood vessels were more abundantly observed within the scar area of rats treated with GYY compared to PAG-treated rats, 2 days after infarct ($P<0.05$) and when compared to all the other infarcted groups at day 7 post-MI ($P<0.001$ for all comparisons) (**Figure 3.6J**). These results showed that GYY treatment promoted angiogenesis within the LV scar area.

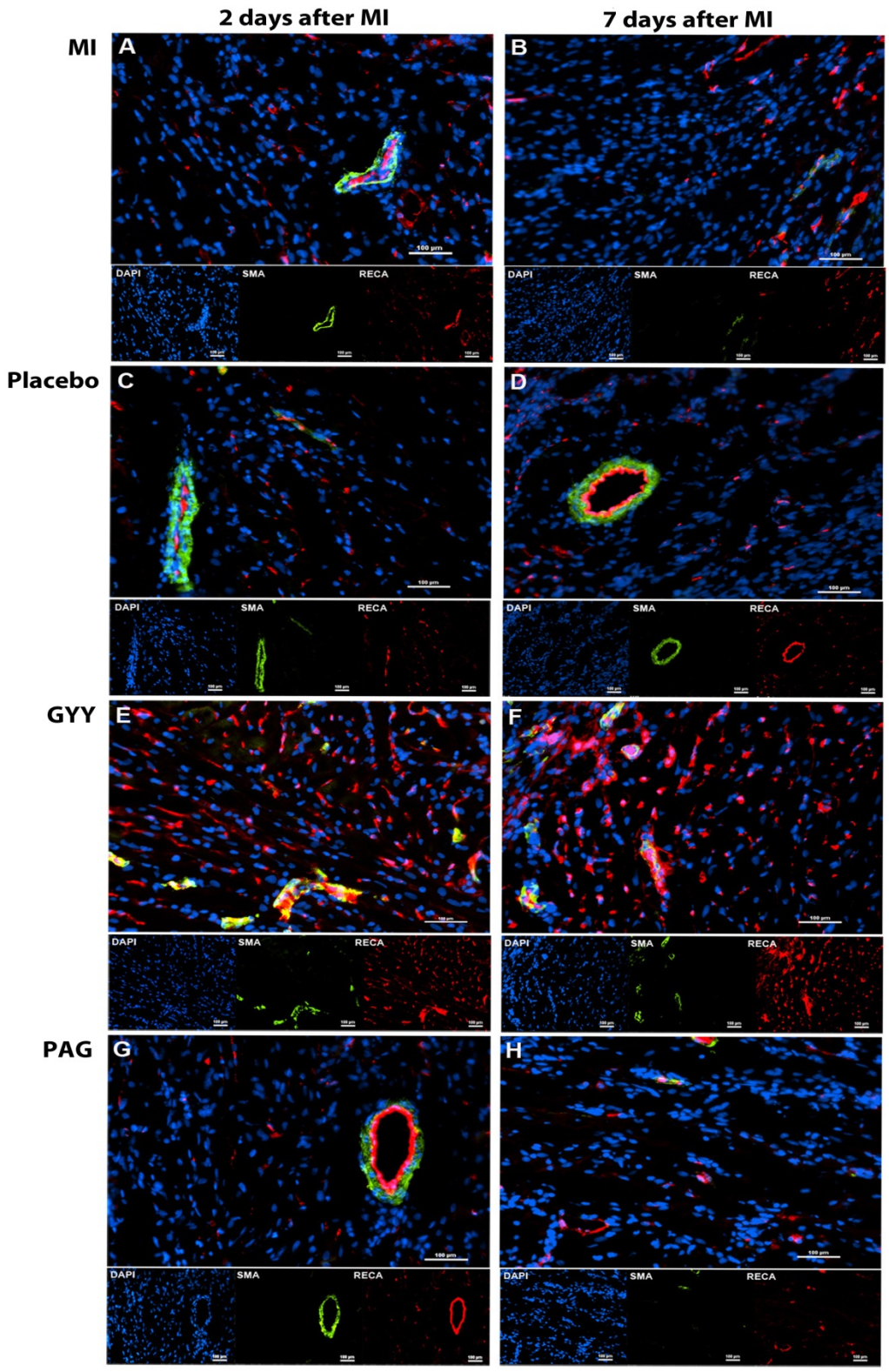

Figure 3.6 Evaluation of vascularization in the infarct area post-MI. Figure to continue on the next page.

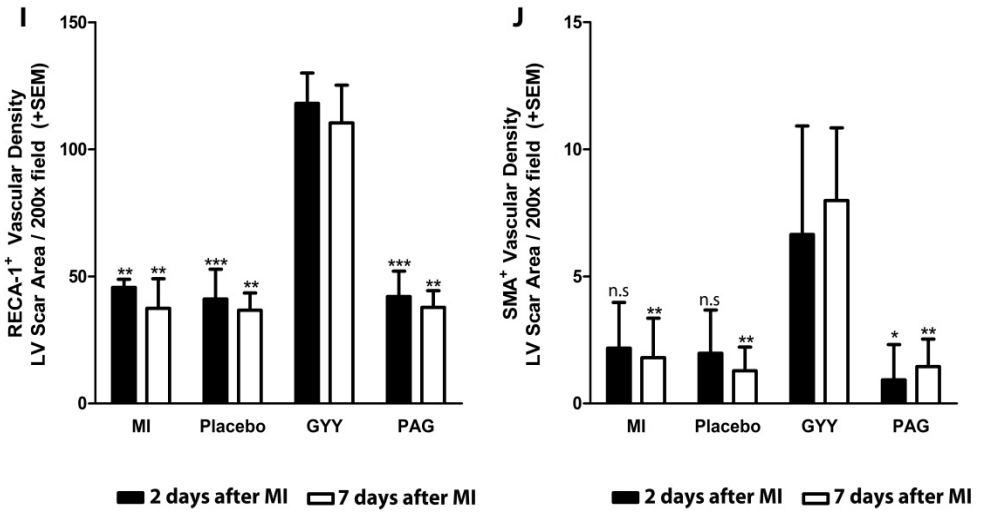

Figure 3.6 Evaluation on vascularization in the infarct area post-MI. Representative micrographs of the LV scar area stained with rat endothelial cell antigen-1 (RECA-1$^+$; red) and α-smooth muscle actin (SMA$^+$; green) and DAPI (nucleus; blue) to visualize blood vessels in (**A, B**) infarcted untreated rat hearts (MI), and in treated rats with (**C, D**) placebo, (**E, F**) GYY, and (**G, H**) PAG, at days 2 and 7 after MI as indicated; (200x; n=3-4/group/time-point). Individual immunofluorescence staining can be observed underneath the merged image. Scale bar indicates 100μm. (**I**) Quantification of RECA-1$^+$ blood vessels density among groups at day 2 and 7 post-infarct (**P<0.01 vs. GYY and ***P<0.001 vs. GYY to each respective time-point). (**J**) Quantification of SMA$^+$ blood vessels density among groups at day 2 and 7 post-infarct (*P<0.05 vs. GYY and **P<0.01 vs. GYY to each respective time-point; n.s, not significant). Data were presented as mean ± SEM.

3.5 Effect of GYY treatment on neurohormonal activation in the acute and late phases following MI

3.4.1 Post-ischemic treatment of GYY increased plasma ANP and BNP levels

In order to investigate whether GYY treatment has effect on neurohormonal activation, plasma samples from each group were evaluated for their ANP and BNP levels. A trend towards increased plasma ANP level in GYY-treated animals could be observed at day 2 post-MI (**Figure 3.7A**). The elevated level of ANP in GYY-treated groups was significantly maintained at day 7 (271.4 ± 66pmol/L) compared to reduced level observed

in sham (81.1 ± 12.4pmol/L), MI (97.2 ± 27.2pmol/L), placebo (88.1 ± 32.9pmol/L) and PAG group (75.33 ± 9.7pmol/L) (P<0.05, respectively) (**Figure 3.7A**). Plasma BNP level was initially comparable among groups at day 2 post-injury but at day 7, BNP level was significantly higher in GYY-treated rats when compared to sham (105.3 ± 9.3pg/mL vs. 59.3 ±3.0pg/mL, P<0.01), as well as to MI (67.7 ± 5.4pg/mL, P<0.01) and PAG-treated animals (64.7 ± 6.7 P<0.01) (**Figure 3.7B**). These results demonstrated that GYY enhanced ANP and BNP levels at the late phase following MI.

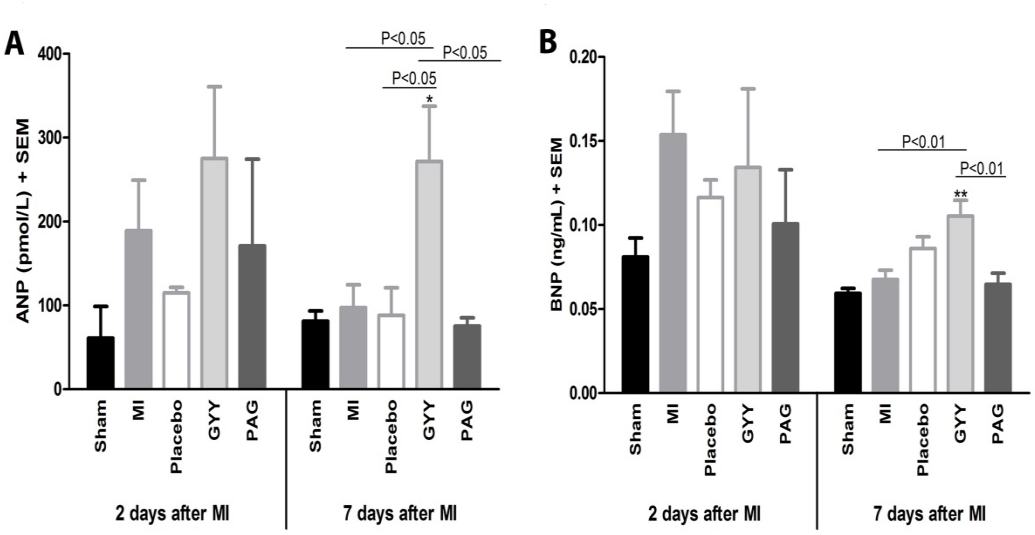

Figure 3.7 Assessment on plasma cardiac NPs levels. Plasma (**A**) ANP and (**B**) BNP levels were evaluated in healthy sham-operated rats, infarcted untreated rats (MI), infarcted placebo-, GYY-, and PAG- treated rats, 2 and 7 days after MI (*P<0.05 vs. sham and **P<0.01 vs. sham; n=3/group/time-point). Data were presented as mean ± SEM.

3.4.2 Post-ischemic treatment of GYY affected cardiac NPs and their receptors at mRNA level

To evaluate whether treatment of GYY has any effect on NPs and NPs receptors at mRNA level, we performed QPCR on heart tissue collected from infarct and peri-infarct area. At day 2 post-MI, mRNA expression of cardiac ANP (*NPPA* mRNA) was

significantly elevated in GYY-treated rats compared to all other animal groups (**Figure 3.8A**). Expression of *NPPA* was increased by 10 fold in GYY-treated rats (10.4 ± 1.9) relative to sham animals ($P<0.001$), and 2-fold relative to the other infarcted groups (i.e. MI, placebo- and PAG-treated, $P<0.05$ respectively; **Figure 3.8A**). At day 7, *NPPA* expression level of GYY-treated animals was not statistically significant when compared to sham group; while in the other infarcted groups, *NPPA* level remained significantly elevated relative to sham group (**Figure 3.8B**). In contrast, there were no significant differences in BNP mRNA levels (*NPPB*) in heart tissue between sham and all the infarcted groups at both time-points (**Figure 3.8C and D**). mRNA expression level of *NPR1*, the guanylyl-cyclase receptor for ANP and BNP, was initially similar among all groups at day 2 post-MI (**Figure 3.8E**), but was found to be down-regulated in MI rats compared to sham ($P<0.01$), GYY- ($P<0.05$) and PAG- treated animals ($P<0.05$) at day 7 post-MI (**Figure 3.8F**). *NPR3* (clearance receptor for NPs) mRNA expression level was overall down-regulated in all infarcted groups relative to sham group at both time-points (**Figure 3.8G and H**). However, it was noted that cardiac *NPR3* expression in GYY-treated animals was less repressed than in the other infarcted groups, and was significantly higher than in PAG-treated rats at day 2 after injury ($P<0.05$; **Figure 3.8G**). These results demonstrated that treatment of GYY influenced mRNA expression level of ANP and NPs clearance receptor.

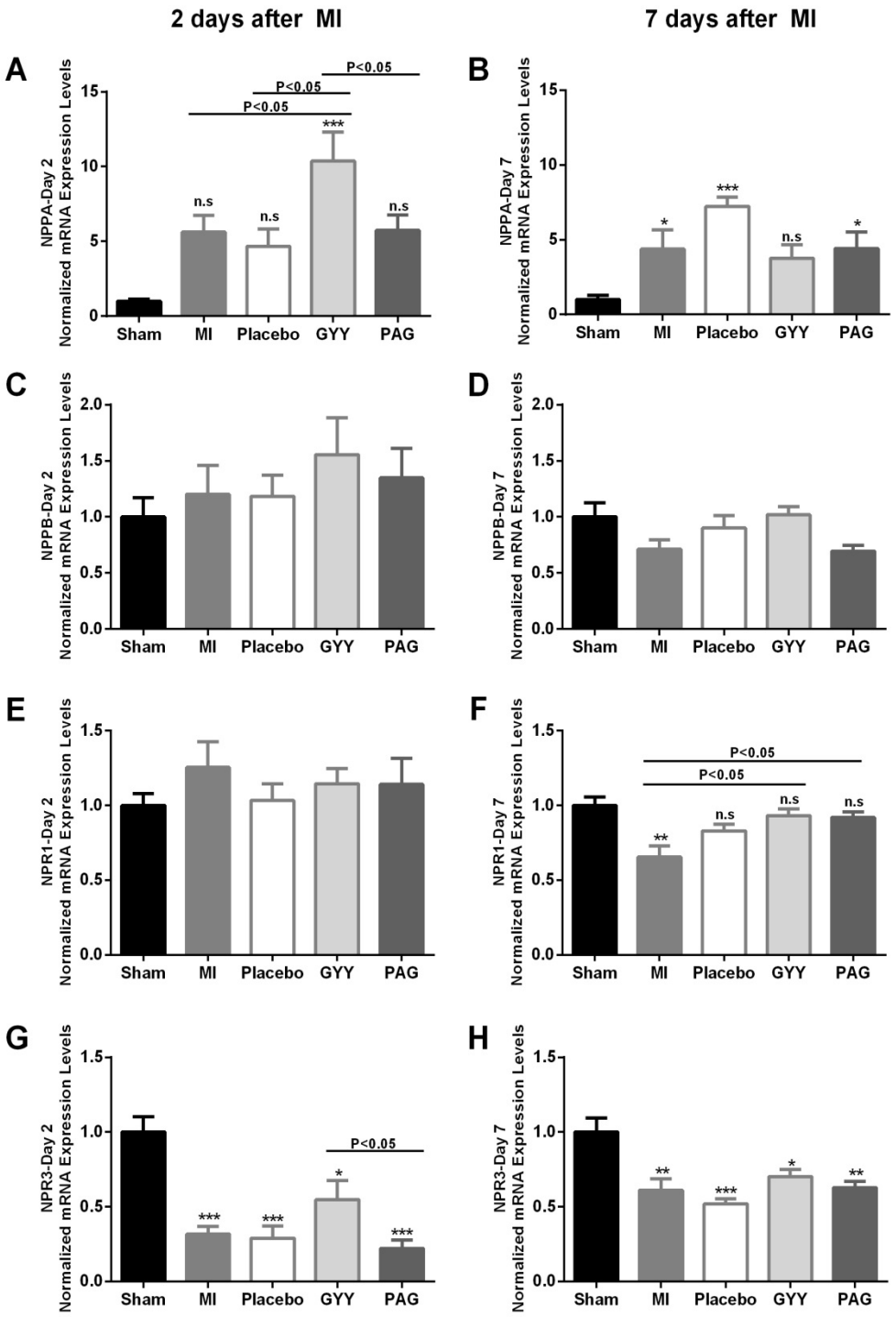

Figure 3.8 Evaluation of mRNA level of NPs and their receptors. Expression of *NPPA*, *NPPB*, *NPR1*, *NPR3* mRNA level at (**A, C, E, G**) day 2 post-MI and (**B, D, F, H**) day 7 post-MI in healthy sham-operated rats, infarcted untreated rats (MI), infarcted placebo-, GYY-, and PAG- treated rats (n=6/group/time point). n.s, not significant; *P<0.05; **P<0.01; ***P<0.001; ****P<0.0001 vs. sham. Data were presented as mean ± SEM.

3.4.3 Effect of GYY treatment on other neurohormones

To evaluate whether GYY treatment influences other neurohormones, their levels in the plasma were measured. There was no difference in plasma aldosterone level in GYY-treated rats compared to sham, MI and placebo group at both time-points (**Figure 3.9A**), although it was noted that plasma aldosterone level in PAG-treated rats was significantly lower compared to sham and GYY-treated rats ($P<0.01$ respectively), as well as to MI and placebo rats ($P<0.05$ respectively) at day 2 post-MI (**Figure 3.9A)**. Plasma endothelin level (**Figure 3.9B**) and plasma renin activity (PRA; **Figure 3.9C**) remained unaltered among the groups at both time-points. These results showed that GYY treatment had no effect on plasma aldosterone, endothelin and PRA.

Apelin, an endogenous ligand for the Ang 2 receptor-like 1 (APJ), has been reported to exert cardioprotective effect in acute MI[135]. As such, we evaluated the effect of GYY treatment on apelin expression. Cardiac apelin mRNA level was found to be up-regulated in GYY-treated rats compared to PAG at day 2 post-injury ($P<0.05$) (**Figure 3.9D**). At day 7 post-MI, GYY-treated rats displayed apelin mRNA level that was significantly elevated compared to untreated infarcted (MI) animals ($P<0.001$), as well as in placebo- ($P<0.05$) and PAG-treated animals ($P<0.0001$), although not statistically significant when compared to sham animals. Whereas, PAG-treated animals demonstrated down-regulation of apelin mRNA relative to sham ($p<0.05$) at day 7 post-MI (**Figure 3.9D**). Likewise, as seen in **Figure 3.9E**, there was an overall down-regulation of *APJ* mRNA, as an effect of infarction, at day 2 in MI-, placebo-, and PAG-treated group. However, importantly, GYY treatment prevented this down-regulation as observed from a similar *APJ* mRNA level to the sham group. This resulted in a significant difference when compared to that of PAG treatment ($P<0.05$). At day 7, *APJ* mRNA level was maintained

in GYY group while it remained down-regulated in PAG-treated animals relative to both sham and GYY-treated rats (P<0.05 and P<0.01; **Figure 3.9E**).

Collectively, these results demonstrated that GYY increased apelin expression while preventing down-regulation of its receptor, APJ. This is important as apelin is involved in cardioprotection.

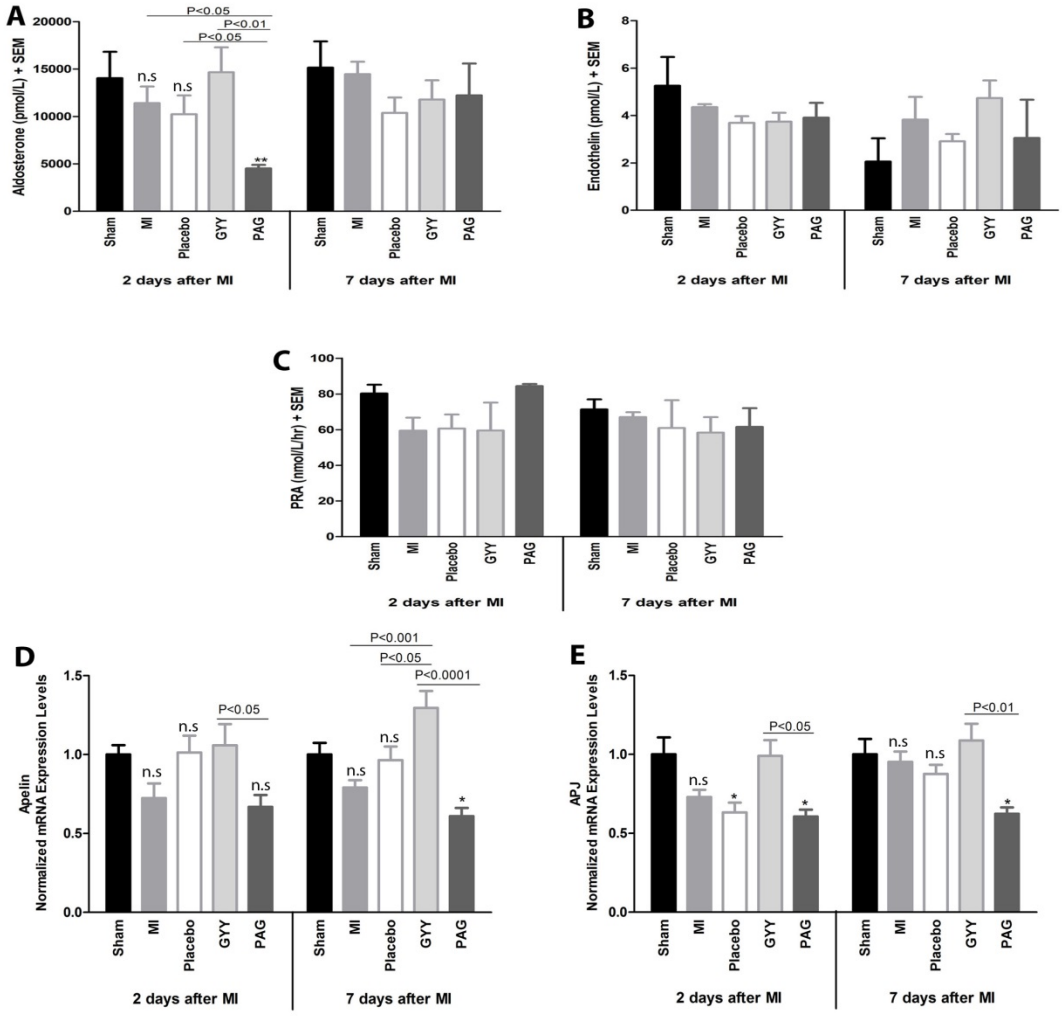

Figure 3.9 Effect of GYY treatment on other neurohormones. Plasma (**A**) aldosterone, (**B**) endothelin and (**C**) plasma renin activity (PRA) levels in sham, infarcted untreated (MI) rats, placebo-, GYY-, and PAG-treated rats were analyzed at day 2 and 7 following myocardial infarction (n=3/group). Cardiac mRNA levels for (**D**) apelin and (**E**) APJ for the above-mentioned groups were also evaluated 2 and 7 days post-injury (n=6/group). *P<0.05 vs. sham; **P<0.01 vs. sham; n.s, not significant. Data were presented as mean ± SEM.

3.5 Post-ischemic treatment of GYY increased plasma cGMP and NO levels in the late post-MI period

cGMP is the intracellular second messenger of ANP and BNP upon binding to NPR1[94]. As such, we examined the downstream effect from the increased ANP and BNP. In agreement to the previously observed elevation of plasma ANP and BNP level in GYY-treated animals at day 7 post-MI, plasma cGMP was also found to be significantly elevated at this time-point in animals treated with GYY (6.15 ± 1.84 pmol/mL) when compared to sham rats (1.33 ± 0.30 pmol/mL), MI- (1.37 ± 0.25 pmol/mL), placebo- (1.76 ± 0.41 pmol/mL) and PAG-treated rats (1.86 ± 0.27 pmol/mL; $P<0.05$, respectively) (**Figure 3.10A**). It has been known that cGMP is also generated by the activation of soluble guanylate cyclase by nitric oxide (NO)[95]. Thus, NO metabolites (i.e. nitrite (NO^{2-}) and nitrate (NO^{3-})) levels in plasma were investigated. Plasma NO level in GYY-treated rats was notably increased compared to sham animals at day 7 post-injury ($P<0.05$) (**Figure 3.10B**). In addition, protein expression level of cGKIα, one of the downstream effectors of cGMP[95], in the heart tissue was determined through immunoblotting. Interestingly, it was observed that in GYY-treated animals, cGKIα protein was significantly increased compared to sham animals ($P<0.01$), at day 2 post-MI as seen in **Figure 3.10C** and its quantification in **Figure 3.10D**, while protein expression of cGKIα remained unchanged among all groups at day 7 post-MI. These results demonstrated that GYY treatment induced increases in plasma NO together with the increases in plasma ANP and BNP, contributed to the activation of the cGMP pathway.

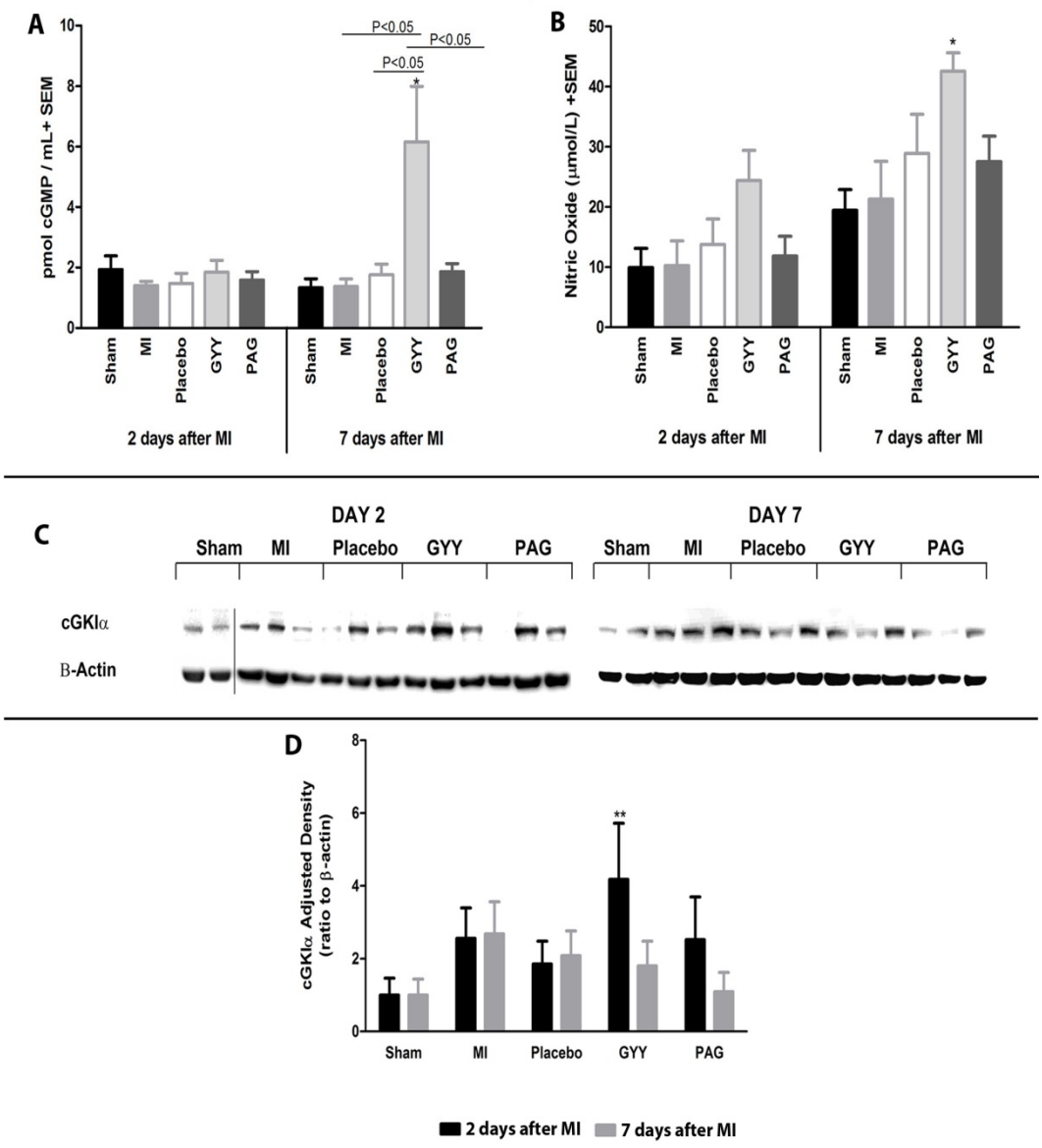

Figure 3.10 Effect of GYY treatment on plasma cGMP and NO levels post-MI. Evaluation of plasma (**A**) cGMP, (**B**) NO (nitrite/nitrate) level at both time-points in sham-operated, infarcted untreated (MI), placebo-, GYY-, and PAG- treated rats (*P<0.05 vs. sham; n=3-4/group/time-point) (**C**) Representative blots showing the expression of cGK1α protein level in heart tissue from the infarct and peri-infarct area at both time-points. Gray line indicating separation of images from 2 different blots (**D**) Densitometry analysis on expression of cGKα protein levels normalized to β-actin (**P<0.01 vs. sham; n=3/group/time-point). Data were presented as mean ± SEM.

3.6 Effect of GYY on cardiac VEGF-A and BCL-2 expression in the acute and late phases following MI

In order to investigate whether the cardioprotective effect exerted by GYY following acute MI was associated with modulation of the expression of *VEGF-A* and *BCL-2*, both of their mRNA and protein level were assessed. Evaluation on *VEGF-A* mRNA expression level in tissue from the infarct and peri-infarct zones demonstrated significant down-regulation in the infarcted groups at both time-points of evaluation (**Figure 3.11A**). At day 2 post-infarction, *VEGF-A* levels in GYY-treated animals were less repressed ($P<0.05$ relative to sham group), while animals from MI ($P<0.001$), placebo ($P<0.0001$) and PAG ($P<0.0001$) groups displayed significant suppression of *VEGF-A* mRNA expression relative to sham groups (**Figure 3.11A**). There were no differences in mRNA expression of the anti-apoptotic gene *BCL-2* among the groups at day 2 post-ischemic injury (**Figure 3.11B**). However, it was noted that *BCL-2* expression was increased in GYY- compared to PAG-treated hearts ($P<0.05$) at day 7 (**Figure 3.11B**). At protein level, high inter-individual variation was observed among all groups at both time-points (**Figure 3.11C and D**). Only a trend towards increased *BCL-2* (**Figure 3.11E**) and *VEGF-A* (**Figure 3.11G**) protein could be seen at day 2, whereas both *BCL-2* (**Figure 3.11F**) and *VEGF-A* (**Figure 3.11H**) protein at day 7 were comparable among all groups. These results suggested that GYY might modulate VEGF-A and BCL-2 at different phases following myocardial infarction.

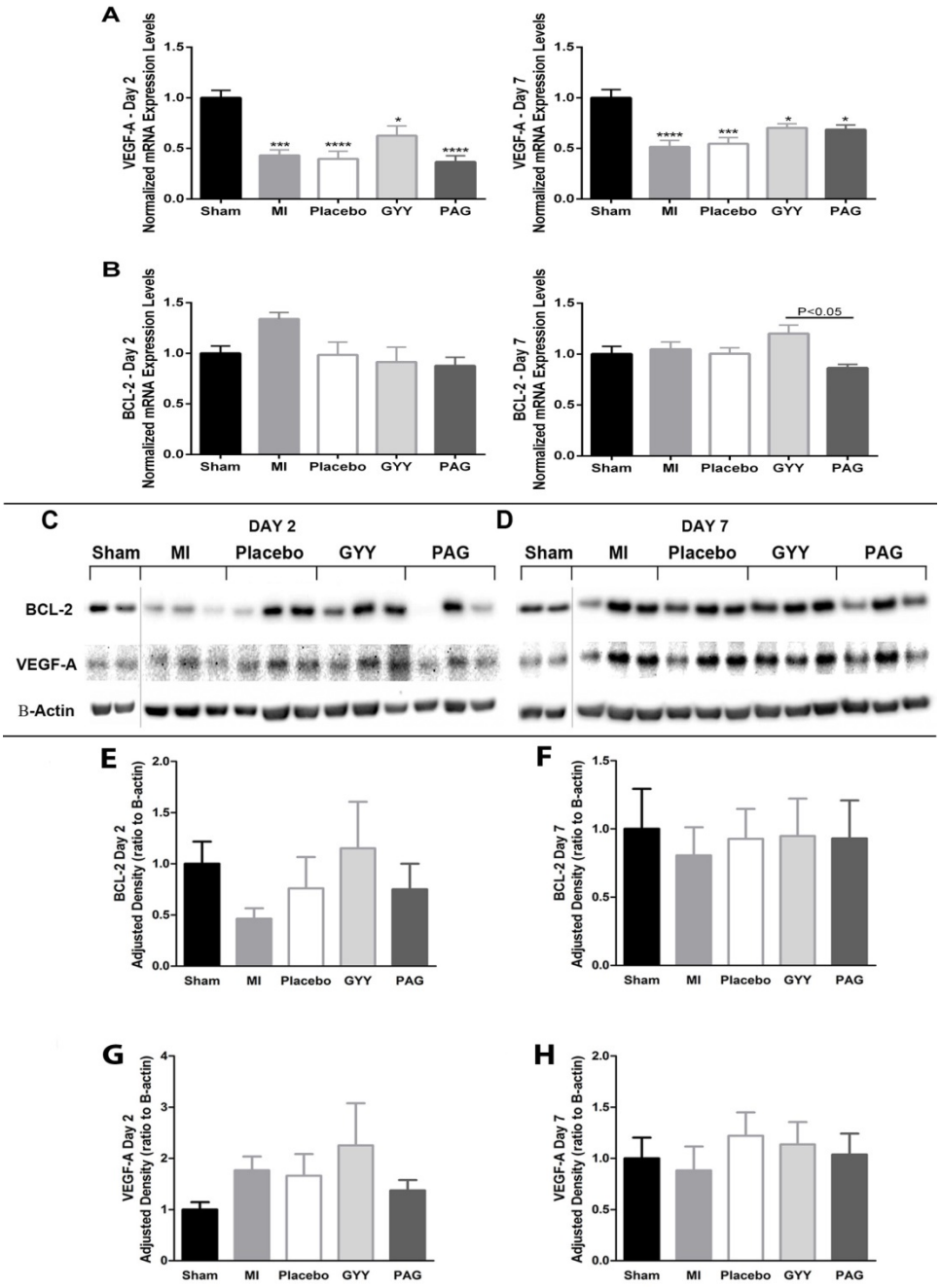

Figure 3.11 Effect of GYY on cardiac VEGF-A and BCL-2 expression at both time-points. mRNA expression level of (**A**) VEGF-A and (**B**) BCL-2 in heart tissue from the infarct and peri-infarct area of sham-operated, infarcted untreated (MI), placebo-, GYY and PAG- treated rats, at days 2 and 7 after MI (*P<0.05; **P<0.01; ***P<0.001 and ****P<0.0001; n=3-6/group/time-point). (**C-D**) Representative blots for VEGF-A and BCL-2 protein expression in rat hearts, as described above (n=4-5/group). Gray line indicating separation of images from 2 different blots. Densitometry analysis was performed for BCL-2 protein levels at (**E**) day 2 and (**F**) day 7 post-MI and VEGF-A protein levels at (**G**) day 2 and (**H**) day 7 post-MI. Protein expressions were normalized to β-actin. Data were presented as mean ± SEM.

3.7 Effect of post-ischemic treatment of GYY on miRNA profiles in the acute and late phases following MI

3.7.1 miRNA profiles in the acute and late phases following MI

To investigate effect of GYY treatment on miRNAs response to cardiac injury, we carried out miRNAs profiling of total RNA isolated from heart tissue from the LV infarct and peri-infarct areas from pooled samples (i.e. three samples/group/time-point were pooled together). miRNAs profiling detected 140 dysregulated miRNAs at 2 days post-MI (**Appendix 1**) and 142 dysregulated miRNAs at day 7 post-MI (all infarcted groups vs. healthy sham) (**Appendix 2**). Analysis was done in comparison to sham group in order to eliminate those miRNAs that are related to muscle injury upon lateral thoracotomy. Box whisker plot for both time-points after quantile normalization demonstrated that the normalized intensity values were of similar distribution among all groups suggesting that all technical and sample variations have been normalized (**Figure 3.12**). Few outliers were observed at day 2 of PAG-treated group as seen from box whisker plot (**Figure 3.12A**) namely miR-30c, miR-30e, miR-342-3p, miR-370, miR-378 and miR-378*.

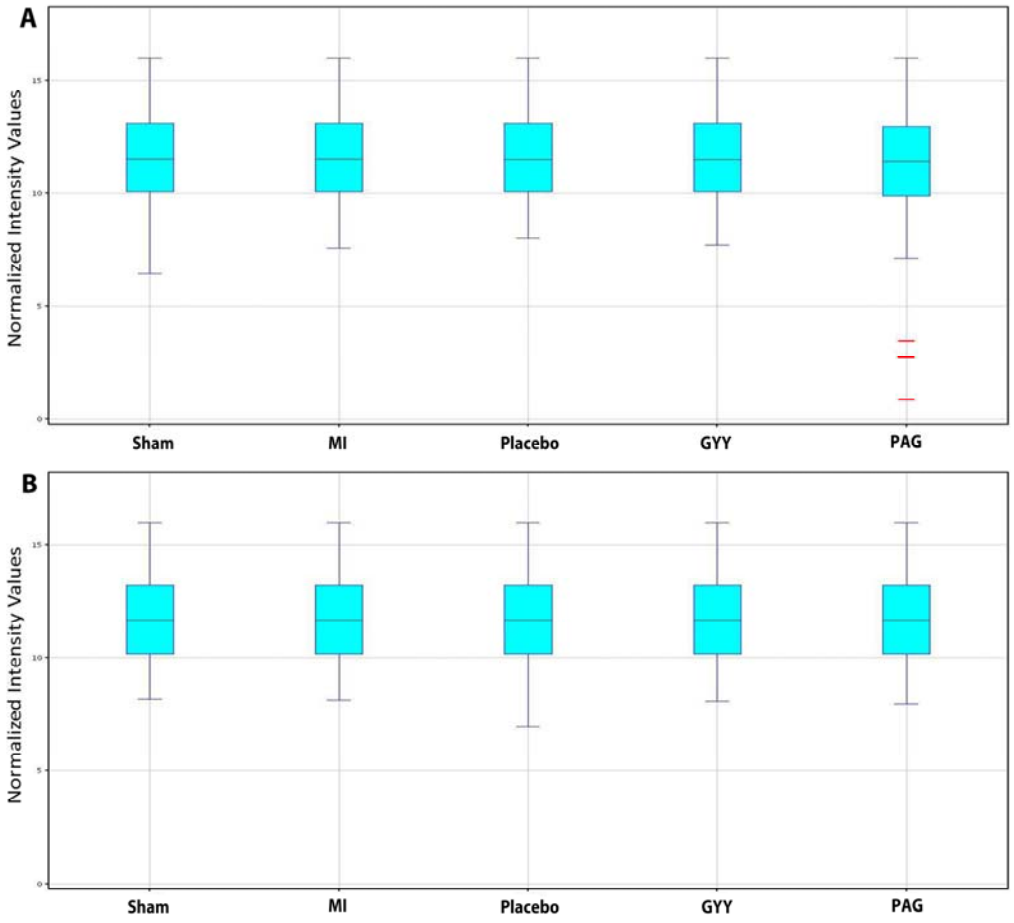

Figure 3.12 Box whisker plots of quantile normalized intensity values for both time-points. Box whisker plot for (**A**) day 2 and (**B**) day 7 post-MI. Red line indicates outliers.

Hierarchical clustering plot with average linkage and Euclidean distance metric was plotted from the fold change (FC) of all infarcted groups versus sham group. The scaling of FC value for hierarchical clustering at day 2 post-MI excluded the exaggerated FCs from the outliers found in PAG-treated group (**Figure 3.12A**) for better representative of the miRNA expression profiles. As seen from hierarchical clustering plot (**Figure 3.13A**), many of detected miRNAs were down-regulated at day 2 post-MI. Hierarchical clustering analyses of infarcted groups versus healthy sham at day 2 post-MI showed that miRNA profiles of untreated (MI), placebo- and GYY-treated group were clustered together

whereas miRNA profiles of PAG-treated group was different from the other infarcted group (**Figure 3.13A**). Although clustered together, miRNA profiles of GYY-treated group displayed different miRNAs distribution pattern compared to MI and placebo-treated group. Compared to day 2 post-MI, many of the detected miRNAs were up-regulated at late phases following MI (day 7 post-MI; **Figure 3.13B**). Hierarchical clustering analyses of infarcted groups versus healthy sham at day 7 post-MI demonstrated that MI and PAG groups were clustered together, followed by clustering with GYY group, whereas miRNA profiles of placebo-treated group was different compared to all other infarcted groups (**Figure 3.13B**). Nonetheless, miRNA profiles of GYY-treated group displayed different miRNAs distribution compared to other infarcted groups at day 7 post-MI. These results demonstrated that GYY treatment affected the miRNAs profiles of the heart tissue 2 day and 7 day after MI.

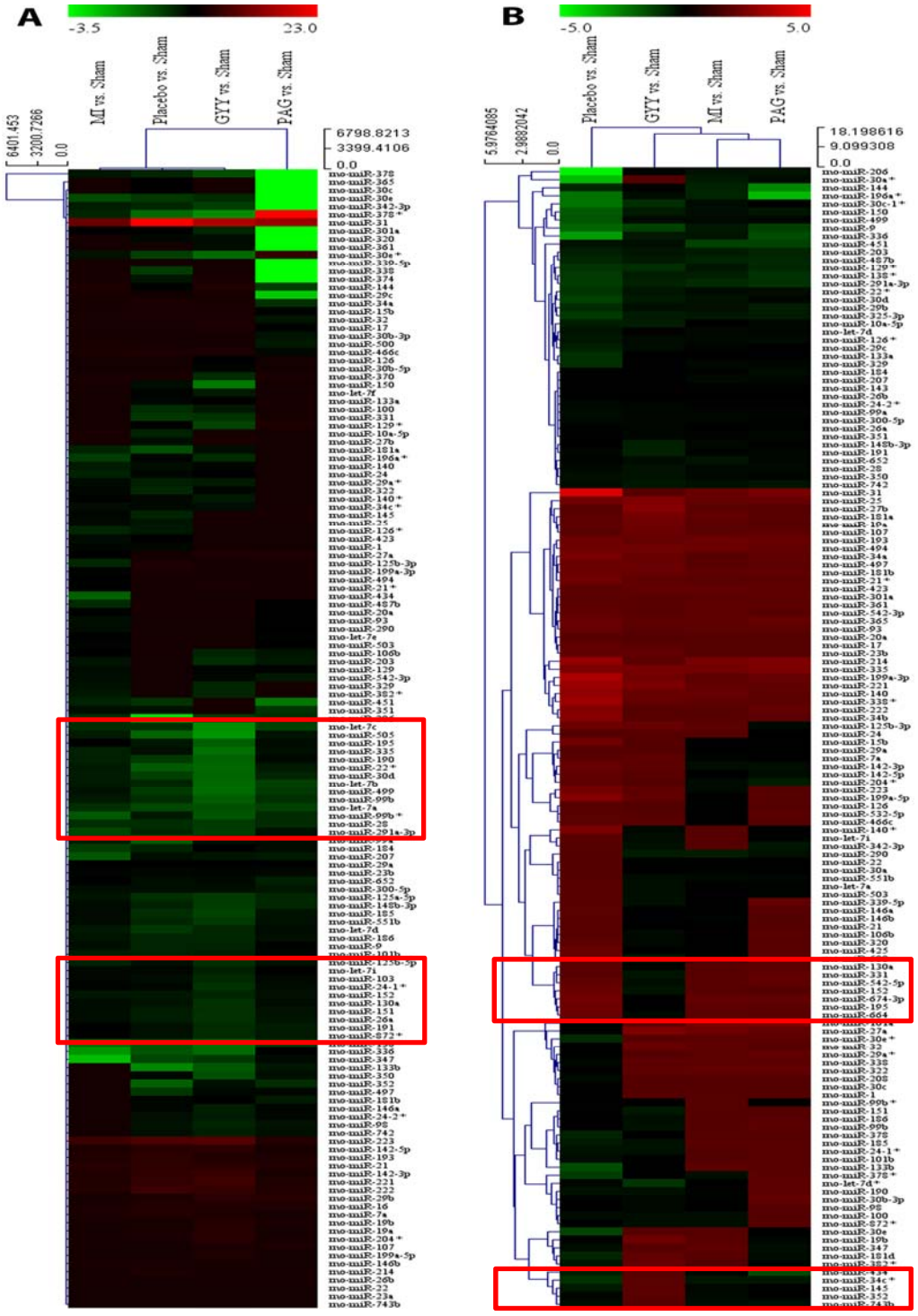

Figure 3.13 miRNAs expression profiles in the acute and late phases following MI. Hierarchical clustering plot (heatmap) with average linkage and Euclidean distance metric of fold change of miRNAs in pooled samples of heart tissue of all infarcted groups versus sham at (**A**) day 2 and (**B**) day 7 post-MI (n=1 pooled sample/group/time-point). Highlighted red boxes represent clusters of miRNAs that are possibly distinct for GYY-treated group. The up-regulated miRNAs are shown in red and down-regulated miRNAs are shown in green.

3.7.2 QPCR validation demonstrated distinct expression of miR-31 upon GYY treatment

Thirteen dysregulated miRNAs that were highly conserved in human, mouse and rat were chosen for validation using quantitative stem-loop real time-PCR on individual samples (n=6/group) by taking into consideration of the following criteria: miRNAs that had FC >1.2 or FC<-1.2 in at least one group, or were distinct in GYY-treated group, or were expressed differently at both time-points (**Figure 3.14**).

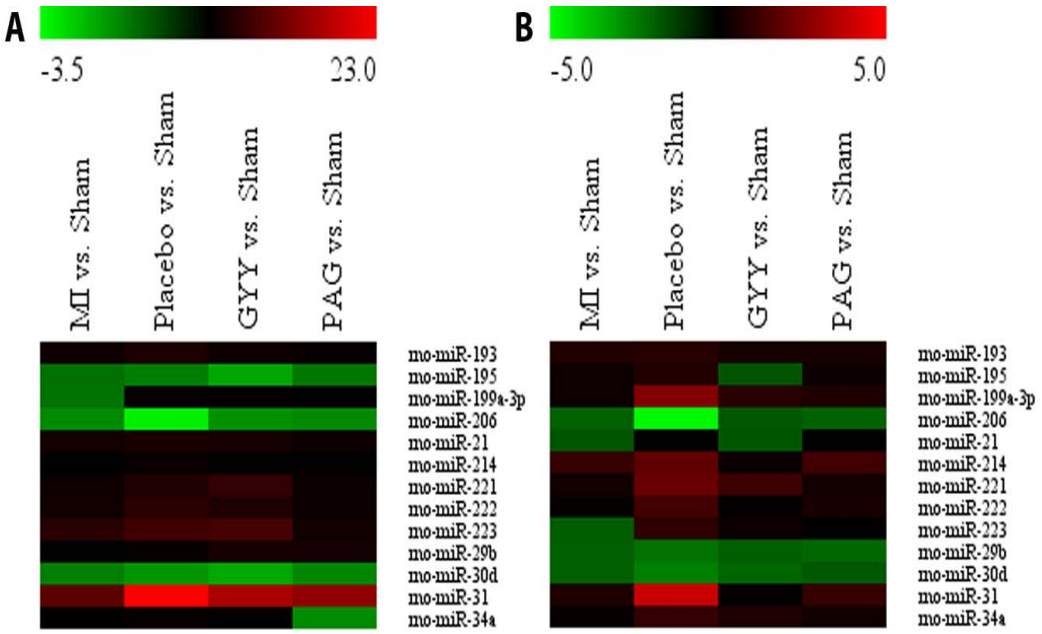

Figure 3.14 Thirteen dysregulated miRNAs for QPCR validation. Hierarchical clustering plot (heatmap) of fold change of thirteen dysregulated miRNAs expression in pooled samples of heart tissue of all infarcted groups versus sham chosen for QPCR validation in (**A**) day 2 and (**B**) day 7 post-MI (n=1 pooled sample/group/time-point). The up-regulated miRNAs are shown in red and down-regulated miRNAs are shown in green.

We then validated these miRNAs with QPCR. At both time-points of evaluation, expression of seven miRNAs (miR-31, miR-221, miR-193, miR-206, miR-214, miR-222 and miR-30d) could be validated in all groups (**Figure 3.15**) i.e. showed similar

expression pattern (either up-regulated or down-regulated) to the array data (**Figure 3.14**). miR-31 expression in the non GYY infarcted groups was significantly elevated relative to sham group at day 2 post-MI (8.69±2.64, $P<0.05$; 8.08±2.20, $P<0.05$; 11.75±1.17, $P<0.001$; **Figure 3.15A**) and markedly increased by 20-30 fold relative to sham at day 7 post-MI (32.14±2.95, $P<0.0001$; 30.38±3.39, $P<0.0001$; 21.25±5.41, $P<0.01$; **Figure 3.15A**). miR-31 expression of untreated MI and placebo-treated group was also significantly increased in a time dependent manner from day 2 to day 7 post-MI ($P<0.0001$; **Figure 3.15A**). Notably, the GYY-treated group displayed significantly distinct miR-31 expression (**Figure 3.15A**). Although expression of miR-31 in the GYY-treated group appeared somewhat elevated compared to sham at both time-points (7.42±1.02 at day 2 and 13.76±2.06 at day 7), these elevations were not statistically significant (**Figure 3.15A**) and were far less pronounced than observed in the other infarct groups. miR-31 expression in GYY-treated rats was significantly repressed compared to MI and placebo-treated rats at day 7 ($P<0.01$ and $P<0.0.5$; **Figure 3.15A**). Hence, GYY treatment suppressed the increase in miR-31 that resulted from infarction.

At day 2 post-MI, expression of mir-221 was significantly up-regulated in PAG-treated group relative to sham ($P<0.01$; **Figure 3.15B**) while the expression in the remaining groups did not differ significantly relative to the sham group. At day 7 post-MI, the expression level of miR-221 in GYY-treated rats (2.85±0.30), was not statistically significant when compared to sham rats; whereas, it was significantly increased in other infarcted groups (3.52±0.66, $P<0.01$; 4.49±0.43, $P<0.0001$; 3.09±0.46, $P<0.05$). There were also no significant changes in miR-221 level in GYY group when compared to MI or placebo group (**Figure 3.15B**). Likewise, no significant difference could be observed in the expression of miR-193 among all groups at day 2 post-MI, with significance only seen in MI group relative to sham at day 7 post-MI ($P<0.05$; **Figure 3.15C**).

Furthermore, presence of GYY did not alter miR-193 expression when compared to MI, placebo and PAG-treated group (**Figure 3.15C**). The expression profile of miR-206 (**Figure 3.15D**) and miR-30d (**Figure 3.15E**) exhibited similar observation. Their expression were significantly down-regulated (relative to sham) at day 2 post-MI among all infarcted groups while their expression at day 7 post-MI went back to baseline (similar to that of sham group) with the exception of miR-206 expression in placebo-treated group (**Figure 3.15D and E**). Although not significant, the expression of miR-206 at day 2 post-MI was not as suppressed in GYY-treated group compared to the other infarcted groups (**Figure 3.15D**). On the other hand, miR-222 expression remained elevated at both time-point of evaluation and GYY treatment did not change the expression level when compared to MI-, placebo- and PAG-treated group (**Figure 3.15F**). Expression of miR-214 at day 2 post-MI was comparable among groups and it was elevated significantly in MI and placebo-treated group at day 7 post-MI relative to sham ($P<0.05$ and $P<0.001$; **Figure 3.15G**). In addition, miR-214 expression in GYY-treated group at day 7 post-MI was not statistically different to its expression at day 2 post-MI; whereas, in other infarcted groups, miR-214 level continued to increase when compared to day 2 post-MI.

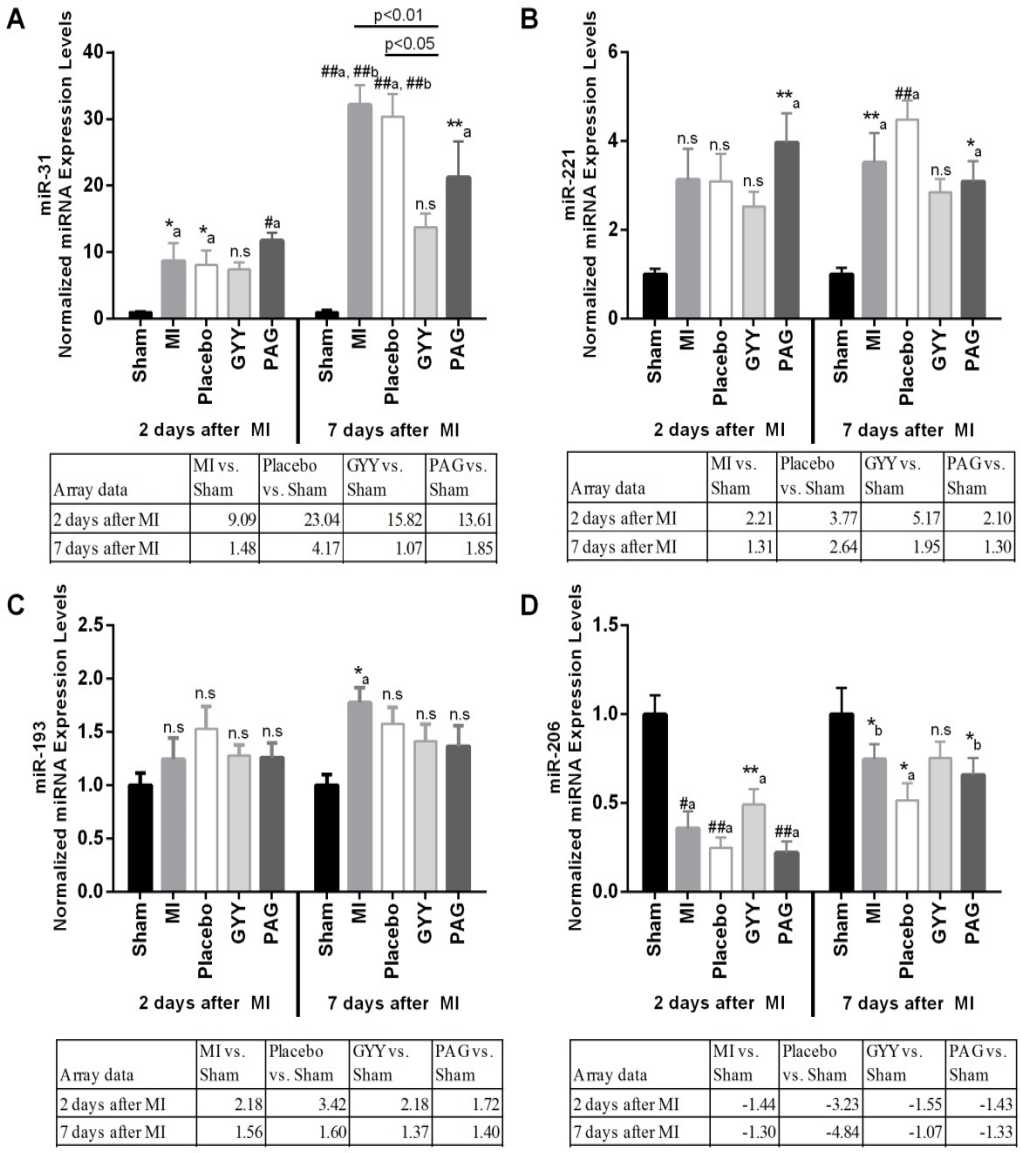

Array data	MI vs. Sham	Placebo vs. Sham	GYY vs. Sham	PAG vs. Sham
2 days after MI	9.09	23.04	15.82	13.61
7 days after MI	1.48	4.17	1.07	1.85

Array data	MI vs. Sham	Placebo vs. Sham	GYY vs. Sham	PAG vs. Sham
2 days after MI	2.21	3.77	5.17	2.10
7 days after MI	1.31	2.64	1.95	1.30

Array data	MI vs. Sham	Placebo vs. Sham	GYY vs. Sham	PAG vs. Sham
2 days after MI	2.18	3.42	2.18	1.72
7 days after MI	1.56	1.60	1.37	1.40

Array data	MI vs. Sham	Placebo vs. Sham	GYY vs. Sham	PAG vs. Sham
2 days after MI	-1.44	-3.23	-1.55	-1.43
7 days after MI	-1.30	-4.84	-1.07	-1.33

Figure 3.15 Validation of seven miRNAs by QPCR for both time-points of evaluation. Figure to continue on the next page.

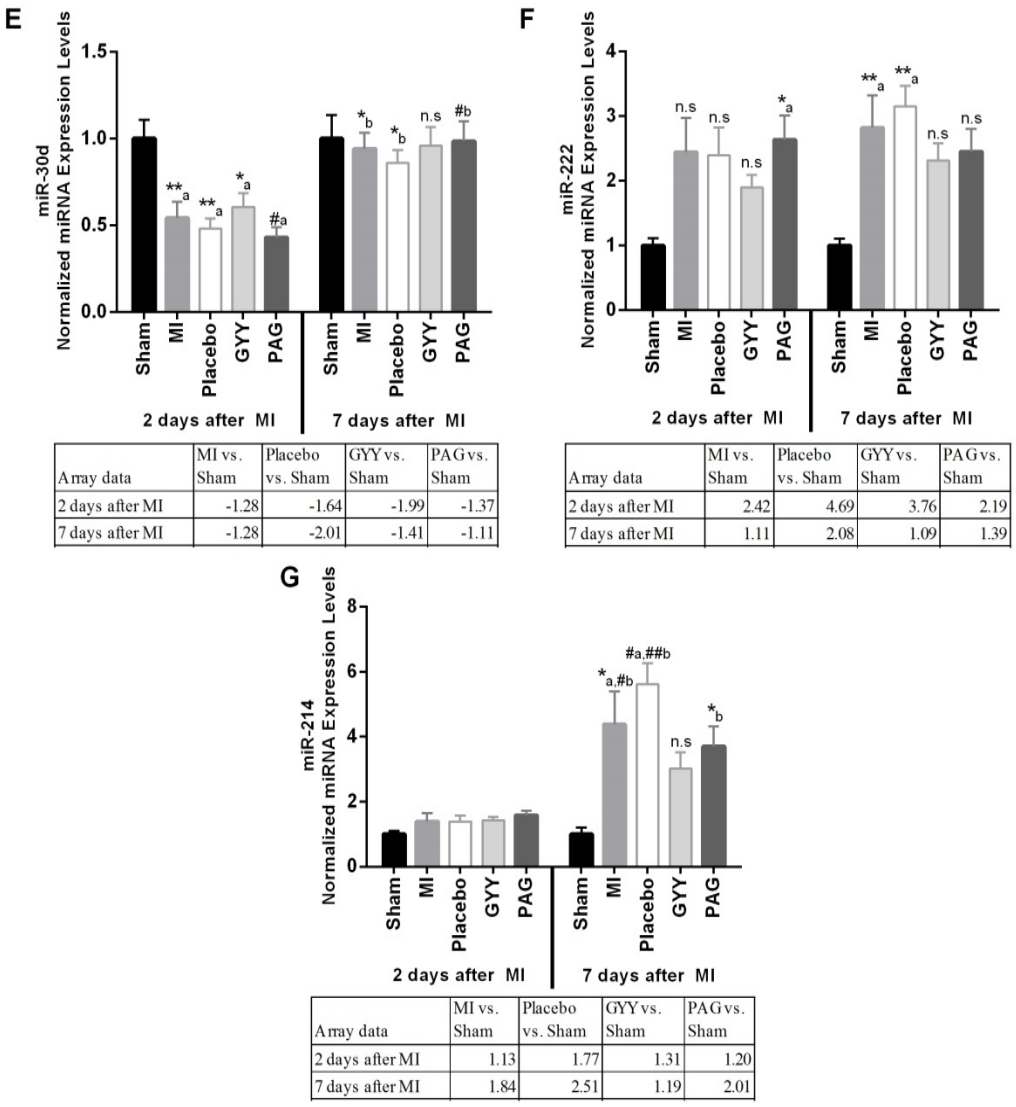

Array data	MI vs. Sham	Placebo vs. Sham	GYY vs. Sham	PAG vs. Sham
2 days after MI	-1.28	-1.64	-1.99	-1.37
7 days after MI	-1.28	-2.01	-1.41	-1.11

Array data	MI vs. Sham	Placebo vs. Sham	GYY vs. Sham	PAG vs. Sham
2 days after MI	2.42	4.69	3.76	2.19
7 days after MI	1.11	2.08	1.09	1.39

Array data	MI vs. Sham	Placebo vs. Sham	GYY vs. Sham	PAG vs. Sham
2 days after MI	1.13	1.77	1.31	1.20
7 days after MI	1.84	2.51	1.19	2.01

Figure 3.15 Validation of seven miRNAs by QPCR for both time-points of evaluation. Expression of (**A**) miR-31, (**B**) miR-221, (**C**) miR-193, (**D**) miR-206, (**E**) miR-30d, (**F**) miR-222 and (**G**) miR-214 in heart tissue of sham, untreated (MI), placebo-, GYY-, PAG-treated rats validated by QPCR. Array data of each miRNA is presented in the table underneath the bar graph. Positive numbers represent up-regulated expression relative to sham group. Negative numbers with (-) represent down-regulated expression relative to sham group. Values are presented as mean fold change (FC) ± SEM for QPCR and FC for miRNAs array data. Group-time interaction statistical significance indicated as follows: *a P<0.05 vs. Sham; **a P<0.01 vs. Sham; #a P<0.001 vs. Sham; ##a P<0.0001 vs. Sham; *b P<0.05 vs. Day 2; #b P<0.001 vs. Day 2; ##b P<0.0001 vs. Day 2; n.s, not significant.

On the other hand, expression of miR-21, miR-195 and miR-223 could only be validated in all groups at day 2 post-MI (**Figure 3.16 A-C),** while the profiles of these miRNAs at day 7 post-MI did not match the array data. At day 7 post-MI, contrasting expression profile was found in miR-21 expression in MI and GYY-treated group (**Figure 3.16A**), miR-195 expression in GYY-treated group (**Figure 3.16B**), and miR-223 expression in MI group (**Figure 3.16C**) when compared to miRNA array data, although the expression of these three miRNAs could be validated in the remaining groups.

Similarly, the expression of miR-199a-3p, miR29b and miR-34a could only be validated through QPCR in all groups at day 7 post-MI (**Figure 3.16D-F**). As seen in **Figure 3.16D**, expression of miR-199a-3p was only validated in MI group whereas the other infarcted groups demonstrated opposite expression compared to miRNA array data at day 2 post-MI. Contradicting expression pattern was also found at day 2 post-MI in miR-29b expression in all groups (**Figure 3.16E**) and in miR-34a expression in GYY- and PAG-treated group (**Figure 3.16F**) when compared to miRNA array data.

There was no significant change in the expression of miR-199a-3p and miR-34a among all groups at day 2 post-MI (**Figure 3.16 D and F**) while expression of miR195 remained unchanged among all groups at day 7 post-MI (**Figure 3.16B**). The expression level of miR-195 and miR-199a-3p in all infarcted groups displayed a bi-phasic expression pattern from being down-regulated (relative to sham group) at day 2 post-MI to being up-regulated (relative to sham group) at day 7 post-MI (**Figure 3.16B and D**). In addition, GYY-treated group had significantly lower expression of miR-199a-3p relative to placebo-treated group at day 7 post-MI ($P<0.05$; **Figure 3.16D**) which may suggest that GYY treatment might contribute to suppress the up-regulation of miR-199a-3p, although no significant difference could be seen between GYY and PAG-treated group. Expression of miR-21 in all groups remained elevated (relative to sham group) at both time-points of

evaluation, yet this expression was only significant in MI- and PAG-treated groups at day 2 post-MI and in MI- and placebo-treated groups at day 7 post-MI (**Figure 3.16A**).

Taken together, these results demonstrated that only miR-31 was distinctively modulated by GYY while the expression of other aberrantly expressed miRNAs was comparable to other infarcted groups.

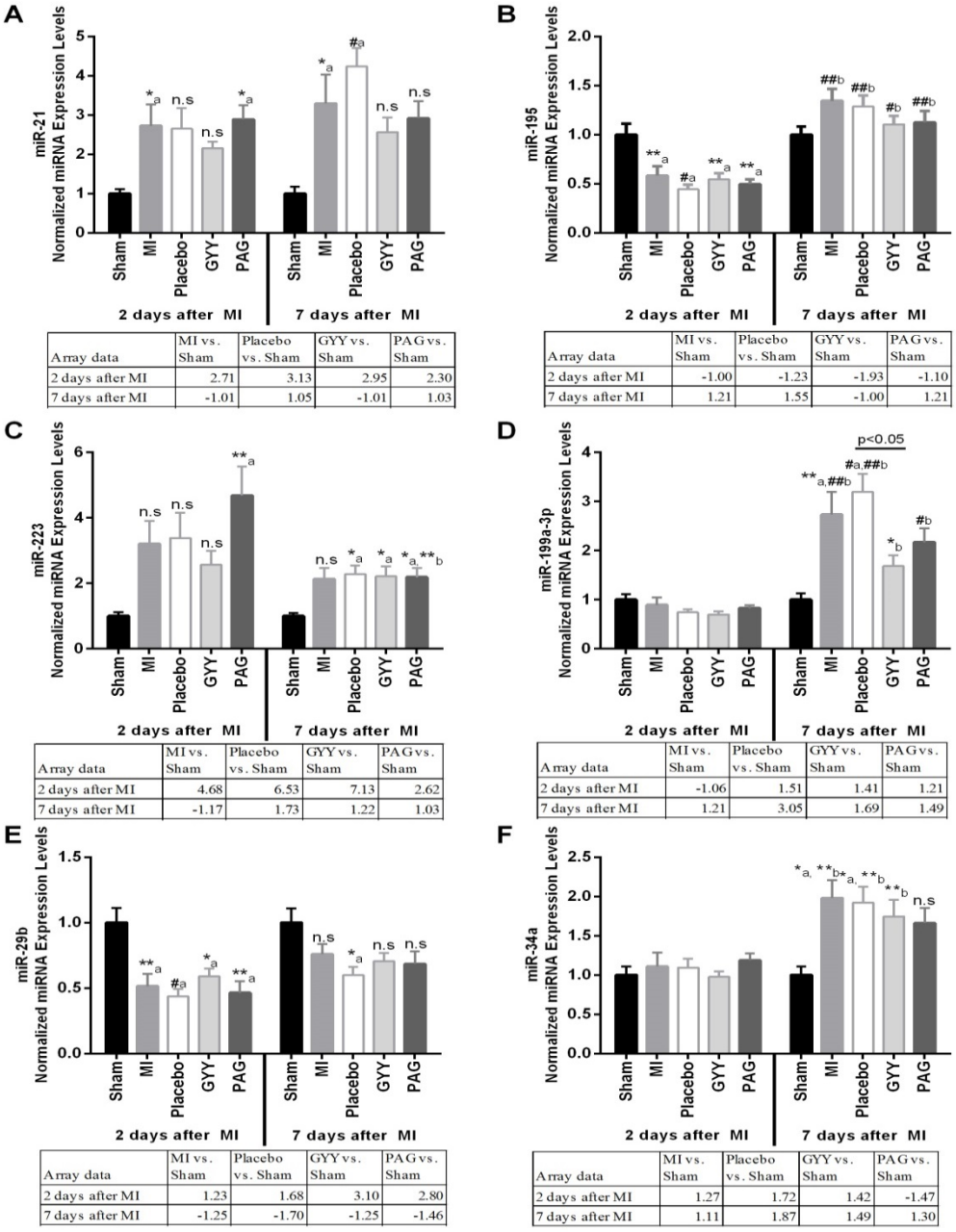

A	Array data	MI vs. Sham	Placebo vs. Sham	GYY vs. Sham	PAG vs. Sham
	2 days after MI	2.71	3.13	2.95	2.30
	7 days after MI	-1.01	1.05	-1.01	1.03

B	Array data	MI vs. Sham	Placebo vs. Sham	GYY vs. Sham	PAG vs. Sham
	2 days after MI	-1.00	-1.23	-1.93	-1.10
	7 days after MI	1.21	1.55	-1.00	1.21

C	Array data	MI vs. Sham	Placebo vs. Sham	GYY vs. Sham	PAG vs. Sham
	2 days after MI	4.68	6.53	7.13	2.62
	7 days after MI	-1.17	1.73	1.22	1.03

D	Array data	MI vs. Sham	Placebo vs. Sham	GYY vs. Sham	PAG vs. Sham
	2 days after MI	-1.06	1.51	1.41	1.21
	7 days after MI	1.21	3.05	1.69	1.49

E	Array data	MI vs. Sham	Placebo vs. Sham	GYY vs. Sham	PAG vs. Sham
	2 days after MI	1.23	1.68	3.10	2.80
	7 days after MI	-1.25	-1.70	-1.25	-1.46

F	Array data	MI vs. Sham	Placebo vs. Sham	GYY vs. Sham	PAG vs. Sham
	2 days after MI	1.27	1.72	1.42	-1.47
	7 days after MI	1.11	1.87	1.49	1.30

Figure 3.16 Validation of six miRNAs by QPCR in either time-point of evaluation. Expression of (**A**) miR-21, (**B**) miR-195, (**C**) miR-223, (**D**) miR-19a-3p, (**E**) miR-29b and (**F**) miR-34a in heart tissue of sham, untreated (MI), placebo-, GYY-, PAG-treated rats validated by QPCR. Array data of each miRNA is presented in the table underneath the bar graph. Positive numbers represent up-regulated expression relative to sham group. Negative numbers with (-) represent down-regulated expression relative to sham group. Values are presented as mean fold change (FC) ± SEM for QPCR and FC for miRNAs array data. Group-time interaction statistical significance indicated as follows: *a P<0.05 vs. Sham; **a P<0.01 vs. Sham; #a P<0.001 vs. Sham; *b P<0.05 vs. Day 2; **b P<0.01 vs. Day 2; #b P<0.001 vs. Day 2; ##b P<0.0001 vs. Day 2; n.s, not significant.

4. DISCUSSION

H_2S is emerging as an important endogenous gasotransmitter that protects against numerous injurious stimuli through activation of signaling pathways that are protective in cardiac injury[46, 71, 136]. The neurohormonal response is critical in the evolution of MI to adverse LV remodeling, and all pharmacotherapies (ARBs, β-adrenoceptors blocker therapy, and ACE inhibitors) currently proven to ameliorate adverse remodeling in clinical HF operate via neurohormonal pathways[137]. In this study, the possibility of H_2S – mediated modulation of neurohormonal activation has been raised. *In vitro*, high concentration of H_2S inhibited ACE in endothelial cells[138] while *in vivo*, it has also been implicated in regulating the renin-angiotensin system by inhibiting degranulation of mast cells and blocking thereby renin release in a isoproterenol (ISO)-induced HF model[139]. In addition, various miRNAs have been found to be associated with pathological changes after MI[121-128]. H_2S has been reported to up-regulate miR-133a, which inhibited cardiomyocyte hypertrophy in an *in vitro* model[140] while *in vivo*, H_2S attenuated myocardial injury via induction of miR-21[141]. The implications of H_2S in modulating neurohormonal response and miRNAs are critical for a better understanding of potential therapeutic role during myocardial injury, as this would provide further insights on the cardioprotective effect of H_2S and its future application. To date, most of H_2S studies in the context of cardiac injury have utilized NaHS, as it is commercially available and easy to handle. However, NaHS is a very volatile and short-lived donor that might not be physiologically relevant to study H_2S therapeutic potential *in vivo*[67]. In this study, GYY, a slow-releasing H_2S donor that mimics its endogenous physiological release, was employed. The effects of GYY on LV remodeling and function following myocardial injury have not been characterized yet. We hypothesized that GYY is cardioprotective in

a rat model of myocardial infarction and exerts this effect, in part, through modulation of the neurohormonal response and miRNAs.

The animal model used in this study was a permanent LAD ligation-induced MI model. This model is one of the most widely used and standard technique of inducing regional injury and subsequent HF in rodents[142, 143]. It is also a useful model to understand further the pathophysiology of post-MI cardiac remodeling due to changes in extracellular matrix and neurohormonal activation[144-146]. In rats, mortality of this model happens within the first hour after infraction due to ventricular fibrillation and it ranges between 35-50%[147]. In our study, we observed 10-20% mortality with the highest observed in PAG-treated group. PAG has been reported to also inhibit other metabolic processes that could lead to possible diuresis and toxic renal effects[148] that could explain the slightly higher mortality rate observed in this group.

4.1 Modulation of H_2S system by GYY

Exogenous administration of GYY increased plasma H_2S levels at both day 2 and 7 post-MI (**Figure 3.1**) indicating that dose regimen used in this study was sufficient and therefore, therapeutic effects exerted by this treatment were indeed because of increased H_2S level. Although it has been reported that plasma H_2S level in rat model of ISO-induced myocardial injury was decreased[59], in this study however, plasma H_2S level in untreated infarcted rats and placebo-treated rats were comparable to sham. Apart from the difference in animal model, this discrepancy might also be due to difference in the method of measuring plasma H_2S level. In the above-mentioned study, Geng and colleagues measured the endogenous plasma H_2S level using methylene blue method. Though this method is very common, it has been shown to pose limitation as it measures

not only free H_2S but also other molecules (sulfide and hydrosulfide anion)[43, 148]. In this study, we employed fluorimetric-based method which used monobromobimane (MBB) to trap free H_2S and the resulting dibimane was then separated by HPLC and detected through its fluorescence property[149]. Baseline level of free H_2S measured by MBB method has been proven to be more physiologically relevant compared to methylene blue method[40]. However, it is important to note that various biological effects of H_2S most probably happen inside the cell. Thus, H_2S measurement either in plasma or in homogenized tissue might not reflect its cellular site of action. However, up until now, there are no assays that are sensitive, selective and capable to measure real-time intracellular H_2S[43].

Most endogenously generated H_2S is derived from the metabolism of L-cysteine by two pyridoxal-5′-phosphate-dependent enzymes: cystathionine β synthase (CBS) and cystathionine γ lyase (CSE) which are inhibited by PAG[43]. CSE is abundantly expressed in liver as well as in vascular and non-vascular smooth muscle[78, 132]. In this study, expression of CSE protein was detected in liver tissue from all animal groups and as expected, no inter-group difference was apparent at either time-point (**Figure 3.2C and D**). Treatment with PAG significantly reduced H_2S synthesizing activity of CSE as observed through the exogenous addition of L-cysteine in liver homogenates (**Figure 3.2E**). Thus, this indicated that the dose regimen used was effective in inhibiting tissue CSE activity despite not detecting reduction in plasma H_2S level.

4.2 Modulation of early neurohormonal response by GYY is cardioprotective

GYY increased the expression and release of ANP and BNP; importantly, plasma ANP concentration increased several fold higher compared to those of comparator groups in

the late phase after MI (**Figure 3.7**). The main stimulus for NP release is myocardial stretch[95], and yet, the highest expression and release of NPs was observed in GYY-treated group that had the best preserved hearts with lowest intra-cardiac pressures. This pattern of elevated plasma NP in the presence of preserved LV structure, function and intra-cardiac pressures is striking and unusual. In addition, we also observed that ANP mRNA level upon GYY treatment increased several fold higher relative to other comparator groups in the early phase after MI (**Figure 3.8A**). These results are strongly suggestive of a specific and direct effect by the H_2S donor to enhance NP expression and secretion. Increased in ANP mRNA expression upon H_2S treatment in both phenylephrine (PE)-induced hypertrophied and non-hypertrophied cardiomyocytes has also been reported previously[140]. Interestingly, mRNA level of NPR3, the receptor clearance, was found to be not as repressed in GYY group at day 2 post-MI though this effect was abolished at day 7 post-MI (**Figure 3.8G and H**). Although the implications of this result were not clear, it may be possible that ANP clearance through NPR3 contributed to the level of plasma ANP in GYY group which was not as elevated at day 2 post-MI. The effect of GYY on NPR3 needs to be further investigated.

A growing body of evidence supports a role for ANP and BNP as cardioprotective hormones despite being used as diagnostic marker to monitor severity of hypertrophy and HF in clinical settings. They counteract the cardiac hypertrophic effects of Ang 2[150-152]. Both ANP and BNP affect multiple neurohormonal (including RAAS system, endothelin and sympathetic nerve activity) and anti-proliferative pathways involved in pathological LV remodeling and progression to HF[153]. Genetic abrogation of ANP or NPR-1 resulted in cardiac hypertrophy and fibrosis[97, 154], while ANP deficiency in mice with dilated cardiomyopathy led to further impairment of LV systolic function[155]. Infusion of ANP in dogs following LAD ligation had significantly lower LVEDP and less severity of

myocardial injury compared to placebo control[156]. In rats, treatment with recombinant BNP immediately after coronary ligation decreased infarct size[157] and enhanced cardiac contractility[158]. Short-term constant infusion of BNP conserved LV systolic function and dimension, and prevented the development of systolic heart failure after persistent ischemic injury in dogs subjected to repetitive coronary embolization[159]. Whereas, long-term administration of BNP after MI for eight weeks in rats attenuated ventricular remodeling and improved cardiac function and this effect was associated with the inhibition of transforming growth factor β1 (TGF-β1)/ mothers against decapentaplegic homolog 2 (Smad2) pathway[160]. In a clinical study, early administration of human recombinant BNP, nesiritide, after MI increased plasma cGMP and C-type natriuretic peptide while decreasing other cardiac peptides with a neutral outcome on renal function and an inclination towards attenuation of LV remodeling[161]. In a clinical study, administration of human atrial natriuretic peptide (hANP, carperitide) prevented LV remodeling and preserved LV function[162] and increased collateral blood flow[163] in MI patients after PCI. Infusion of hANP before MI provided cardioprotection probably through a NO-PKC dependent pathway followed by activation of mitochondrial K_{ATP} channel[164]. hANP also exhibited an antioxidant action, which may ameliorate ischemia-reperfusion injury and limit infarct size, increased collateral blood flow and decreased LVEDP[165, 166]. Moreover, activation of NPR1 upon binding of ANP or BNP generated an increase in its second messenger, cGMP, which was clearly increased in parallel to plasma ANP and BNP in our study (**Figure 3.10A**). cGMP mediates natriuresis and inhibition of renin and aldosterone, attenuates hypertrophy and, adverse remodeling, as well as promotes angiogenesis[105, 106, 152, 155], although in our results, plasma renin activity and aldosterone remained unchanged. Given these promising actions, the NP system serves as an important compensatory mechanism against deleterious neurohormonal activation following MI, and an enhanced early endogenous NP response is a plausible

contributor to the cardioprotection offered by GYY. However, further studies are necessary to investigate the exact mechanism of GYY-induced ANP and BNP activation and long-term effect of GYY on ANP and BNP activation and consequence results of these sustained activations to the heart function.

In addition, GYY treatment had an effect on apelin expression, an adipokine that binds to APJ, which has been reported as cadioprotective in acute myocardial ischemia[135]. Cardiac apelin mRNA level was up-regulated in GYY-treated rats compared to PAG treatment at day 2 post-injury, while suppressed in infarcted groups relative to sham group (**Figure 3.9D**). Likewise, cardiac apelin was up-regulated in the GYY rats relative to all infarcted groups at day 7 post-injury. In parallel, APJ mRNA level was up-regulated in animals treated with GYY compared to PAG-treated animals (**Figure 3.9E**). Consistently, it has been reported that apelin level following LAD ligation was reduced in the infarct and peri-infarct regions at 1 day post-MI which persevered up to 7 days post-MI; whereas APJ, was up-regulated 1 day post- MI followed by down-regulation at day 7[167]. Apelin has lasting cardioprotective effects after MI through reduction of cardiac tissue damage and lipid peroxidation with augmentation of NO production[135]. Apelin also prevented TGF β-induced activation of cardiac fibroblasts and collagen production *in vitro*[168]. Administration of apelin-12 peptide during reperfusion following ischemia in rats limited infarct size and decreased post-ischemic cardiomyocyte membrane damage through NO-dependent mechanisms[169], while treatment with apelin-13 promoted angiogenesis in infarcted hearts[170] and improved cardiac repair post-MI[171]. Apelin treatment also increased cardiac contractility and angiotensin converting enzyme-2 (ACE-2) level in APJ-deficient mice and a coupling of the RAAS and apelin system via ACE-2 has been suggested[172]. Hence, an H_2S-induced increase in endogenous cardiac apelin could also have contributed to the cardioprotective effect observed in this study.

4.3 cGMP-dependent and -independent signal transduction may mediate the therapeutic effect of GYY

Previous reports have shown that H_2S mediated improvement of survival and attenuation of cardiac dysfunction and infarct size in infarcted rodents[66, 173]. In our study, treatment with GYY limited final infarct size (as assessed by LV scar dimensions), attenuated adverse remodeling and provided sustained preservation of cardiac structure and function following MI in a rat model, as evidenced by echocardiography (**Figure 3.3 and 3.4**), hemodynamic measurements (**Table 3.1**) and morphometric studies (**Figure 3.5**). Furthermore, GYY preserved LV end-systolic and diastolic volumes, LV end-diastolic pressure and LV ejection fraction (**Figure 3.4**), all of which are reliable indicators of cardiac function and accepted predictors of adverse outcomes in clinical practice. Furthermore, our results demonstrated that GYY promoted angiogenesis within the LV scar following ischemic injury (**Figure 3.6**). Angiogenesis is one of the vital mechanisms to heal the injured myocardium after infarction[27].

We found that GYY treatment increased cGKIα protein level at day 2 post-MI (**Figure 3.10C and D**). However, increased in cGKIα protein level does not represent the catalytic activity of cGKI. Therefore, the implication of this result is not clear as we did not perform an assay to measure the catalytic activity of cGKI which could provide a better correlation with our results showing an increase of plasma cGMP at day 7 post-MI. Nonetheless, the early increased of cardiac cGKIα protein, in parallel with increased of plasma cGMP may have played a role in the pro-angiogenic effect observed in GYY-treated animals, since in vascular endothelial cells, cGMP-cGK signaling modulates cell migration, motility, and proliferation, all of which are essential for angiogenesis[95]. H_2S was reported to promote angiogenesis under ischemic conditions both *in vitro* and *in vivo* and could elicit protective effects through activation of VEGF-Akt-eNOS-NO-cGMP

signaling pathway, while elevating NO bioavailability in pressure-overload induced HF in rodents[174]. We found post-MI down-regulation of cardiac *VEGF-A* mRNA in both infarct and peri-infarct tissues from all groups relative to sham group; yet, mRNA level in GYY-treated animals were less suppressed than in the other infarcted groups and showed a trend towards higher protein expression post-MI (**Figure 3.11**). H_2S and NO cross-talk have been shown to promote angiogenesis through the cGMP-cGK signaling pathway[175, 176]. Accordingly, we detected increases in plasma NO and cGMP in GYY-treated rats post-MI. Since ANP and BNP levels were also significantly increased in GYY-treated animals at the same time-point, this suggests that the rise observed in plasma cGMP could reflect both increased plasma NPs and NO (**Figure 3.10A and B**). In addition, ANP and BNP have been demonstrated to regulate angiogenesis in the heart and skeletal muscle through cGKI[106, 109]. GYY-induced angiogenesis may also occur through cGK-independent pathways. Notably, GYY has been shown to induce a minor increase in cGMP compared to NaHS in isolated aortic ring experiments and promotes vasorelaxation through a cGK-independent pathway[177]. In addition, NPs could act on vascular tissue through cGMP regulated phosphodiesterases (PDEs)[178] and cyclic nucleotide-gated ion channels (CNGs)[179]. PDEs are involved in endothelial cell migration, proliferation and angiogenesis[180], while CNGs are Ca^{2+}-permeable non-selective cation channels that open upon adenosine 3'-5'-cyclic monophosphate (cAMP) or cGMP binding[181]. CNGA2, a CNG subunit expressed in human and rat vascular tissues, was activated by ANP more readily than NO in CNGA2-expressing vascular smooth muscle cells[182]. Furthermore, increased expression of apelin in our study at day 7 (**Figure 3.9 D**) might be associated with increase in plasma cGMP at the same time-point as apelin secretion has been reported to be regulated through cAMP and cGMP dependent pathways in the adipocytes[183]. Thus, it is possible that GYY plays a role in angiogenesis and arteriogenesis through cGMP-cGK downstream signaling or cGMP-

cGK-independent pathways during cardiac ischemic injury and this warrants further investigation.

Cardiac mitochondrial protection has been implicated as one of the mechanisms behind NaHS cardioprotection through increased expression of anti-apoptotic *BCL-2*, decreased expression of pro-apoptotic BAX and caspase-3 and reduction of cytochrome c protein leakage from mitochondria to cytoplasm[173]. NaHS, administered 5mins before MI and 60mins after MI in mice, was shown to improve survival by preserving LV function and reducing infarct size, through the regulation of BAX/BCL-2 pathway and anti-inflammatory response[66]. We have found that *BCL-2* mRNA expression was increased and there was a trend towards increased *BCL-2* protein in GYY-treated rats compared to PAG-treated (**Figure 3.11**). Discrepancies between mRNA and protein expression in this study could be due to a higher protein degradation/lower stability secondary pathology. Another possible explanation is that, in this study, we have evaluated tissues only from the infarct and peri-infarct area and did not incorporate the remote healthy myocardium.

4.4 Modulation of miRNAs by GYY

Since normalization in analyzing miRNA array data is important to eliminate variations that arise from technical and sample variations, we performed global quantile normalization method that has been reported to work best and more robust in reducing difference in miRNAs expression values. This method adjusts the differential bias across the scale of expression values[184, 185].

Seven out of thirteen selected dysregulated miRNAs in heart tissue after myocardial infarction namely: miR-31, miR-221, miR-193, miR-206, miR-214, miR-222 and miR-30d from the miRNA array data could be validated (showed similar pattern of up-

regulation or down-regulation) through QPCR for both time-points (**Figure 3.15**). miRNAs from day 2 post-MI (miR-199a-3p, miR-29b and miR-34a) and day 7 post-MI (miR-21, miR-195 and miR-223) that could not be validated were detected in QPCR with opposite expression from miRNA array data (**Figure 3.16**). In the microarray platform, signals obtained depend on hybridization temperature, specificity and length of the probe[186, 187]. As a result, binding affinities vary among miRNAs and there could be false positive results. Thus, miRNA array should only be used to seek out possible unique miRNAs and alone should not be used to make quantitative statements and needs to be validated with other platform. Stem-loop QPCR quantification of miRNAs expression used in this study has been commonly used to validate miRNA array data as it has high specificity[187, 188]. Besides, our miRNA array was performed with pooled samples of three whereas QPCR was performed on six individual samples. Therefore, results obtained from QPCR are more reliable for quantitative measurements of miRNAs expression.

Post-ischemic treatment with GYY suppressed the expression of miR-31 in the late phase after MI whereas the other infarcted groups expressed 20-30 folds higher relative to sham group by day 7 post-MI (**Figure 3.15A**). miR-31 has been shown to target myogenic determination gene, Myf5, thereby repressing myogenesis[189]. Through Islet-1, miR-31 regulates cardiac fibrogenic epithelial-to-mesenchymal transition (EMT)[190]. Evidence suggests that epicardial mesothelial cells undergo fibrogenic EMT upon cardiac stress to generate myofibroblast-like cells[191-193] that contribute to the development of fibrosis[194]. miR-31 also directly binds to cellular repressor of E1A-stimulated genes that plays a vital role in modulating vascular smooth muscle cells (VSMCs) phenotype by retaining these cells in the differentiated mature phenotype state[195]. Restenosis after PCI is linked to VSMC phenotype modulation, whereby VSCMs de-differentiate from a contractile to synthetic phenotype after vascular injury[196]. In parallel to this, serum miR-31 level is

elevated in coronary artery disease (CAD) patients with restenosis compared to CAD patients without restenosis and to healthy controls, suggesting that miR-31 may be a potential biomarker in diseases concerning VSMC phenotypic modulation[195]. In addition, a parallel study carried out by our group has also demonstrated that miR-31 is deleterious to cardiac function and its inhibition after MI *in vivo* ameliorates cardiac dysfunction (data not shown- manuscript in preparation). Using target prediction database, miRWalk[197], miR-31 is predicted to target cardiac troponin T type 2 (TNNT2) and E2 factor transcription factor 6 (E2F6) genes in the 3'UTR. TNNT2 plays an important role in the regulation of contractile function[198]. Mutations in this gene are involved in the progression of molecular and structural ventricular remodeling[199] and associated with familial hypertrophic cardiomyopathy as well as with dilated cardiomyopathy[200]. E2F6 plays a role as a repressor of gene transcription during cell cycle progression and growth,[201] and it has been validated as target of miR-31 in the highly malignant prostate cancer cell line and over-expression of E2F6 contributes to apoptosis resistance in benign prostate cancer cell line[202]. Interestingly, during myocyte hypertrophy, E2F6 protein is significantly up-regulated and this is in parallel with the re-entry of myocytes to the cell cycle. In addition, knocking down E2F6 gene decreases viability of cultured neonatal myocytes suggesting that E2F6 is possibly involved in myocardial regeneration[203].

We also found that miR-221 was not so elevated in GYY treated-rats 7 days after MI in comparison to the other infarcted groups (**Figure 3.15B**). This finding is in agreement with a recent report that demonstrated inhibition of miR-221 by organosulfur garlic compound, DATS, in human EPCs *in vitro*. Furthermore, inhibition of miR-221 causes up-regulation of vasculogenic c-kit protein, promoting thereby neovasculogenesis[204]. Up-regulation of miR-221 suppresses the expression of c-kit protein and this obstructs the

angiogenesis process in human endothelial cells *in vitro*[205]. Likewise, miR-221 level is significantly higher in EPCs from patients with CAD compared to healthy subjects[206].

Moreover, based on miRWalk predictions, both miR-31 and miR-221 possibly target apelin in the 3'UTR. Since miRNAs repress their targets, it is important to note that suppression of miR-31 and possibly miR-221 by GYY in parallel with the increase in apelin expression observed in our study strongly suggest this association. However, direct interaction between miR-31 and miR-221 with apelin needs to be further investigated. Taken together, modulation of miRNAs expression, namely miR-31 and possibly miR-221, may contribute to the observed cardioprotective and pro-angiogenic effects of GYY.

GYY-treated rats also expressed slightly different expression of miR-206, miR-214 and miR-199a-3p compared to other infarcted groups (**Figure 3.15 and 3.16**). These miRNAs have been associated with cardiac injury. miR-206 is expressed specifically in muscle and plays a role in myogenesis[207, 208]. It suppresses hypertrophy in myogenic cells through inhibition of histone deacetylase 4 (HDAC4) *in vitro*[209]. miR-206 also targets tissue inhibitor of metalloproteinase 3 (TIMP-3) and it contributes to the high mobility group box-1 protein (HMGB1)-mediated attenuation of cardiac remodeling after MI[210]. miR-214 is up-regulated in response to ischemic injury and heart failure[211]. It protects the heart against ischemia reperfusion injury by regulating calcium influx and cell death through sodium/calcium exchanger 1 *in vivo*[212]. Inhibition of miR-214 suppresses proliferation and differentiation of mouse myoblast cell line (C2C12)[213]. Moreover, miR-214 also regulates angiogenesis by targeting Quaking, a key regulator of vascular development and remodeling, as well as decreasing angiogenic growth factor release[214]. Likewise, miR-199a-3p is up-regulated four days after pulmonary artery constriction in the right ventricle hypertrophy and failure model and it is associated with cardiomyocyte size and fibrosis[215]. In contrast to inhibition of miR-214, inhibiting miR-199a-3p with antisense

oligonucleotides induces C2C12 differentiation and myotube hypertrophy by targeting insulin-like growth factor 1 (IGF-1), mTOR and ribosomal protein S6 kinase (RPS6KA6) in the iGF-1/AKT/mTOR signaling pathway[216]. Further studies are needed to investigate the contribution of miR-206, miR-214 and miR-199a-3p to the GYY-mediated cardioprotective effect.

Although it has been reported that H_2S induces miR-133a *in vitro*[140], we did not observe it in our *in vivo* study (**Appendix 1 and 2**). We also did not find increase of miR-21 in GYY-treated group compared to placebo group (**Figure 3.16A**) as reported by Toldo and colleagues[141]. This might be due to the difference in animal model, H_2S donor used, and the time-point of miR-21 measurement. In their study, Toldo and colleagues measured the level of miR-21 one hour after sodium sulfide or saline administration and before the ischemia/reperfusion injury while we measured the level of miR-21 2 days and 7 days after MI and treatment.

4.5 Limitations of H_2S donors including GYY in clinical application

H_2S donors including GYY are potential clinical therapeutic agents in cardiovascular diseases. However, there are some limitations of these donors that need to be addressed before they can be used clinically. One of the major challenges is to develop an accurate and non-invasive method of H_2S measurement in plasma, as well as at the cellular and in intracellular compartments[217]. This would allow to determining the efficacy of H_2S donors after its administration in delivering H_2S to intracellular targets and to monitor any potentially toxic high levels. Another limitation is that the byproducts that are produced after H_2S release from these donors including GYY are still unclear[218]. It is important to identify these products and investigate their biological activities to prevent

any future side effects for chronic clinical application that could potentially arise, such as hypotension and excessive angiogenesis. In the future, a targeted delivery of H_2S donors to the heart might help to circumvent these potential systemic side effects.

In conclusion, we demonstrated that post-ischemic therapeutic intervention with the slow-releasing H_2S donor, GYY, preserves cardiac function and attenuates adverse remodeling during the acute and late phases following MI. The mechanisms involved behind GYY cardioprotection may include a specific enhancement of the beneficial natriuretic peptide response to cardiac stress and suppression of miRNAs deleterious to cardiac function with associated post-ischemic promotion of pro-angiogenesis, anti-apoptotic and anti-fibrotic effects.

5. FUTURE PERSPECTIVES

This study raises the novel possibility that GYY may exert cardioprotective actions *in vivo* through H_2S-induced natriuretic peptide activation and H_2S-mediated miRNAs modulation. Exogenous recombinant NPs have been used therapeutically in clinical MI and acute HF with mixed results[219-221] and further prospective studies are necessary to address the controversy about safety of these recombinant drugs[87, 113]. Therefore, definition of long-term effects of GYY administration following ischemic injury on NPs activation need to be further investigated. It is also important to study the exact mechanisms behind NP activation. Since GYY up-regulated mRNA expression of ANP and prevented down-regulation of NPR3, it will be interesting to know if H_2S can regulate the promoter of the ANP and NPR3 gene to regulate their mRNA biosynthesis and degradation. GYY could also modulate ANP at the protein level since plasma ANP was found to be several folds higher at the late phase post-MI. In addition, protein level of cGKIα was also increased upon GYY treatment. A recent study has suggested that H_2S signals through proteins s-sulfhydration (converting cysteine –SH groups to –SSH) and this process augments the activity of the targeted proteins[45]. Following that, various studies have reported protein targets of s-sulfhydration including ion channels[222, 223], p65 subunit of NF-κB that is involved in apoptosis pathway[224] and phospholamban that is involved in cardiac contractility and relaxation[225]. Based on these studies, post-translation modification by H_2S, i.e. s-sulfhydration, could possibly play a role on ANP and cGKIα at protein level. Therefore, s-sulfhydration study using mass-spectometry platform can be used to identify specifically targets of GYY including NPs, cGKIα and apelin that contribute to its cardioprotective effect. Additionally, catalytic activity of cGKIα and PDE can be performed in upon GYY treatment to determine its effect on the downstream effectors of cGMP.

Moreover, GYY also modulated two of the dysregulated miRNAs that are predicted to target apelin. It will be necessary to confirm the direct binding of apelin to miR-31 or miR-221 using gene reporter assay. Validation of other possible predicted targets of miR-31 (including TNNT2) and miR-221 that may play a role in angiogenesis, fibrosis and apoptosis will also be of particular interest to further understand the mechanism of observed therapeutic effect of H_2S-mediated miRNAs modulation. Alternatively, modulating expression of miR-31 and miR-221 expression with mimics or inhibitors and subsequently evaluating the downstream effect on target genes can also be carried out to confirm the presence of direct binding. Additionally, the role of miR-206, miR-214 and miR-199a-3p in GYY-treated rats needs to be further investigated. Validation of targets of these miRNAs that may contribute to GYY-mediated cardioprotective effect is also necessary. Furthermore, there may be other miRNAs that are distinctively modulated by GYY that have not been validated. Thus, validation of these miRNAs and their downstream targets is also necessary and is underway.

In addition to mechanistic studies, it will be of particular clinical relevance to evaluate the effect of delayed treatment of GYY after early LV remodeling and dysfunction has happened. Immediate treatment (30min) after myocardial injury might not be clinically applicable, as in most cases, patients who have heart attack do not receive treatment within that short time frame following the ischemic event. Thus, it is necessary to evaluate whether the cardioprotective effect of GYY can still be observed when its administration is delayed. In addition, it is also important to evaluate the effect of GYY in the chronic (long-term) setting and investigate its effect on HF. Moreover, combination therapy of GYY with inhibitors of miR-31 or miR-221 can be administered after MI to obtain an enhanced synergistic cardioprotective effect. It is important to note, however, that each miRNA may target hundreds of genes; thus, off-target effects should be taken

into careful consideration when one or both of miRNAs is/are inhibited *in vivo*. Lastly, the effect of H_2S deficiency on cardiac function and remodeling can be assessed using *in vitro* and *in vivo* models of myocardial injury in mice with CSE knockout/ overexpression. Importantly, these models might reveal whether slow H_2S release by GYY may really mimic the endogenous H_2S release pattern in physiological conditions and also whether GYY suffices to rescue CSE deficient mice/ cells from ischemic injury.

BIBLIOGRAPHY

1. Pepine CJ and Nichols WW. The pathophysiology of chronic ischemic heart disease. *Clin Cardiol*. 2007;30:I4-9.
2. Miller LW and Missov ED. Epidemiology of heart failure. *Cardiol Clin*. 2001;19:547-55.
3. Health Facts Singapore: "Principal Causes of Death", MOH Website. *http://wwwmohgovsg/content/moh_web/home/statistics/Health_Facts_Singapore/Principal_Causes_of_Deathhtml*. 2014:Health Facts Singapore: "Principal Causes of Death", MOH Website.
4. White HD and Chew DP. Acute myocardial infarction. *Lancet*. 2008;372:570-84.
5. Konstam MA, Kramer DG, Patel AR, Maron MS and Udelson JE. Left ventricular remodeling in heart failure: current concepts in clinical significance and assessment. *JACC Cardiovasc Imaging*. 2011;4:98-108.
6. Mann DL and Bristow MR. Mechanisms and models in heart failure: the biomechanical model and beyond. *Circulation*. 2005;111:2837-49.
7. Tang WH, Shrestha K, Martin MG, Borowski AG, Jasper S, Yandle TG, Richards AM, Klein AL and Troughton RW. Clinical significance of endogenous vasoactive neurohormones in chronic systolic heart failure. *J Card Fail*. 2010;16:635-40.
8. Sigurdsson A, Held P and Swedberg K. Short- and long-term neurohormonal activation following acute myocardial infarction. *Am Heart J*. 1993;126:1068-76.
9. Abraham WT, Greenberg BH and Yancy CW. Pharmacologic therapies across the continuum of left ventricular dysfunction. *Am J Cardiol*. 2008;102:21G-28G.
10. Kemp CD and Conte JV. The pathophysiology of heart failure. *Cardiovasc Pathol*. 2012;21:365-71.
11. Williams RE. The effect of neurohormonal antagonists in reducing heart failure hospitalizations. *Curr Med Res Opin*. 2006;22:139-50.
12. Swedberg K. Importance of neuroendocrine activation in chronic heart failure. Impact on treatment strategies. *Eur J Heart Fail*. 2000;2:229-33.
13. Schnee JM and Hsueh WA. Angiotensin II, adhesion, and cardiac fibrosis. *Cardiovasc Res*. 2000;46:264-8.
14. Leri A, Liu Y, Li B, Fiordaliso F, Malhotra A, Latini R, Kajstura J and Anversa P. Up-regulation of AT(1) and AT(2) receptors in postinfarcted hypertrophied myocytes and stretch-mediated apoptotic cell death. *Am J Pathol*. 2000;156:1663-72.
15. Delcayre C and Swynghedauw B. Molecular mechanisms of myocardial remodeling. The role of aldosterone. *J Mol Cell Cardiol*. 2002;34:1577-84.
16. Rocha R, Rudolph AE, Frierdich GE, Nachowiak DA, Kekec BK, Blomme EA, McMahon EG and Delyani JA. Aldosterone induces a vascular inflammatory phenotype in the rat heart. *Am J Physiol Heart Circ Physiol*. 2002;283:H1802-10.
17. Cea LB. Natriuretic peptide family: new aspects. *Curr Med Chem Cardiovasc Hematol Agents*. 2005;3:87-98.
18. Ellis KL, Newton-Cheh C, Wang TJ, Frampton CM, Doughty RN, Whalley GA, Ellis CJ, Skelton L, Davis N, Yandle TG, Troughton RW, Richards AM and Cameron VA. Association of genetic variation in the natriuretic peptide system with cardiovascular outcomes. *J Mol Cell Cardiol*. 2011;50:695-701.
19. Richards AM. Therapeutic potential of infused cardiac natriuretic peptides in myocardial infarction. *Heart*. 2009;95:1299-300.

20. Haynes WG, Strachan FE and Webb DJ. Endothelin ETA and ETB receptors cause vasoconstriction of human resistance and capacitance vessels in vivo. *Circulation*. 1995;92:357-63.
21. Kurihara H, Yamaoki K, Nagai R, Yoshizumi M, Takaku F, Satoh H, Inui J and Yazaki Y. Endothelin: a potent vasoconstrictor associated with coronary vasospasm. *Life Sci*. 1989;44:1937-43.
22. Huang Y, Zhang H, Shao Z, O'Hara KA, Kopilas MA, Yu L, Netticadan T and Anderson HD. Suppression of endothelin-1-induced cardiac myocyte hypertrophy by PPAR agonists: role of diacylglycerol kinase zeta. *Cardiovasc Res*. 2011;90:267-75.
23. Khan SQ, Dhillon O, Struck J, Quinn P, Morgenthaler NG, Squire IB, Davies JE, Bergmann A and Ng LL. C-terminal pro-endothelin-1 offers additional prognostic information in patients after acute myocardial infarction: Leicester Acute Myocardial Infarction Peptide (LAMP) Study. *Am Heart J*. 2007;154:736-42.
24. Mann DL, Kent RL, Parsons B and Cooper Gt. Adrenergic effects on the biology of the adult mammalian cardiocyte. *Circulation*. 1992;85:790-804.
25. A clinical trial comparing primary coronary angioplasty with tissue plasminogen activator for acute myocardial infarction. The Global Use of Strategies to Open Occluded Coronary Arteries in Acute Coronary Syndromes (GUSTO IIb) Angioplasty Substudy Investigators. *N Engl J Med*. 1997;336:1621-8.
26. Keeley EC, Boura JA and Grines CL. Primary angioplasty versus intravenous thrombolytic therapy for acute myocardial infarction: a quantitative review of 23 randomised trials. *Lancet*. 2003;361:13-20.
27. Rossini R, Senni M, Musumeci G, Ferrazzi P and Gavazzi A. Prevention of left ventricular remodelling after acute myocardial infarction: an update. *Recent Pat Cardiovasc Drug Discov*. 2010;5:196-207.
28. Thai HM, Van HT, Gaballa MA, Goldman S and Raya TE. Effects of AT1 receptor blockade after myocardial infarct on myocardial fibrosis, stiffness, and contractility. *Am J Physiol*. 1999;276:H873-80.
29. Sun Y, Zhang JQ, Zhang J and Ramires FJ. Angiotensin II, transforming growth factor-beta1 and repair in the infarcted heart. *J Mol Cell Cardiol*. 1998;30:1559-69.
30. Nakamura Y, Yoshiyama M, Omura T, Yoshida K, Izumi Y, Takeuchi K, Kim S, Iwao H and Yoshikawa J. Beneficial effects of combination of ACE inhibitor and angiotensin II type 1 receptor blocker on cardiac remodeling in rat myocardial infarction. *Cardiovasc Res*. 2003;57:48-54.
31. Doughty RN, Whalley GA, Walsh HA, Gamble GD, Lopez-Sendon J and Sharpe N. Effects of carvedilol on left ventricular remodeling after acute myocardial infarction: the CAPRICORN Echo Substudy. *Circulation*. 2004;109:201-6.
32. Ibanez B, Macaya C, Sanchez-Brunete V, Pizarro G, Fernandez-Friera L, Mateos A, Fernandez-Ortiz A, Garcia-Ruiz JM, Garcia-Alvarez A, Iniguez A, Jimenez-Borreguero J, Lopez-Romero P, Fernandez-Jimenez R, Goicolea J, Ruiz-Mateos B, Bastante T, Arias M, Iglesias-Vazquez JA, Rodriguez MD, Escalera N, Acebal C, Cabrera JA, Valenciano J, Perez de Prado A, Fernandez-Campos MJ, Casado I, Garcia-Rubira JC, Garcia-Prieto J, Sanz-Rosa D, Cuellas C, Hernandez-Antolin R, Albarran A, Fernandez-Vazquez F, de la Torre-Hernandez JM, Pocock S, Sanz G and Fuster V. Effect of early metoprolol on infarct size in ST-segment-elevation myocardial infarction patients undergoing primary percutaneous coronary intervention: the Effect of Metoprolol in Cardioprotection During an Acute Myocardial Infarction (METOCARD-CNIC) trial. *Circulation*. 2013;128:1495-503.

33. Lamas GA, Flaker GC, Mitchell G, Smith SC, Jr., Gersh BJ, Wun CC, Moye L, Rouleau JL, Rutherford JD, Pfeffer MA and et al. Effect of infarct artery patency on prognosis after acute myocardial infarction. The Survival and Ventricular Enlargement Investigators. *Circulation*. 1995;92:1101-9.
34. Dominguez-Rodriguez A, Abreu-Gonzalez P and Reiter RJ. Cardioprotection and pharmacological therapies in acute myocardial infarction: Challenges in the current era. *World J Cardiol*. 2014;6:100-6.
35. Deedwania PC and Carbajal E. Evidence-based therapy for heart failure. *Med Clin North Am*. 2012;96:915-31.
36. Go AS, Mozaffarian D, Roger VL, Benjamin EJ, Berry JD, Borden WB, Bravata DM, Dai S, Ford ES, Fox CS, Franco S, Fullerton HJ, Gillespie C, Hailpern SM, Heit JA, Howard VJ, Huffman MD, Kissela BM, Kittner SJ, Lackland DT, Lichtman JH, Lisabeth LD, Magid D, Marcus GM, Marelli A, Matchar DB, McGuire DK, Mohler ER, Moy CS, Mussolino ME, Nichol G, Paynter NP, Schreiner PJ, Sorlie PD, Stein J, Turan TN, Virani SS, Wong ND, Woo D and Turner MB. Executive summary: heart disease and stroke statistics--2013 update: a report from the American Heart Association. *Circulation*. 2013;127:143-52.
37. McAllister DA, Halbesma N, Carruthers K, Denvir M and Fox KA. GRACE score predicts heart failure admission following acute coronary syndrome. *Eur Heart J Acute Cardiovasc Care*. 2014.
38. Wang R. Two's company, three's a crowd: can H2S be the third endogenous gaseous transmitter? *Faseb J*. 2002;16:1792-8.
39. Guo W, Cheng ZY and Zhu YZ. Hydrogen sulfide and translational medicine. *Acta Pharmacol Sin*. 2013;34:1284-91.
40. Liu YH, Lu M, Hu LF, Wong PT, Webb GD and Bian JS. Hydrogen sulfide in the mammalian cardiovascular system. *Antioxid Redox Signal*. 2012;17:141-85.
41. Kabil O and Banerjee R. Redox biochemistry of hydrogen sulfide. *J Biol Chem*. 2010;285:21903-7.
42. Singh S and Banerjee R. PLP-dependent H(2)S biogenesis. *Biochim Biophys Acta*. 2011;1814:1518-27.
43. Li L, Rose P and Moore PK. Hydrogen sulfide and cell signaling. *Annu Rev Pharmacol Toxicol*. 2011;51:169-87.
44. Bian JS, Yong QC, Pan TT, Feng ZN, Ali MY, Zhou S and Moore PK. Role of hydrogen sulfide in the cardioprotection caused by ischemic preconditioning in the rat heart and cardiac myocytes. *J Pharmacol Exp Ther*. 2006;316:670-8.
45. Mustafa AK, Gadalla MM, Sen N, Kim S, Mu W, Gazi SK, Barrow RK, Yang G, Wang R and Snyder SH. H2S signals through protein S-sulfhydration. *Sci Signal*. 2009;2:ra72.
46. Li L, Salto-Tellez M, Tan CH, Whiteman M and Moore PK. GYY4137, a novel hydrogen sulfide-releasing molecule, protects against endotoxic shock in the rat. *Free Radic Biol Med*. 2009;47:103-13.
47. Aggarwal BB, Kunnumakkara AB, Harikumar KB, Gupta SR, Tharakan ST, Koca C, Dey S and Sung B. Signal transducer and activator of transcription-3, inflammation, and cancer: how intimate is the relationship? *Ann N Y Acad Sci*. 2009;1171:59-76.
48. Calvert JW, Jha S, Gundewar S, Elrod JW, Ramachandran A, Pattillo CB, Kevil CG and Lefer DJ. Hydrogen sulfide mediates cardioprotection through Nrf2 signaling. *Circ Res*. 2009;105:365-74.

49. Yong QC, Lee SW, Foo CS, Neo KL, Chen X and Bian JS. Endogenous hydrogen sulphide mediates the cardioprotection induced by ischemic postconditioning. *Am J Physiol Heart Circ Physiol*. 2008;295:H1330-H1340.
50. Zhao W, Zhang J, Lu Y and Wang R. The vasorelaxant effect of H(2)S as a novel endogenous gaseous K(ATP) channel opener. *Embo J*. 2001;20:6008-16.
51. Hosoki R, Matsuki N and Kimura H. The possible role of hydrogen sulfide as an endogenous smooth muscle relaxant in synergy with nitric oxide. *Biochem Biophys Res Commun*. 1997;237:527-31.
52. Cheng Y, Ndisang JF, Tang G, Cao K and Wang R. Hydrogen sulfide-induced relaxation of resistance mesenteric artery beds of rats. *Am J Physiol Heart Circ Physiol*. 2004;287:H2316-23.
53. Li L, Whiteman M, Guan YY, Neo KL, Cheng Y, Lee SW, Zhao Y, Baskar R, Tan CH and Moore PK. Characterization of a novel, water-soluble hydrogen sulfide-releasing molecule (GYY4137): new insights into the biology of hydrogen sulfide. *Circulation*. 2008;117:2351-60.
54. Zhang Z, Huang H, Liu P, Tang C and Wang J. Hydrogen sulfide contributes to cardioprotection during ischemia-reperfusion injury by opening K ATP channels. *Can J Physiol Pharmacol*. 2007;85:1248-53.
55. Ji Y, Pang QF, Xu G, Wang L, Wang JK and Zeng YM. Exogenous hydrogen sulfide postconditioning protects isolated rat hearts against ischemia-reperfusion injury. *Eur J Pharmacol*. 2008;587:1-7.
56. Johansen D, Ytrehus K and Baxter GF. Exogenous hydrogen sulfide (H2S) protects against regional myocardial ischemia-reperfusion injury--Evidence for a role of K ATP channels. *Basic Res Cardiol*. 2006;101:53-60.
57. Kimura Y, Goto Y and Kimura H. Hydrogen sulfide increases glutathione production and suppresses oxidative stress in mitochondria. *Antioxid Redox Signal*. 2010;12:1-13.
58. Rossoni G, Sparatore A, Tazzari V, Manfredi B, Del Soldato P and Berti F. The hydrogen sulphide-releasing derivative of diclofenac protects against ischaemia-reperfusion injury in the isolated rabbit heart. *Br J Pharmacol*. 2008;153:100-9.
59. Geng B, Chang L, Pan C, Qi Y, Zhao J, Pang Y, Du J and Tang C. Endogenous hydrogen sulfide regulation of myocardial injury induced by isoproterenol. *Biochem Biophys Res Commun*. 2004;318:756-63.
60. Jiang HL, Wu HC, Li ZL, Geng B and Tang CS. [Changes of the new gaseous transmitter H2S in patients with coronary heart disease]. *Di Yi Jun Yi Da Xue Xue Bao*. 2005;25:951-4.
61. Zhu YZ, Wang ZJ, Ho P, Loke YY, Zhu YC, Huang SH, Tan CS, Whiteman M, Lu J and Moore PK. Hydrogen sulfide and its possible roles in myocardial ischemia in experimental rats. *J Appl Physiol (1985)*. 2007;102:261-8.
62. Pan TT, Chen YQ and Bian JS. All in the timing: a comparison between the cardioprotection induced by H2S preconditioning and post-infarction treatment. *Eur J Pharmacol*. 2009;616:160-5.
63. Qipshidze N, Metreveli N, Mishra PK, Lominadze D and Tyagi SC. Hydrogen sulfide mitigates cardiac remodeling during myocardial infarction via improvement of angiogenesis. *Int J Biol Sci*. 2012;8:430-41.
64. Cucoranu I, Clempus R, Dikalova A, Phelan PJ, Ariyan S, Dikalov S and Sorescu D. NAD(P)H oxidase 4 mediates transforming growth factor-beta1-induced differentiation of cardiac fibroblasts into myofibroblasts. *Circ Res*. 2005;97:900-7.

65. Pan LL, Liu XH, Shen YQ, Wang NZ, Xu J, Wu D, Xiong QH, Deng HY, Huang GY and Zhu YZ. Inhibition of NADPH oxidase 4-related signaling by sodium hydrosulfide attenuates myocardial fibrotic response. *Int J Cardiol*. 2013;168:3770-8.
66. Zhang Y, Li H, Zhao G, Sun A, Zong NC, Li Z, Zhu H, Zou Y, Yang X and Ge J. Hydrogen sulfide attenuates the recruitment of CD11b(+)Gr-1(+) myeloid cells and regulates Bax/Bcl-2 signaling in myocardial ischemia injury. *Sci Rep*. 2014;4:4774.
67. Zhao Y, Wang H and Xian M. Cysteine-activated hydrogen sulfide (H2S) donors. *J Am Chem Soc*. 2011;133:15-7.
68. Benavides GA, Squadrito GL, Mills RW, Patel HD, Isbell TS, Patel RP, Darley-Usmar VM, Doeller JE and Kraus DW. Hydrogen sulfide mediates the vasoactivity of garlic. *Proc Natl Acad Sci U S A*. 2007;104:17977-82.
69. Amagase H. Clarifying the real bioactive constituents of garlic. *J Nutr*. 2006;136:716S-725S.
70. Gu X and Zhu YZ. Therapeutic applications of organosulfur compounds as novel hydrogen sulfide donors and/or mediators. *Expert Rev Clin Pharmacol*. 2011;4:123-33.
71. Wang Q, Wang XL, Liu HR, Rose P and Zhu YZ. Protective effects of cysteine analogues on acute myocardial ischemia: novel modulators of endogenous H(2)S production. *Antioxid Redox Signal*. 2010;12:1155-65.
72. Chuah SC, Moore PK and Zhu YZ. S-allylcysteine mediates cardioprotection in an acute myocardial infarction rat model via a hydrogen sulfide-mediated pathway. *Am J Physiol Heart Circ Physiol*. 2007;293:H2693-701.
73. Li L, Rossoni G, Sparatore A, Lee LC, Del Soldato P and Moore PK. Anti-inflammatory and gastrointestinal effects of a novel diclofenac derivative. *Free Radic Biol Med*. 2007;42:706-19.
74. Sidhapuriwala J, Li L, Sparatore A, Bhatia M and Moore PK. Effect of S-diclofenac, a novel hydrogen sulfide releasing derivative, on carrageenan-induced hindpaw oedema formation in the rat. *Eur J Pharmacol*. 2007;569:149-54.
75. Baskar R, Sparatore A, Del Soldato P and Moore PK. Effect of S-diclofenac, a novel hydrogen sulfide releasing derivative inhibit rat vascular smooth muscle cell proliferation. *Eur J Pharmacol*. 2008;594:1-8.
76. Whiteman M, Li L, Rose P, Tan CH, Parkinson DB and Moore PK. The effect of hydrogen sulfide donors on lipopolysaccharide-induced formation of inflammatory mediators in macrophages. *Antioxid Redox Signal*. 2010;12:1147-54.
77. Bass SE, Sienkiewicz P, Macdonald CJ, Cheng RY, Sparatore A, Del Soldato P, Roberts DD, Moody TW, Wink DA and Yeh GC. Novel dithiolethione-modified nonsteroidal anti-inflammatory drugs in human hepatoma HepG2 and colon LS180 cells. *Clin Cancer Res*. 2009;15:1964-72.
78. Whiteman M and Winyard PG. Hydrogen sulfide and inflammation: the good, the bad, the ugly and the promising. *Expert Rev Clin Pharmacol*. 2011;4:13-32.
79. Sparatore A, Santus G, Giustarini D, Rossi R and Del Soldato P. Therapeutic potential of new hydrogen sulfide-releasing hybrids. *Expert Rev Clin Pharmacol*. 2011;4:109-21.
80. Li L, Fox B, Keeble J, Salto-Tellez M, Winyard PG, Wood ME, Moore PK and Whiteman M. The complex effects of the slow-releasing hydrogen sulfide donor GYY4137 in a model of acute joint inflammation and in human cartilage cells. *J Cell Mol Med*. 2013;17:365-76.

81. Lee ZW, Zhou J, Chen CS, Zhao Y, Tan CH, Li L, Moore PK and Deng LW. The slow-releasing hydrogen sulfide donor, GYY4137, exhibits novel anti-cancer effects in vitro and in vivo. *PLoS One*. 2011;6:e21077.
82. Robinson H and Wray S. A new slow releasing, H(2)S generating compound, GYY4137 relaxes spontaneous and oxytocin-stimulated contractions of human and rat pregnant myometrium. *PLoS One*. 2012;7:e46278.
83. Vadivel A, Alphonse RS, Ionescu L, Machado DS, O'Reilly M, Eaton F, Haromy A, Michelakis ED and Thebaud B. Exogenous hydrogen sulfide (H2S) protects alveolar growth in experimental O2-induced neonatal lung injury. *PLoS One*. 2014;9:e90965.
84. Grambow E, Mueller-Graf F, Delyagina E, Frank M, Kuhla A and Vollmar B. Effect of the hydrogen sulfide donor GYY4137 on platelet activation and microvascular thrombus formation in mice. *Platelets*. 2013.
85. Liu Z, Han Y, Li L, Lu H, Meng G, Li X, Shirhan M, Peh MT, Xie L, Zhou S, Wang X, Chen Q, Dai W, Tan CH, Pan S, Moore PK and Ji Y. The hydrogen sulfide donor, GYY4137, exhibits anti-atherosclerotic activity in high fat fed apolipoprotein E(-/-) mice. *Br J Pharmacol*. 2013;169:1795-809.
86. Wei WB, Hu X, Zhuang XD, Liao LZ and Li WD. GYY4137, a novel hydrogen sulfide-releasing molecule, likely protects against high glucose-induced cytotoxicity by activation of the AMPK/mTOR signal pathway in H9c2 cells. *Mol Cell Biochem*. 2014;389:249-56.
87. Nishikimi T, Maeda N and Matsuoka H. The role of natriuretic peptides in cardioprotection. *Cardiovasc Res*. 2006;69:318-28.
88. Chopra S, Cherian D, Verghese PP and Jacob JJ. Physiology and clinical significance of natriuretic hormones. *Indian J Endocrinol Metab*. 2013;17:83-90.
89. Yan W, Wu F, Morser J and Wu Q. Corin, a transmembrane cardiac serine protease, acts as a pro-atrial natriuretic peptide-converting enzyme. *Proc Natl Acad Sci U S A*. 2000;97:8525-9.
90. Thibault G, Charbonneau C, Bilodeau J, Schiffrin EL and Garcia R. Rat brain natriuretic peptide is localized in atrial granules and released into the circulation. *Am J Physiol*. 1992;263:R301-9.
91. Thuerauf DJ, Hanford DS and Glembotski CC. Regulation of rat brain natriuretic peptide transcription. A potential role for GATA-related transcription factors in myocardial cell gene expression. *J Biol Chem*. 1994;269:17772-5.
92. Vanneste Y, Michel A, Dimaline R, Najdovski T and Deschodt-Lanckman M. Hydrolysis of alpha-human atrial natriuretic peptide in vitro by human kidney membranes and purified endopeptidase-24.11. Evidence for a novel cleavage site. *Biochem J*. 1988;254:531-7.
93. Pankow K, Wang Y, Gembardt F, Krause E, Sun X, Krause G, Schultheiss HP, Siems WE and Walther T. Successive action of meprin A and neprilysin catabolizes B-type natriuretic peptide. *Circ Res*. 2007;101:875-82.
94. Takimoto E. Cyclic GMP-dependent signaling in cardiac myocytes. *Circ J*. 2012;76:1819-25.
95. Tsai EJ and Kass DA. Cyclic GMP signaling in cardiovascular pathophysiology and therapeutics. *Pharmacol Ther*. 2009;122:216-38.
96. Horio T, Nishikimi T, Yoshihara F, Matsuo H, Takishita S and Kangawa K. Inhibitory regulation of hypertrophy by endogenous atrial natriuretic peptide in cultured cardiac myocytes. *Hypertension*. 2000;35:19-24.

97. Holtwick R, van Eickels M, Skryabin BV, Baba HA, Bubikat A, Begrow F, Schneider MD, Garbers DL and Kuhn M. Pressure-independent cardiac hypertrophy in mice with cardiomyocyte-restricted inactivation of the atrial natriuretic peptide receptor guanylyl cyclase-A. *J Clin Invest*. 2003;111:1399-407.
98. Kishimoto I, Rossi K and Garbers DL. A genetic model provides evidence that the receptor for atrial natriuretic peptide (guanylyl cyclase-A) inhibits cardiac ventricular myocyte hypertrophy. *Proc Natl Acad Sci U S A*. 2001;98:2703-6.
99. Zahabi A, Picard S, Fortin N, Reudelhuber TL and Deschepper CF. Expression of constitutively active guanylate cyclase in cardiomyocytes inhibits the hypertrophic effects of isoproterenol and aortic constriction on mouse hearts. *J Biol Chem*. 2003;278:47694-9.
100. Lin X, Hanze J, Heese F, Sodmann R and Lang RE. Gene expression of natriuretic peptide receptors in myocardial cells. *Circ Res*. 1995;77:750-8.
101. Cao L and Gardner DG. Natriuretic peptides inhibit DNA synthesis in cardiac fibroblasts. *Hypertension*. 1995;25:227-34.
102. Maki T, Horio T, Yoshihara F, Suga S, Takeo S, Matsuo H and Kangawa K. Effect of neutral endopeptidase inhibitor on endogenous atrial natriuretic peptide as a paracrine factor in cultured cardiac fibroblasts. *Br J Pharmacol*. 2000;131:1204-10.
103. Franco V, Chen YF, Oparil S, Feng JA, Wang D, Hage F and Perry G. Atrial natriuretic peptide dose-dependently inhibits pressure overload-induced cardiac remodeling. *Hypertension*. 2004;44:746-50.
104. Takahashi T, Allen PD and Izumo S. Expression of A-, B-, and C-type natriuretic peptide genes in failing and developing human ventricles. Correlation with expression of the Ca(2+)-ATPase gene. *Circ Res*. 1992;71:9-17.
105. Chen H, Levine YC, Golan DE, Michel T and Lin AJ. Atrial natriuretic peptide-initiated cGMP pathways regulate vasodilator-stimulated phosphoprotein phosphorylation and angiogenesis in vascular endothelium. *J Biol Chem*. 2008;283:4439-47.
106. Kuhn M, Volker K, Schwarz K, Carbajo-Lozoya J, Flogel U, Jacoby C, Stypmann J, van Eickels M, Gambaryan S, Hartmann M, Werner M, Wieland T, Schrader J and Baba HA. The natriuretic peptide/guanylyl cyclase--a system functions as a stress-responsive regulator of angiogenesis in mice. *J Clin Invest*. 2009;119:2019-30.
107. Shmilovich H, Ben-Shoshan J, Tal R, Afek A, Barshack I, Maysel-Auslander S, Harats D, Keren G and George J. B-type natriuretic peptide enhances vasculogenesis by promoting number and functional properties of early endothelial progenitor cells. *Tissue Eng Part A*. 2009;15:2741-9.
108. Yamahara K, Itoh H, Chun TH, Ogawa Y, Yamashita J, Sawada N, Fukunaga Y, Sone M, Yurugi-Kobayashi T, Miyashita K, Tsujimoto H, Kook H, Feil R, Garbers DL, Hofmann F and Nakao K. Significance and therapeutic potential of the natriuretic peptides/cGMP/cGMP-dependent protein kinase pathway in vascular regeneration. *Proc Natl Acad Sci U S A*. 2003;100:3404-9.
109. Tokudome T, Kishimoto I, Yamahara K, Osaki T, Minamino N, Horio T, Sawai K, Kawano Y, Miyazato M, Sata M, Kohno M, Nakao K and Kangawa K. Impaired recovery of blood flow after hind-limb ischemia in mice lacking guanylyl cyclase-A, a receptor for atrial and brain natriuretic peptides. *Arterioscler Thromb Vasc Biol*. 2009;29:1516-21.
110. Saito Y, Nakao K, Nishimura K, Sugawara A, Okumura K, Obata K, Sonoda R, Ban T, Yasue H and Imura H. Clinical application of atrial natriuretic polypeptide in patients

with congestive heart failure: beneficial effects on left ventricular function. *Circulation*. 1987;76:115-24.
111. Cody RJ, Atlas SA, Laragh JH, Kubo SH, Covit AB, Ryman KS, Shaknovich A, Pondolfino K, Clark M, Camargo MJ and et al. Atrial natriuretic factor in normal subjects and heart failure patients. Plasma levels and renal, hormonal, and hemodynamic responses to peptide infusion. *J Clin Invest*. 1986;78:1362-74.
112. Crozier IG, Nicholls MG, Ikram H, Espiner EA, Gomez HJ and Warner NJ. Haemodynamic effects of atrial peptide infusion in heart failure. *Lancet*. 1986;2:1242-5.
113. Saito Y. Roles of atrial natriuretic peptide and its therapeutic use. *J Cardiol*. 2010;56:262-70.
114. Hayashi M, Tsutamoto T, Wada A, Maeda K, Mabuchi N, Tsutsui T, Horie H, Ohnishi M and Kinoshita M. Intravenous atrial natriuretic peptide prevents left ventricular remodeling in patients with first anterior acute myocardial infarction. *J Am Coll Cardiol*. 2001;37:1820-6.
115. Kitakaze M, Asakura M, Kim J, Shintani Y, Asanuma H, Hamasaki T, Seguchi O, Myoishi M, Minamino T, Ohara T, Nagai Y, Nanto S, Watanabe K, Fukuzawa S, Hirayama A, Nakamura N, Kimura K, Fujii K, Ishihara M, Saito Y, Tomoike H and Kitamura S. Human atrial natriuretic peptide and nicorandil as adjuncts to reperfusion treatment for acute myocardial infarction (J-WIND): two randomised trials. *Lancet*. 2007;370:1483-93.
116. Krol J, Loedige I and Filipowicz W. The widespread regulation of microRNA biogenesis, function and decay. *Nat Rev Genet*. 2010;11:597-610.
117. Nelson P, Kiriakidou M, Sharma A, Maniataki E and Mourelatos Z. The microRNA world: small is mighty. *Trends Biochem Sci*. 2003;28:534-40.
118. Lagos-Quintana M, Rauhut R, Yalcin A, Meyer J, Lendeckel W and Tuschl T. Identification of tissue-specific microRNAs from mouse. *Curr Biol*. 2002;12:735-9.
119. Jansson MD and Lund AH. MicroRNA and cancer. *Mol Oncol*. 2012.
120. van Rooij E, Marshall WS and Olson EN. Toward microRNA-based therapeutics for heart disease: the sense in antisense. *Circ Res*. 2008;103:919-28.
121. Shan ZX, Lin QX, Fu YH, Deng CY, Zhou ZL, Zhu JN, Liu XY, Zhang YY, Li Y, Lin SG and Yu XY. Upregulated expression of miR-1/miR-206 in a rat model of myocardial infarction. *Biochem Biophys Res Commun*. 2009;381:597-601.
122. Lu Y, Zhang Y, Shan H, Pan Z, Li X, Li B, Xu C, Zhang B, Zhang F, Dong D, Song W, Qiao G and Yang B. MicroRNA-1 downregulation by propranolol in a rat model of myocardial infarction: a new mechanism for ischaemic cardioprotection. *Cardiovasc Res*. 2009;84:434-41.
123. Bonauer A, Carmona G, Iwasaki M, Mione M, Koyanagi M, Fischer A, Burchfield J, Fox H, Doebele C, Ohtani K, Chavakis E, Potente M, Tjwa M, Urbich C, Zeiher AM and Dimmeler S. MicroRNA-92a controls angiogenesis and functional recovery of ischemic tissues in mice. *Science*. 2009;324:1710-3.
124. Hu S, Huang M, Li Z, Jia F, Ghosh Z, Lijkwan MA, Fasanaro P, Sun N, Wang X, Martelli F, Robbins RC and Wu JC. MicroRNA-210 as a novel therapy for treatment of ischemic heart disease. *Circulation*. 2010;122:S124-31.
125. Liang H, Zhang C, Ban T, Liu Y, Mei L, Piao X, Zhao D, Lu Y, Chu W and Yang B. A novel reciprocal loop between microRNA-21 and TGFbetaRIII is involved in cardiac fibrosis. *Int J Biochem Cell Biol*. 2012;44:2152-2160.
126. Pan Z, Sun X, Shan H, Wang N, Wang J, Ren J, Feng S, Xie L, Lu C, Yuan Y, Zhang Y, Wang Y, Lu Y and Yang B. MicroRNA-101 inhibited postinfarct cardiac fibrosis and

improved left ventricular compliance via the FBJ osteosarcoma oncogene/transforming growth factor-beta1 pathway. *Circulation*. 2012;126:840-50.
127. Johnnidis JB, Harris MH, Wheeler RT, Stehling-Sun S, Lam MH, Kirak O, Brummelkamp TR, Fleming MD and Camargo FD. Regulation of progenitor cell proliferation and granulocyte function by microRNA-223. *Nature*. 2008;451:1125-9.
128. van Rooij E, Sutherland LB, Thatcher JE, DiMaio JM, Naseem RH, Marshall WS, Hill JA and Olson EN. Dysregulation of microRNAs after myocardial infarction reveals a role of miR-29 in cardiac fibrosis. *Proc Natl Acad Sci U S A*. 2008;105:13027-32.
129. Ai J, Zhang R, Li Y, Pu J, Lu Y, Jiao J, Li K, Yu B, Li Z, Wang R, Wang L, Li Q, Wang N, Shan H and Yang B. Circulating microRNA-1 as a potential novel biomarker for acute myocardial infarction. *Biochem Biophys Res Commun*. 2010;391:73-7.
130. D'Alessandra Y, Devanna P, Limana F, Straino S, Di Carlo A, Brambilla PG, Rubino M, Carena MC, Spazzafumo L, De Simone M, Micheli B, Biglioli P, Achilli F, Martelli F, Maggiolini S, Marenzi G, Pompilio G and Capogrossi MC. Circulating microRNAs are new and sensitive biomarkers of myocardial infarction. *Eur Heart J*. 2010;31:2765-73.
131. Wang GK, Zhu JQ, Zhang JT, Li Q, Li Y, He J, Qin YW and Jing Q. Circulating microRNA: a novel potential biomarker for early diagnosis of acute myocardial infarction in humans. *Eur Heart J*. 2010;31:659-66.
132. Szabo C. Hydrogen sulphide and its therapeutic potential. *Nat Rev Drug Discov*. 2007;6:917-35.
133. White HD, Norris RM, Brown MA, Brandt PW, Whitlock RM and Wild CJ. Left ventricular end-systolic volume as the major determinant of survival after recovery from myocardial infarction. *Circulation*. 1987;76:44-51.
134. Jugdutt BI. Remodeling of the myocardium and potential targets in the collagen degradation and synthesis pathways. *Curr Drug Targets Cardiovasc Haematol Disord*. 2003;3:1-30.
135. Azizi Y, Faghihi M, Imani A, Roghani M and Nazari A. Post-infarct treatment with [Pyr1]-apelin-13 reduces myocardial damage through reduction of oxidative injury and nitric oxide enhancement in the rat model of myocardial infarction. *Peptides*. 2013;46:76-82.
136. Calvert JW, Elston M, Nicholson CK, Gundewar S, Jha S, Elrod JW, Ramachandran A and Lefer DJ. Genetic and pharmacologic hydrogen sulfide therapy attenuates ischemia-induced heart failure in mice. *Circulation*. 2010;122:11-9.
137. Yancy CW, Jessup M, Bozkurt B, Butler J, Casey DE, Jr., Drazner MH, Fonarow GC, Geraci SA, Horwich T, Januzzi JL, Johnson MR, Kasper EK, Levy WC, Masoudi FA, McBride PE, McMurray JJ, Mitchell JE, Peterson PN, Riegel B, Sam F, Stevenson LW, Tang WH, Tsai EJ and Wilkoff BL. 2013 ACCF/AHA guideline for the management of heart failure: a report of the American College of Cardiology Foundation/American Heart Association Task Force on Practice Guidelines. *J Am Coll Cardiol*. 2013;62:e147-239.
138. Laggner H, Hermann M, Esterbauer H, Muellner MK, Exner M, Gmeiner BM and Kapiotis S. The novel gaseous vasorelaxant hydrogen sulfide inhibits angiotensin-converting enzyme activity of endothelial cells. *J Hypertens*. 2007;25:2100-4.
139. Liu YH, Lu M, Xie ZZ, Hua F, Xie L, Gao JH, Koh YH and Bian JS. Hydrogen sulfide prevents heart failure development via inhibition of renin release from mast cells in isoproterenol-treated rats. *Antioxid Redox Signal*. 2014;20:759-69.
140. Liu J, Hao DD, Zhang JS and Zhu YC. Hydrogen sulphide inhibits cardiomyocyte hypertrophy by up-regulating miR-133a. *Biochem Biophys Res Commun*. 2011;413:342-7.

141. Toldo S, Das A, Mezzaroma E, Chau VQ, Marchetti C, Durrant D, Samidurai A, Van Tassell BW, Yin C, Ockaili RA, Vigneshwar N, Mukhopadhyay ND, Kukreja RC, Abbate A and Salloum FN. Induction of MicroRNA-21 With Exogenous Hydrogen Sulfide Attenuates Myocardial Ischemic and Inflammatory Injury in Mice. *Circ Cardiovasc Genet*. 2014;7:311-20.
142. Bayat H, Swaney JS, Ander AN, Dalton N, Kennedy BP, Hammond HK and Roth DM. Progressive heart failure after myocardial infarction in mice. *Basic Res Cardiol*. 2002;97:206-13.
143. Gould KE, Taffet GE, Michael LH, Christie RM, Konkol DL, Pocius JS, Zachariah JP, Chaupin DF, Daniel SL, Sandusky GE, Jr., Hartley CJ and Entman ML. Heart failure and greater infarct expansion in middle-aged mice: a relevant model for postinfarction failure. *Am J Physiol Heart Circ Physiol*. 2002;282:H615-21.
144. Bialik GM, Abassi ZA, Hammel I, Winaver J and Lewinson D. Evaluation of atrial natriuretic peptide and brain natriuretic peptide in atrial granules of rats with experimental congestive heart failure. *J Histochem Cytochem*. 2001;49:1293-300.
145. Patten RD and Hall-Porter MR. Small animal models of heart failure: development of novel therapies, past and present. *Circ Heart Fail*. 2009;2:138-44.
146. Redfield MM. Epidemiology and pathophysiology of heart failure. *Curr Cardiol Rep*. 2000;2:179-80.
147. Gomes AC, Falcao-Pires I, Pires AL, Bras-Silva C and Leite-Moreira AF. Rodent models of heart failure: an updated review. *Heart Fail Rev*. 2013;18:219-49.
148. Whiteman M, Le Trionnaire S, Chopra M, Fox B and Whatmore J. Emerging role of hydrogen sulfide in health and disease: critical appraisal of biomarkers and pharmacological tools. *Clin Sci (Lond)*. 2011;121:459-88.
149. Shen X, Pattillo CB, Pardue S, Bir SC, Wang R and Kevil CG. Measurement of plasma hydrogen sulfide in vivo and in vitro. *Free Radic Biol Med*. 2011;50:1021-31.
150. Fujita S, Shimojo N, Terasaki F, Otsuka K, Hosotani N, Kohda Y, Tanaka T, Nishioka T, Yoshida T, Hiroe M, Kitaura Y, Ishizaka N and Imanaka-Yoshida K. Atrial natriuretic peptide exerts protective action against angiotensin II-induced cardiac remodeling by attenuating inflammation via endothelin-1/endothelin receptor A cascade. *Heart Vessels*. 2013;28:646-57.
151. Takahashi N, Saito Y, Kuwahara K, Harada M, Kishimoto I, Ogawa Y, Kawakami R, Nakagawa Y, Nakanishi M and Nakao K. Angiotensin II-induced ventricular hypertrophy and extracellular signal-regulated kinase activation are suppressed in mice overexpressing brain natriuretic peptide in circulation. *Hypertens Res*. 2003;26:847-53.
152. Rosenkranz AC, Hood SG, Woods RL, Dusting GJ and Ritchie RH. B-type natriuretic peptide prevents acute hypertrophic responses in the diabetic rat heart: importance of cyclic GMP. *Diabetes*. 2003;52:2389-95.
153. Kasama S, Furuya M, Toyama T, Ichikawa S and Kurabayashi M. Effect of atrial natriuretic peptide on left ventricular remodelling in patients with acute myocardial infarction. *Eur Heart J*. 2008;29:1485-94.
154. Mori T, Chen YF, Feng JA, Hayashi T, Oparil S and Perry GJ. Volume overload results in exaggerated cardiac hypertrophy in the atrial natriuretic peptide knockout mouse. *Cardiovasc Res*. 2004;61:771-9.
155. Wang D, Gladysheva IP, Fan TH, Sullivan R, Houng AK and Reed GL. Atrial natriuretic peptide affects cardiac remodeling, function, heart failure, and survival in a mouse model of dilated cardiomyopathy. *Hypertension*. 2014;63:514-9.

156. Rastegar MA, Vegh A, Papp JG and Parratt JR. Atrial natriuretic peptide reduces the severe consequences of coronary artery occlusion in anaesthetized dogs. *Cardiovasc Drugs Ther*. 2000;14:471-9.
157. Ren B, Shen Y, Shao H, Qian J, Wu H and Jing H. Brain natriuretic peptide limits myocardial infarct size dependent of nitric oxide synthase in rats. *Clin Chim Acta*. 2007;377:83-7.
158. George I, Xydas S, Klotz S, Hay I, Ng C, Chang J, Xu K, Li Z, Protter AA, Wu EX, Oz MC and Wang J. Long-term effects of B-type natriuretic peptide infusion after acute myocardial infarction in a rat model. *J Cardiovasc Pharmacol*. 2010;55:14-20.
159. George I, Morrow B, Xu K, Yi GH, Holmes J, Wu EX, Li Z, Protter AA, Oz MC and Wang J. Prolonged effects of B-type natriuretic peptide infusion on cardiac remodeling after sustained myocardial injury. *Am J Physiol Heart Circ Physiol*. 2009;297:H708-17.
160. He J, Chen Y, Huang Y, Yao F, Wu Z, Chen S, Wang L, Xiao P, Dai G, Meng R, Zhang C, Tang L and Li Z. Effect of long-term B-type natriuretic peptide treatment on left ventricular remodeling and function after myocardial infarction in rats. *Eur J Pharmacol*. 2009;602:132-7.
161. Hillock RJ, Frampton CM, Yandle TG, Troughton RW, Lainchbury JG and Richards AM. B-type natriuretic peptide infusions in acute myocardial infarction. *Heart*. 2008;94:617-22.
162. Kuga H, Ogawa K, Oida A, Taguchi I, Nakatsugawa M, Hoshi T, Sugimura H, Abe S and Kaneko N. Administration of atrial natriuretic peptide attenuates reperfusion phenomena and preserves left ventricular regional wall motion after direct coronary angioplasty for acute myocardial infarction. *Circ J*. 2003;67:443-8.
163. Kyriakides ZS, Sbarouni E, Antoniadis A, Iliodromitis EK, Mitropoulos D and Kremastinos DT. Atrial natriuretic peptide augments coronary collateral blood flow: a study during coronary angioplasty. *Clin Cardiol*. 1998;21:737-42.
164. Okawa H, Horimoto H, Mieno S, Nomura Y, Yoshida M and Shinjiro S. Preischemic infusion of alpha-human atrial natriuretic peptide elicits myoprotective effects against ischemia reperfusion in isolated rat hearts. *Mol Cell Biochem*. 2003;248:171-7.
165. Koga H, Hagiwara S, Kusaka J, Matsumoto S, Nishida T, Yokoi I and Noguchi T. Human atrial natriuretic peptide attenuates renal ischemia-reperfusion injury. *J Surg Res*. 2012;173:348-53.
166. Takagi G, Kiuchi K, Endo T, Yamamoto T, Sato N, Nejima J and Takano T. Alpha-human atrial natriuretic peptide, carperitide, reduces infarct size but not arrhythmias after coronary occlusion/reperfusion in dogs. *J Cardiovasc Pharmacol*. 2000;36:22-30.
167. Wang W, McKinnie SM, Patel VB, Haddad G, Wang Z, Zhabyeyev P, Das SK, Basu R, McLean B, Kandalam V, Penninger JM, Kassiri Z, Vederas JC, Murray AG and Oudit GY. Loss of Apelin exacerbates myocardial infarction adverse remodeling and ischemia-reperfusion injury: therapeutic potential of synthetic Apelin analogues. *J Am Heart Assoc*. 2013;2:e000249.
168. Pchejetski D, Foussal C, Alfarano C, Lairez O, Calise D, Guilbeau-Frugier C, Schaak S, Seguelas MH, Wanecq E, Valet P, Parini A and Kunduzova O. Apelin prevents cardiac fibroblast activation and collagen production through inhibition of sphingosine kinase 1. *Eur Heart J*. 2012;33:2360-9.
169. Pisarenko OI, Serebriakova LI, Pelogeikina Iu A, Studneva IM, Kkhatri DN, Tskitishvili OV, Bespalova Zh D, Az'muko AA, Sidorova MV, Pal'keeva ME and Chazov EI.

[Involvement of NO-dependent mechanisms of apelin action in myocardial protection against ischemia/reperfusion damage]. *Kardiologiia*. 2012;52:52-8.
170. Zhang BH, Guo CX, Wang HX, Lu LQ, Wang YJ, Zhang LK, Du FH and Zeng XJ. Cardioprotective effects of adipokine apelin on myocardial infarction. *Heart Vessels*. 2013.
171. Li L, Zeng H and Chen JX. Apelin-13 increases myocardial progenitor cells and improves repair postmyocardial infarction. *Am J Physiol Heart Circ Physiol*. 2012;303:H605-18.
172. Sato T, Suzuki T, Watanabe H, Kadowaki A, Fukamizu A, Liu PP, Kimura A, Ito H, Penninger JM, Imai Y and Kuba K. Apelin is a positive regulator of ACE2 in failing hearts. *J Clin Invest*. 2013;123:5203-11.
173. Wang X, Wang Q, Guo W and Zhu YZ. Hydrogen sulfide attenuates cardiac dysfunction in a rat model of heart failure: a mechanism through cardiac mitochondrial protection. *Biosci Rep*. 2011;31:87-98.
174. Kondo K, Bhushan S, King AL, Prabhu SD, Hamid T, Koenig S, Murohara T, Predmore BL, Gojon G, Sr., Gojon G, Jr., Wang R, Karusula N, Nicholson CK, Calvert JW and Lefer DJ. H(2)S protects against pressure overload-induced heart failure via upregulation of endothelial nitric oxide synthase. *Circulation*. 2013;127:1116-27.
175. Coletta C, Papapetropoulos A, Erdelyi K, Olah G, Modis K, Panopoulos P, Asimakopoulou A, Gero D, Sharina I, Martin E and Szabo C. Hydrogen sulfide and nitric oxide are mutually dependent in the regulation of angiogenesis and endothelium-dependent vasorelaxation. *Proc Natl Acad Sci U S A*. 2012;109:9161-6.
176. Bir SC, Kolluru GK, McCarthy P, Shen X, Pardue S, Pattillo CB and Kevil CG. Hydrogen sulfide stimulates ischemic vascular remodeling through nitric oxide synthase and nitrite reduction activity regulating hypoxia-inducible factor-1alpha and vascular endothelial growth factor-dependent angiogenesis. *J Am Heart Assoc*. 2012;1:e004093.
177. Bucci M, Papapetropoulos A, Vellecco V, Zhou Z, Zaid A, Giannogonas P, Cantalupo A, Dhayade S, Karalis KP, Wang R, Feil R and Cirino G. cGMP-dependent protein kinase contributes to hydrogen sulfide-stimulated vasorelaxation. *PLoS One*. 2012;7:e53319.
178. Conti M and Beavo J. Biochemistry and physiology of cyclic nucleotide phosphodiesterases: essential components in cyclic nucleotide signaling. *Annu Rev Biochem*. 2007;76:481-511.
179. Biel M and Michalakis S. Function and dysfunction of CNG channels: insights from channelopathies and mouse models. *Mol Neurobiol*. 2007;35:266-77.
180. Pullamsetti SS, Banat GA, Schmall A, Szibor M, Pomagruk D, Hanze J, Kolosionek E, Wilhelm J, Braun T, Grimminger F, Seeger W, Schermuly RT and Savai R. Phosphodiesterase-4 promotes proliferation and angiogenesis of lung cancer by crosstalk with HIF. *Oncogene*. 2013;32:1121-34.
181. Cheng KT, Chan FL, Huang Y, Chan WY and Yao X. Expression of olfactory-type cyclic nucleotide-gated channel (CNGA2) in vascular tissues. *Histochem Cell Biol*. 2003;120:475-81.
182. Piggott LA, Hassell KA, Berkova Z, Morris AP, Silberbach M and Rich TC. Natriuretic peptides and nitric oxide stimulate cGMP synthesis in different cellular compartments. *J Gen Physiol*. 2006;128:3-14.
183. Than A, Tee WT and Chen P. Apelin secretion and expression of apelin receptors in 3T3-L1 adipocytes are differentially regulated by angiotensin type 1 and type 2 receptors. *Mol Cell Endocrinol*. 2012;351:296-305.

184. Pradervand S, Weber J, Thomas J, Bueno M, Wirapati P, Lefort K, Dotto GP and Harshman K. Impact of normalization on miRNA microarray expression profiling. *Rna*. 2009;15:493-501.
185. Rao Y, Lee Y, Jarjoura D, Ruppert AS, Liu CG, Hsu JC and Hagan JP. A comparison of normalization techniques for microRNA microarray data. *Stat Appl Genet Mol Biol*. 2008;7:Article22.
186. Yin JQ, Zhao RC and Morris KV. Profiling microRNA expression with microarrays. *Trends Biotechnol*. 2008;26:70-6.
187. van Rooij E. The art of microRNA research. *Circ Res*. 2011;108:219-34.
188. Benes V and Castoldi M. Expression profiling of microRNA using real-time quantitative PCR, how to use it and what is available. *Methods*. 2010;50:244-9.
189. Crist CG, Montarras D and Buckingham M. Muscle satellite cells are primed for myogenesis but maintain quiescence with sequestration of Myf5 mRNA targeted by microRNA-31 in mRNP granules. *Cell Stem Cell*. 2012;11:118-26.
190. Bronnum H, Andersen DC, Schneider M, Nossent AY, Nielsen SB and Sheikh SP. Islet-1 is a dual regulator of fibrogenic epithelial-to-mesenchymal transition in epicardial mesothelial cells. *Exp Cell Res*. 2013;319:424-35.
191. Di Meglio F, Castaldo C, Nurzynska D, Romano V, Miraglia R, Bancone C, Langella G, Vosa C and Montagnani S. Epithelial-mesenchymal transition of epicardial mesothelium is a source of cardiac CD117-positive stem cells in adult human heart. *J Mol Cell Cardiol*. 2010;49:719-27.
192. Russell JL, Goetsch SC, Gaiano NR, Hill JA, Olson EN and Schneider JW. A dynamic notch injury response activates epicardium and contributes to fibrosis repair. *Circ Res*. 2011;108:51-9.
193. Smart N, Risebro CA, Melville AA, Moses K, Schwartz RJ, Chien KR and Riley PR. Thymosin beta4 induces adult epicardial progenitor mobilization and neovascularization. *Nature*. 2007;445:177-82.
194. Porter KE and Turner NA. Cardiac fibroblasts: at the heart of myocardial remodeling. *Pharmacol Ther*. 2009;123:255-78.
195. Wang J, Yan CH, Li Y, Xu K, Tian XX, Peng CF, Tao J, Sun MY and Han YL. MicroRNA-31 controls phenotypic modulation of human vascular smooth muscle cells by regulating its target gene cellular repressor of E1A-stimulated genes. *Exp Cell Res*. 2013;319:1165-75.
196. Rzucidlo EM, Martin KA and Powell RJ. Regulation of vascular smooth muscle cell differentiation. *J Vasc Surg*. 2007;45 Suppl A:A25-32.
197. Dweep H, Sticht C, Pandey P and Gretz N. miRWalk--database: prediction of possible miRNA binding sites by "walking" the genes of three genomes. *J Biomed Inform*. 2011;44:839-47.
198. Sehnert AJ, Huq A, Weinstein BM, Walker C, Fishman M and Stainier DY. Cardiac troponin T is essential in sarcomere assembly and cardiac contractility. *Nat Genet*. 2002;31:106-10.
199. Moore RK, Grinspan LT, Jimenez J, Guinto PJ, Ertz-Berger B and Tardiff JC. HCM-linked 160E cardiac troponin T mutation causes unique progressive structural and molecular ventricular remodeling in transgenic mice. *J Mol Cell Cardiol*. 2013;58:188-98.
200. Lombardi R, Bell A, Senthil V, Sidhu J, Noseda M, Roberts R and Marian AJ. Differential interactions of thin filament proteins in two cardiac troponin T mouse models of hypertrophic and dilated cardiomyopathies. *Cardiovasc Res*. 2008;79:109-17.

201. Trimarchi JM, Fairchild B, Verona R, Moberg K, Andon N and Lees JA. E2F-6, a member of the E2F family that can behave as a transcriptional repressor. *Proc Natl Acad Sci U S A*. 1998;95:2850-5.
202. Bhatnagar N, Li X, Padi SK, Zhang Q, Tang MS and Guo B. Downregulation of miR-205 and miR-31 confers resistance to chemotherapy-induced apoptosis in prostate cancer cells. *Cell Death Dis*. 2010;1:e105.
203. Movassagh M, Bicknell KA and Brooks G. Characterisation and regulation of E2F-6 and E2F-6b in the rat heart: a potential target for myocardial regeneration? *J Pharm Pharmacol*. 2006;58:73-82.
204. Chiang EP, Chiu SC, Pai MH, Wang YC, Wang FY, Kuo YH and Tang FY. Organosulfur garlic compounds induce neovasculogenesis in human endothelial progenitor cells through a modulation of MicroRNA 221 and the PI3-K/Akt signaling pathways. *J Agric Food Chem*. 2013;61:4839-49.
205. Liu X, Cheng Y, Yang J, Xu L and Zhang C. Cell-specific effects of miR-221/222 in vessels: molecular mechanism and therapeutic application. *J Mol Cell Cardiol*. 2012;52:245-55.
206. Minami Y, Satoh M, Maesawa C, Takahashi Y, Tabuchi T, Itoh T and Nakamura M. Effect of atorvastatin on microRNA 221 / 222 expression in endothelial progenitor cells obtained from patients with coronary artery disease. *Eur J Clin Invest*. 2009;39:359-67.
207. Malizia AP and Wang DZ. MicroRNAs in cardiomyocyte development. *Wiley Interdiscip Rev Syst Biol Med*. 2011;3:183-90.
208. Sweetman D, Goljanek K, Rathjen T, Oustanina S, Braun T, Dalmay T and Munsterberg A. Specific requirements of MRFs for the expression of muscle specific microRNAs, miR-1, miR-206 and miR-133. *Dev Biol*. 2008;321:491-9.
209. Winbanks CE, Beyer C, Hagg A, Qian H, Sepulveda PV and Gregorevic P. miR-206 represses hypertrophy of myogenic cells but not muscle fibers via inhibition of HDAC4. *PLoS One*. 2013;8:e73589.
210. Limana F, Esposito G, D'Arcangelo D, Di Carlo A, Romani S, Melillo G, Mangoni A, Bertolami C, Pompilio G, Germani A and Capogrossi MC. HMGB1 attenuates cardiac remodelling in the failing heart via enhanced cardiac regeneration and miR-206-mediated inhibition of TIMP-3. *PLoS One*. 2011;6:e19845.
211. van Rooij E, Sutherland LB, Liu N, Williams AH, McAnally J, Gerard RD, Richardson JA and Olson EN. A signature pattern of stress-responsive microRNAs that can evoke cardiac hypertrophy and heart failure. *Proc Natl Acad Sci U S A*. 2006;103:18255-60.
212. Aurora AB, Mahmoud AI, Luo X, Johnson BA, van Rooij E, Matsuzaki S, Humphries KM, Hill JA, Bassel-Duby R, Sadek HA and Olson EN. MicroRNA-214 protects the mouse heart from ischemic injury by controlling Ca(2)(+) overload and cell death. *J Clin Invest*. 2012;122:1222-32.
213. Feng Y, Cao JH, Li XY and Zhao SH. Inhibition of miR-214 expression represses proliferation and differentiation of C2C12 myoblasts. *Cell Biochem Funct*. 2011;29:378-83.
214. van Mil A, Grundmann S, Goumans MJ, Lei Z, Oerlemans MI, Jaksani S, Doevendans PA and Sluijter JP. MicroRNA-214 inhibits angiogenesis by targeting Quaking and reducing angiogenic growth factor release. *Cardiovasc Res*. 2012;93:655-65.

215. Reddy S, Zhao M, Hu DQ, Fajardo G, Hu S, Ghosh Z, Rajagopalan V, Wu JC and Bernstein D. Dynamic microRNA expression during the transition from right ventricular hypertrophy to failure. *Physiol Genomics*. 2012;44:562-75.
216. Jia L, Li YF, Wu GF, Song ZY, Lu HZ, Song CC, Zhang QL, Zhu JY, Yang GS and Shi XE. MiRNA-199a-3p regulates C2C12 myoblast differentiation through IGF-1/AKT/mTOR signal pathway. *Int J Mol Sci*. 2014;15:296-308.
217. Kashfi K and Olson KR. Biology and therapeutic potential of hydrogen sulfide and hydrogen sulfide-releasing chimeras. *Biochemical pharmacology*. 2013;85:689-703.
218. Zhao Y, Biggs TD and Xian M. Hydrogen sulfide (H2S) releasing agents: chemistry and biological applications. *Chemical communications*. 2014;50:11788-805.
219. O'Connor CM, Starling RC, Hernandez AF, Armstrong PW, Dickstein K, Hasselblad V, Heizer GM, Komajda M, Massie BM, McMurray JJ, Nieminen MS, Reist CJ, Rouleau JL, Swedberg K, Adams KF, Jr., Anker SD, Atar D, Battler A, Botero R, Bohidar NR, Butler J, Clausell N, Corbalan R, Costanzo MR, Dahlstrom U, Deckelbaum LI, Diaz R, Dunlap ME, Ezekowitz JA, Feldman D, Felker GM, Fonarow GC, Gennevois D, Gottlieb SS, Hill JA, Hollander JE, Howlett JG, Hudson MP, Kociol RD, Krum H, Laucevicius A, Levy WC, Mendez GF, Metra M, Mittal S, Oh BH, Pereira NL, Ponikowski P, Tang WH, Tanomsup S, Teerlink JR, Triposkiadis F, Troughton RW, Voors AA, Whellan DJ, Zannad F and Califf RM. Effect of nesiritide in patients with acute decompensated heart failure. *N Engl J Med*. 2011;365:32-43.
220. Colucci WS, Elkayam U, Horton DP, Abraham WT, Bourge RC, Johnson AD, Wagoner LE, Givertz MM, Liang CS, Neibaur M, Haught WH and LeJemtel TH. Intravenous nesiritide, a natriuretic peptide, in the treatment of decompensated congestive heart failure. Nesiritide Study Group. *N Engl J Med*. 2000;343:246-53.
221. Intravenous nesiritide vs nitroglycerin for treatment of decompensated congestive heart failure: a randomized controlled trial. *Jama*. 2002;287:1531-40.
222. Gade AR, Kang M and Akbarali HI. Hydrogen sulfide as an allosteric modulator of ATP-sensitive potassium channels in colonic inflammation. *Mol Pharmacol*. 2013;83:294-306.
223. Munaron L, Avanzato D, Moccia F and Mancardi D. Hydrogen sulfide as a regulator of calcium channels. *Cell Calcium*. 2013;53:77-84.
224. Sen N, Paul BD, Gadalla MM, Mustafa AK, Sen T, Xu R, Kim S and Snyder SH. Hydrogen sulfide-linked sulfhydration of NF-kappaB mediates its antiapoptotic actions. *Mol Cell*. 2012;45:13-24.
225. Mazza R, Pasqua T, Cerra MC, Angelone T and Gattuso A. Akt/eNOS signaling and PLN S-sulfhydration are involved in H(2)S-dependent cardiac effects in frog and rat. *Am J Physiol Regul Integr Comp Physiol*. 2013;305:R443-51.

APPENDIX

Appendix 1. miRNA array data of infarcted untreated rats (MI), infarcted placebo-, GYY-, and PAG- treated rats vs. sham at 2 days after MI

miRNA ID	FC MI vs Sham	FC Placebo vs Sham	FC GYY vs Sham	FC PAG vs Sham	miRNA ID	FC MI vs Sham	FC Placebo vs Sham	FC GYY vs Sham	FC PAG vs Sham
rno-let-7a	-1.46	-1.73	-1.78	-1.64	rno-miR-24-1*	-1.04	-1.07	-1.49	-1.11
rno-let-7b	-1.25	-1.38	-2.04	-1.64	rno-miR-24-2*	1.01	-1.15	-1.28	-1.07
rno-let-7c	-1.46	-1.46	-2.39	-1.66	rno-miR-25	-1.11	-1.22	1.42	1.07
rno-let-7d	-1.25	-1.55	-1.37	-1.11	rno-miR-26a	-1.11	-1.28	-1.49	-1.21
rno-let-7e	-1.00	1.24	1.08	-1.03	rno-miR-26b	1.29	1.15	1.24	1.29
rno-let-7f	1.23	-1.04	-1.26	1.09	rno-miR-27a	-1.00	1.07	2.00	1.87
rno-let-7i	-1.09	-1.06	-1.32	-1.00	rno-miR-27b	1.39	-1.14	1.56	1.23
rno-miR-1	-1.07	-1.07	1.00	1.00	rno-miR-28	-1.46	-1.46	-1.57	-1.43
rno-miR-100	1.04	-1.46	-1.25	1.19	rno-miR-290	-1.12	1.07	1.16	-1.00
rno-miR-101b	-1.30	-1.36	-1.30	-1.07	rno-miR-291a-3p	-1.71	-1.39	-1.62	-1.17
rno-miR-103	-1.06	-1.12	-1.40	-1.08	rno-miR-29a	-1.02	-1.01	-1.01	-1.01
rno-miR-106b	-1.01	1.06	-1.35	-1.21	rno-miR-29a*	-1.10	-1.31	-1.26	1.11
rno-miR-107	1.25	1.14	1.65	1.65	rno-miR-29b	1.23	1.68	3.10	2.80
rno-miR-10a-5p	1.48	-1.35	1.30	1.07	rno-miR-29c	1.42	1.04	1.42	-3.00
rno-miR-125a-5p	-1.20	-1.47	-1.60	-1.39	rno-miR-300-5p	-1.15	-1.15	-1.15	-1.23
rno-miR-125b-3p	-1.41	1.67	1.08	1.29	rno-miR-301a	-1.00	-1.02	-1.38	-10.27
rno-miR-125b-5p	-1.36	-1.15	-1.46	-1.19	rno-miR-30b-3p	1.33	1.19	1.12	-1.19
rno-miR-126	1.09	1.15	-1.00	1.03	rno-miR-30b-5p	1.06	1.02	-1.05	1.02
rno-miR-126*	-1.37	-1.23	1.10	1.10	rno-miR-30c	1.06	-1.00	1.06	-205.23
rno-miR-129	-1.13	1.02	-1.04	-1.04	rno-miR-30d	-1.28	-1.64	-1.99	-1.37
rno-miR-129*	1.20	-1.01	-1.67	1.81	rno-miR-30e	-1.74	-1.57	-1.41	-62.81
rno-miR-130a	-1.11	-1.21	-1.48	-1.11	rno-miR-30e*	-1.18	-1.62	-2.06	4.12
rno-miR-133a	1.21	-1.07	-1.00	1.28	rno-miR-31	9.09	23.04	15.82	13.61
rno-miR-133b	1.09	-2.34	-1.86	-1.22	rno-miR-32	1.46	1.30	1.57	-1.20
rno-miR-138*	-2.11	-1.81	-2.11	-1.51	rno-miR-320	1.13	-1.09	-1.13	-8.94
rno-miR-140	-1.27	-1.14	-1.05	1.15	rno-miR-322	-1.08	-1.38	-1.08	1.08
rno-miR-140*	-1.03	-1.08	-1.25	1.06	rno-miR-329	-1.18	1.04	-1.37	1.15
rno-miR-142-3p	2.17	3.65	4.33	1.54	rno-miR-331	1.05	-1.55	-1.50	1.24
rno-miR-142-5p	1.80	2.87	3.00	1.39	rno-miR-335	-1.31	-1.15	-2.10	-1.15
rno-miR-144	1.76	-1.04	2.13	-1.60	rno-miR-336	-2.47	-1.84	-2.05	-1.00
rno-miR-145	-1.08	-1.36	1.20	1.28	rno-miR-338	1.28	-1.59	1.19	-5.65
rno-miR-146a	1.12	-1.06	-1.29	-1.06	rno-miR-339-5p	1.23	1.16	1.25	-5.98
rno-miR-146b	1.40	1.54	1.25	1.16	rno-miR-342-3p	-1.29	-1.39	-1.62	-55.96
rno-miR-148b-3p	-1.11	-1.33	-1.60	-1.39	rno-miR-347	-2.86	-1.70	-1.56	-1.10
rno-miR-150	1.33	-1.13	-2.19	1.08	rno-miR-34a	1.27	1.72	1.42	-1.47
rno-miR-151	-1.13	-1.28	-1.47	-1.18	rno-miR-34c*	-1.13	-1.10	-1.13	1.29
rno-miR-152	-1.22	-1.24	-1.37	-1.17	rno-miR-350	1.01	-1.08	-1.79	-1.15
rno-miR-15b	1.21	1.45	1.37	-1.04	rno-miR-351	-1.14	-1.18	1.04	-1.50
rno-miR-16	1.60	2.14	2.14	2.14	rno-miR-352	1.02	-1.95	-1.17	-1.45
rno-miR-17	1.36	1.59	1.68	-1.03	rno-miR-361	1.06	1.15	-1.14	-10.27
rno-miR-181a	-1.36	-1.78	-1.14	1.05	rno-miR-365	1.01	-1.00	1.39	-623.29
rno-miR-181b	1.09	-1.07	-1.00	-1.27	rno-miR-370	1.53	1.51	-1.44	1.51
rno-miR-184	-1.59	-1.35	-1.00	-1.11	rno-miR-374	1.22	-1.22	1.42	-4.15
rno-miR-185	-1.10	-1.46	-1.66	-1.19	rno-miR-378	-1.22	-1.37	-1.79	-6767.54
rno-miR-186	-1.19	-1.38	-1.38	-1.15	rno-miR-378*	-1.36	-2.05	-2.38	63.92
rno-miR-190	-1.33	-1.58	-1.96	-1.09	rno-miR-382*	-1.24	1.08	-1.37	1.24
rno-miR-191	-1.00	-1.15	-1.43	-1.28	rno-miR-423	-1.11	-1.00	1.02	1.11
rno-miR-193	2.18	3.42	2.18	1.72	rno-miR-434	-1.97	1.08	1.16	1.10
rno-miR-195	-1.00	-1.23	-1.93	-1.11	rno-miR-451	-1.35	-1.50	1.35	-2.18
rno-miR-196a*	-1.61	-1.07	-1.42	1.04	rno-miR-466c	1.74	1.65	1.65	-1.09
rno-miR-199a-3p	-1.06	1.51	1.41	1.21	rno-miR-487b	-1.41	1.35	1.31	-1.00
rno-miR-199a-5p	1.08	1.23	1.85	1.05	rno-miR-494	-1.00	1.26	1.26	1.32
rno-miR-19a	1.17	1.53	2.58	1.21	rno-miR-497	1.12	-1.54	-1.08	-1.08
rno-miR-19b	1.19	1.22	2.56	1.53	rno-miR-499	-1.19	-1.57	-2.06	-1.57
rno-miR-203	-1.19	1.13	-1.46	-1.23	rno-miR-500	1.32	1.19	1.19	-1.26

rno-miR-204*	1.41	1.60	2.80	1.27	rno-miR-503	-1.05	1.25	1.04	-1.00
rno-miR-206	-1.44	-3.23	-1.55	-1.43	rno-miR-505	-1.27	-1.99	-2.47	-1.20
rno-miR-207	-1.87	-1.14	-1.21	-1.26	rno-miR-542-3p	-1.14	1.12	-1.06	-1.24
rno-miR-20a	-1.03	1.37	1.41	-1.03	rno-miR-551b	-1.12	-1.39	-1.56	-1.16
rno-miR-21	2.71	3.13	2.95	2.30	rno-miR-652	-1.00	-1.15	-1.10	-1.33
rno-miR-21*	-1.02	1.24	1.48	1.20	rno-miR-742	1.04	-1.17	-1.30	-1.15
rno-miR-214	1.13	1.77	1.31	1.20	rno-miR-743b	1.10	1.07	1.17	1.04
rno-miR-22	1.08	1.12	1.05	1.05	rno-miR-7a	1.63	2.36	1.91	1.24
rno-miR-22*	-1.26	-1.90	-2.01	-1.26	rno-miR-872*	-1.04	-1.17	-1.42	-1.26
rno-miR-221	2.21	3.77	5.17	2.10	rno-miR-9	-1.14	-1.36	-1.35	-1.04
rno-miR-222	2.42	4.69	3.76	2.19	rno-miR-93	-1.14	1.10	1.10	-1.00
rno-miR-223	4.68	6.53	7.13	2.62	rno-miR-98	1.05	-1.18	-1.35	-1.18
rno-miR-23a	1.08	1.12	1.08	1.03	rno-miR-99a	-1.27	-1.92	-1.16	-1.12
rno-miR-23b	-1.06	-1.08	-1.06	-1.08	rno-miR-99b	-1.26	-1.43	-1.92	-1.47
rno-miR-24	-1.33	-1.09	-1.00	1.03	rno-miR-99b*	-1.87	-1.26	-1.84	-1.42

Appendix 2 miRNA array data of infarcted untreated rats (MI), infarcted placebo-, GYY-, and PAG- treated rats vs. sham at 7 days after MI

miRNA ID	FC MI vs Sham	FC Placebo vs Sham	FC GYY vs Sham	FC PAG vs Sham	miRNA ID	FC MI vs Sham	FC Placebo vs Sham	FC GYY vs Sham	FC PAG vs Sham
rno-let-7d*	-1.00	-1.10	-1.82	1.15	rno-miR-31	1.48	4.17	1.07	1.85
rno-let-7d	-1.17	-1.31	-1.02	-1.08	rno-miR-32	1.27	-1.00	1.50	1.05
rno-let-7i	1.07	1.17	-1.22	-1.03	rno-miR-320	-1.00	1.19	-1.14	1.05
rno-miR-100	-1.21	-1.21	-1.18	1.04	rno-miR-331	1.05	1.09	-1.33	1.35
rno-miR-101a	1.89	-1.00	1.25	2.05	rno-miR-335	1.74	1.92	1.86	1.97
rno-miR-106b	-1.02	1.09	-1.16	1.17	rno-miR-338	1.22	-1.12	1.28	1.14
rno-miR-10a-5p	-1.00	-1.47	-1.47	-1.12	rno-miR-338*	1.30	2.71	1.36	1.16
rno-miR-125b-3p	1.20	1.57	1.45	-1.14	rno-miR-339-5p	-1.00	1.08	-1.26	1.36
rno-miR-126*	-1.14	-1.37	-1.17	-1.17	rno-miR-342-3p	1.06	1.06	-1.27	-1.35
rno-miR-126	-1.04	1.06	1.03	1.01	rno-miR-34a	1.11	1.87	1.49	1.30
rno-miR-130a	1.16	1.16	-1.08	1.16	rno-miR-361	1.23	1.18	1.12	1.23
rno-miR-133a	-1.00	-1.75	-1.01	-1.00	rno-miR-365	1.25	1.45	1.28	1.41
rno-miR-138*	-1.50	-1.92	-1.46	-1.79	rno-miR-378*	-1.24	-1.96	-1.00	1.15
rno-miR-140*	1.05	1.92	-1.15	-1.00	rno-miR-378	1.06	-1.56	-1.00	1.06
rno-miR-140	1.41	2.38	1.50	1.21	rno-miR-423	1.31	1.20	1.31	1.27
rno-miR-142-3p	-1.21	1.48	1.20	-1.21	rno-miR-425	-1.04	1.45	-1.04	1.07
rno-miR-142-5p	-1.00	1.30	1.11	-1.18	rno-miR-451	-2.04	-1.28	-1.24	-2.04
rno-miR-143	-1.00	-1.00	-1.00	-1.00	rno-miR-487b	-1.55	-1.60	-1.40	-1.64
rno-miR-144	-1.56	-1.64	-1.05	-3.11	rno-miR-494	1.53	1.62	1.62	1.32
rno-miR-145	-1.13	-1.41	1.13	-1.02	rno-miR-497	1.17	1.52	1.52	1.19
rno-miR-146a	-1.03	1.17	-1.03	1.07	rno-miR-499	-1.16	-2.36	-1.16	-1.11
rno-miR-146b	-1.07	1.16	-1.00	1.02	rno-miR-532-5p	-1.00	1.18	1.02	1.18
rno-miR-148b-3p	-1.13	-1.00	-1.49	-1.02	rno-miR-542-3p	1.26	1.30	1.11	1.11
rno-miR-150	-1.21	-2.42	-1.44	-1.36	rno-miR-542-5p	1.17	1.35	-1.23	1.35
rno-miR-151	1.01	-1.05	-1.41	1.01	rno-miR-551b	-1.14	1.04	-1.20	-1.11
rno-miR-152	1.07	1.50	-1.33	1.01	rno-miR-652	-1.36	-1.07	-1.19	-1.12
rno-miR-15b	-1.02	1.67	1.02	-1.02	rno-miR-7a	-1.07	1.14	1.21	-1.00
rno-miR-181a	1.32	1.18	1.75	1.18	rno-miR-9	-1.37	-2.60	-2.06	-1.99
rno-miR-181d	1.09	-1.60	1.30	-1.16	rno-miR-93	1.22	1.46	1.17	1.22
rno-miR-184	-1.07	-1.04	-1.03	-1.20	rno-miR-98	-1.00	-1.00	-1.13	1.07
rno-miR-185	1.09	-1.42	-1.25	1.06	rno-miR-99a	-1.10	-1.18	-1.10	-1.10
rno-miR-186	1.04	-1.02	-1.23	1.07	rno-miR-99b*	1.05	-1.02	-1.02	-1.06
rno-miR-190	-1.06	-1.28	-1.24	1.19	rno-miR-99b	1.03	-1.00	-1.28	1.14
rno-miR-191	-1.07	-1.10	-1.54	-1.10	rno-let-7a	-1.06	1.08	-1.22	-1.06
rno-miR-193	1.56	1.60	1.37	1.40	rno-miR-101b	1.03	-1.22	-1.04	1.08
rno-miR-195	1.21	1.55	-1.00	1.21	rno-miR-107	1.21	1.13	1.55	1.24
rno-miR-196a*	-1.56	-2.82	-1.19	-3.92	rno-miR-129*	-1.35	-1.81	-1.72	-1.62
rno-miR-199a-3p	1.21	3.05	1.69	1.49	rno-miR-133b	1.26	-2.23	-1.00	1.11
rno-miR-19a	1.12	1.26	1.59	1.07	rno-miR-17	1.02	1.32	1.12	1.02
rno-miR-19b	1.09	-1.05	1.63	-1.10	rno-miR-181b	1.27	1.55	1.48	1.32
rno-miR-203	-1.43	-1.49	-1.36	-1.61	rno-miR-199a-5p	-1.00	2.13	1.28	1.10
rno-miR-206	-1.30	-4.84	-1.07	-1.33	rno-miR-207	-1.15	-1.00	-1.00	-1.10
rno-miR-208	1.00	-1.15	1.00	1.00	rno-miR-20a	1.06	1.10	1.04	1.06
rno-miR-21	-1.01	1.05	-1.01	1.03	rno-miR-21*	1.18	1.70	1.26	1.15
rno-miR-214	1.84	2.51	1.19	2.01	rno-miR-23b	1.07	1.36	1.31	1.07
rno-miR-22*	-1.16	-1.81	-1.34	-1.21	rno-miR-28	-1.14	-1.14	-1.29	-1.14
rno-miR-22	-1.03	1.02	-1.03	-1.00	rno-miR-290	-1.46	1.04	-1.42	-1.28
rno-miR-221	1.31	2.64	1.95	1.30	rno-miR-291a-3p	-1.67	-1.96	-1.51	-1.80
rno-miR-222	1.11	2.08	1.09	1.39	rno-miR-300-5p	-1.08	-1.14	-1.11	-1.05
rno-miR-223	-1.17	1.73	1.22	1.03	rno-miR-30b-3p	-1.04	-1.04	-1.11	1.35
rno-miR-24	1.09	1.07	1.10	-1.00	rno-miR-322	1.32	-1.03	1.24	1.32
rno-miR-24-1*	1.02	-1.27	-1.27	1.06	rno-miR-325-3p	-1.37	-1.91	-1.43	-1.43
rno-miR-24-2*	-1.03	-1.12	-1.08	-1.03	rno-miR-329	-1.15	-1.74	-1.01	-1.09
rno-miR-25	1.37	1.68	2.04	1.42	rno-miR-34b	1.09	2.20	1.09	1.19
rno-miR-26a	-1.00	-1.03	-1.09	-1.05	rno-miR-34c*	-1.35	-1.78	1.12	-1.39
rno-miR-26b	-1.00	-1.00	-1.00	-1.00	rno-miR-350	-1.13	-1.24	-1.31	-1.09
rno-miR-27a	1.61	-1.05	2.01	1.37	rno-miR-351	-1.06	-1.03	-1.12	-1.12
rno-miR-27b	1.18	1.09	2.16	1.07	rno-miR-434	-1.10	-1.47	1.12	-2.21
rno-miR-29a*	1.12	-1.04	1.04	1.32	rno-miR-500	-1.08	1.49	-1.38	1.12

rno-miR-29a	-1.00	1.04	1.02	-1.00	rno-miR-503	-1.00	1.08	-1.23	-1.07
rno-miR-29b	-1.25	-1.70	-1.25	-1.46	rno-miR-674-3p	1.33	1.66	-1.00	1.33
rno-miR-29c	-1.07	-1.50	-1.19	-1.00	rno-miR-872*	-1.23	-1.00	-1.23	1.03
rno-miR-301a	1.20	1.17	1.14	1.28	rno-miR-1	1.00	-1.02	1.00	1.00
rno-miR-30a*	-1.41	-3.94	1.04	-1.20	rno-miR-204*	-1.18	1.22	1.02	-1.46
rno-miR-30a	-1.00	1.00	-1.00	-1.00	rno-miR-336	-1.33	-3.47	-1.40	-2.22
rno-miR-30c	1.00	-1.02	1.00	1.00	rno-miR-347	1.20	-1.22	1.06	-1.22
rno-miR-30c-1*	-1.19	-2.83	-1.73	-1.03	rno-miR-352	-1.17	-1.08	1.15	-1.03
rno-miR-30d	-1.28	-2.01	-1.41	-1.11	rno-miR-382*	1.04	-1.36	1.42	-1.07
rno-miR-30e*	1.15	-1.69	1.08	1.21	rno-miR-466c	-1.00	1.18	1.18	1.10
rno-miR-30e	1.08	-2.07	1.05	-1.00	rno-miR-664	1.21	1.51	-1.15	1.11
rno-let-7d*	-1.00	-1.10	-1.82	1.15	rno-miR-742	-1.28	-1.21	-1.38	-1.33

Appendix 3 List of publications

Lilyanna S, Peh MT, Liew OW, Moore PK, Richards AM, Martinez EC. GYY4137, a slow-releasing hydrogen sulfide donor, attenuates adverser remodeling, preserves cardiac function and modulates the natriuretic peptide response to myocardial ischemic injury. Manuscript under review.

Lilyanna S, Martinez EC, Vu TD, Ling LH, Gan SU, Tan AL, Phan TT, Kofidis T. Cord lining-mesenchymal stem cells graft supplemented with an omental flap induces myocardial revascularization and ameliorates cardiac dysfunction in a rat model of chronic ischemic heart failure. *Tissue Eng Part A*. 2013;19:1303-1315

Martinez EC, Vu DT, Wang J, **Lilyanna S**, Ling LH, Gan SU, Tan AL, Phan TT, Lee CN, Kofidis T. Graftsn enriched with subamnion-cord-lining mesenchymal stem cell angiogenic spheroids induce post-ischemic myocardial revascularization and preserve cardiac function in failing rat hearts. *Stem Cells Dev*. 2013;22:3087-3099

Martinez EC, Wang J, **Lilyanna S**, Ling LH, Gan SU, Singh R, Lee CN, Kofidis T. Post-ischaemic angiogenic therapy using in vivo prevascularized ascorbic acid-enriched myocardial artificial grafts improves heart function in a rat model. *J Tissue Eng Regen Med*. 2013;7:203-212